

Portland State University

PDXScholar

Dissertations and Theses

Dissertations and Theses

5-7-2009

Active Site Chemistry of the NADPH-Dependent:7-Cyano-7-Deazaguanine (PreQ0) Nitrile Oxidoreductase, an Enzyme involved in Queuosine Biosynthesis

Bobby Wai Keung Lee
Portland State University

Follow this and additional works at: https://pdxscholar.library.pdx.edu/open_access_etds

 Part of the [Environmental Sciences Commons](#)

Let us know how access to this document benefits you.

Recommended Citation

Lee, Bobby Wai Keung, "Active Site Chemistry of the NADPH-Dependent:7-Cyano-7-Deazaguanine (PreQ0) Nitrile Oxidoreductase, an Enzyme involved in Queuosine Biosynthesis" (2009). *Dissertations and Theses*. Paper 6157.

<https://doi.org/10.15760/etd.8017>

This Dissertation is brought to you for free and open access. It has been accepted for inclusion in Dissertations and Theses by an authorized administrator of PDXScholar. Please contact us if we can make this document more accessible: pdxscholar@pdx.edu.

ACTIVE SITE CHEMISTRY OF THE NADPH-DEPENDENT:7-CYANO-7-
DEAZAGUANINE (PreQ₀) NITRILE OXIDOREDUCTASE, AN ENZYME
INVOLVED IN QUEUOSINE BIOSYNTHESIS

by

BOBBY WAI KEUNG LEE

A dissertation submitted in partial fulfillment of the
requirements for the degree of

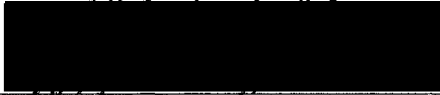
DOCTOR OF PHILOSOPHY
in
ENVIRONMENTAL SCIENCES AND RESOURCES: CHEMISTRY


Portland State University
2007

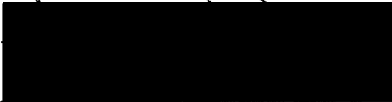
DISSERTATION APPROVAL

The abstract and dissertation of Bobby Wai Keung Lee for the Doctor of
Philosophy in Environmental Sciences and Resources: Chemistry were presented
May 7, 2007, and accepted by the dissertation committee and the doctoral program.


COMMITTEE APPROVALS:


Dirk Iwata-Reuyl, Chair

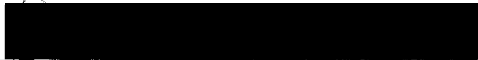

David H. Peyton


Kevin A. Reynolds


Kenneth M. Stedman


Michael S. Bartlett
Representative of the Office of Graduate Studies

DOCTORAL PROGRAM APPROVAL:


M. A. K. Khalil, Director
Environmental Sciences and Resources
Doctoral Program

ABSTRACT

An abstract of the dissertation of Bobby Wai Keung Lee for the Doctor of Philosophy in Environmental Sciences and Resources: Chemistry presented May 7, 2007.

Title: Active Site Chemistry of the NADPH-Dependent:7-Cyano-7-Deazaguanine (PreQ₀) Nitrile Oxidoreductase, An Enzyme Involved in Queuosine Biosynthesis

Queuosine (Q) is a modified nucleoside found at the wobble position of bacterial and eukaryotic transfer RNAs (tRNAs) that are specific for the amino acids tyrosine, histidine, aspartate and asparagine. A recently discovered enzyme in the biosynthetic pathway of Q, the NADPH-dependent 7-cyano-7-deazaguanine oxidoreductase (QueF), carries out the two-fold, four-electron reduction of Q precursor preQ₀ to preQ₁ and represents the first example of the enzymatic conversion of the nitrile functional group to an amine. Presented herein are kinetic, spectroscopic, mutational, biophysical, and isotope labeling studies directed at the elucidation of the chemical and kinetic mechanisms of this new class of protein.

Steady-state kinetic analysis using a NADPH-linked continuous assay provided the kinetic parameters $K_m(\text{NADPH}) = 19 \pm 2 \mu\text{M}$ and $k_{\text{cat}} = 0.69 \pm 0.02$

min⁻¹. To determine the kinetic parameters of preQ₀, a fluorescence assay that was used to follow the formation of NADP⁺ as an alkaline degradation product was optimized, and this method gave the kinetic constants $K_m(\text{preQ}_0) = 0.237 \pm 0.045$ μM , and $k_{\text{cat}} = 0.66 \pm 0.04$ min⁻¹.

Titration of enzyme with preQ₀, inactivation and protection studies with iodoacetamide, and site-directed mutagenesis of a conserved cysteine residue (Cys⁵⁵ in *Bacillus subtilis*), followed by the biochemical and biophysical analysis of the resulting protein products suggest covalent catalysis is employed by QueF, with Cys⁵⁵ serving as the catalytic nucleophile to form a covalent thioimide adduct.

The mechanism of hydride transfer from NADPH to preQ₀ was addressed using isotope labeling studies. The data obtained from ¹H-NMR, ESI-MS and steady-state kinetic analysis of QueF suggests that the protein promotes the stereospecific transfer of the *pro-R* hydride of NADPH.

Mutational and kinetic studies are also described for the substitution of a conserved glutamate (Glu⁹⁷ in *B. subtilis*). As evidenced by 25-fold to 280-fold increases in $K_m(\text{preQ}_0)$ values, the results show this residue is critical for preQ₀ recognition and binding. In addition, the kinetics revealed 13-fold to 20-fold decreases in k_{cat} , suggesting substitution of Glu⁹⁷ also impacts chemistry at the active site.

These data provide insights into the active-site chemistry of the QueF mediated nitrile reduction and a chemical mechanism consistent with our results is proposed.

Dedication

This dissertation is dedicated to my wife Katie, and my mother and father, Amy and Tony Lee. I will always remember your encouragement and unwavering patience throughout the course my doctoral studies and the writing of my dissertation.

Acknowledgments

Prof. Dirk Iwata-Reuyl for his support and guidance throughout this dissertation work

Past and present members of the Iwata-Reuyl Group for their support

Dr. Todd Link for teaching me the fundamentals in art of organic synthesis.

Professor David H. Peyton for performing NMR experiments.

Professor Niles Lehman and Dr. Debra Decker for DNA sequencing of plasmid constructs.

Professor Scott Reed for help in optimizing the fluorescence assays and for instructions on the use of the spectrofluorimeter.

Professor Simoyi and the Simoyi Group for instructions on the use of the stopped-flow spectrometer.

Professor Hans Peter Bächinger for the acquisition of protein circular dichroism data.

Deb McMillen and John Klimek for performing the protein mass spectrometry.

Dr. Andrea DeBarber and Jenny Luo for performing the small molecule mass spectrometry.

Table of Contents

Acknowledgements.....	ii
List of Tables.....	iv
List of Figures.....	v
List of Schemes.....	viii
Abbreviations.....	ix
Introduction.....	1
Experimental Procedures.....	21
Results.....	62
Discussion.....	81
References.....	168
Appendix A. Buffers	191
Appendix B. Primer Sequences.....	192
Appendix C. Derivation of the Initial Velocity Equations for the Ter-Ter Ping Pong Mechanism.....	193
Appendix D. Characterization of Synthetic Compounds.....	195

List of Tables

Table 1.	Steady-state kinetic parameters of YkvM	99
Table 2.	Activity of YkvM and Cys55 mutants measured by UV-vis and fluorescence spectroscopy.....	100
Table 3.	Size exclusion chromatography protein standards	101
Table 4.	Native molecular weight determination of YkvM and YkvM mutants	102
Table 5.	Steady-state kinetic constants for the YkvM catalyzed reaction with stereospecifically deuterium labeled NADPH.....	103
Table 6.	Kinetic characterization of the YkvM Glu ⁹⁷ mutants.....	104

Figure 22.	Molecular weight analysis of wild-type YkvM by mass spectrometry.....	126
Figure 23.	Detection of the YkvM-preQ ₀ covalent adduct by mass spectrometry.....	127
Figure 24.	Thiol inactivation studies of YkvM.....	128
Figure 25.	The purification of YkvM Cys ⁵⁵ mutants Cys55Ser and Cys55Ala..	129
Figure 26.	Mass spectrometry analysis of YkvM C55S and YkvM C55A.....	130
Figure 27.	UV-vis spectroscopy based activity assay of the YkvM Cys ⁵⁵ mutants following the oxidation of NADPH at 340 nm.....	131
Figure 28.	Fluorescence based activity assay of YkvM Cys ⁵⁵ mutants following the formation of the alkaline NADP ⁺ degradation product.....	132
Figure 29.	Substrate titration studies of the YkvM mutants C55A and C55S...	133
Figure 30.	Comparison of circular dichroism spectra of YkvM, C55A, and C55S.....	134
Figure 31.	Size exclusion chromatography of YkvM and the Cys ⁵⁵ mutants....	135
Figure 32.	Comparative trace of YkvM, C55S, and C55A by size exclusion chromatography.....	136
Figure 33.	Stereospecificity of hydride transfer catalyzed by YkvM.....	137
Figure 34.	Purification of <i>pro-S</i> and <i>pro-R</i> deuterium labeled NADPH.....	138
Figure 35.	YkvM reaction using stereoisotopically labeled cofactor.....	139
Figure 36.	Steady-state kinetic analysis of YkvM using <i>pro-R</i> deuterium labeled, <i>pro-S</i> deuterium labeled, and unlabeled NADPH.....	140
Figure 37.	Purification and analysis of preQ ₁ generated from deuterium labeled cofactors.....	141
Figure 38.	¹ H-NMR analysis of preQ ₁ generated from deuterium labeled cofactors and YkvM.....	142

List of Figures

Figure 1.	Structures of the 7-deazaguanosine bases present in tRNA.....	105
Figure 2.	Physiological occurrence of the 7-deazaguanosine modifications in tRNA.....	106
Figure 3.	The <i>de novo</i> biosynthesis of queuosine in bacteria.....	107
Figure 4.	The biosynthesis of archaeosine and the phylogenetic distribution of G* and Q in archaea and bacteria.....	108
Figure 5.	Uncharacterized operon involved in Q biosynthesis.....	109
Figure 6.	The reaction catalyzed by <i>Bacillus subtilis</i> YkvM.....	110
Figure 7.	Sequence alignment of GTP-cyclohydrolase I and QueF.....	111
Figure 8.	Multimeric barrels generated by T-folds for four functionally different enzymes.....	112
Figure 9.	The role of the universally conserved glutamate/glutamine in T-fold proteins.....	113
Figure 10.	Primary structural organization of the YqcD and YkvM subfamilies of QueF.....	114
Figure 11.	Homology model of the putative YkvM active site.....	115
Figure 12.	Different pathways of nitrile metabolism.....	116
Figure 13.	The reaction catalyzed by QueA.....	117
Figure 14.	Regiochemistry of C-N bond formation catalyzed by QueA.....	118
Figure 15.	[1- ¹³ C]AdoMet labeling studies of the QueA reaction.....	119
Figure 16.	The proposed chemical mechanism of QueA.....	120
Figure 17.	SDS-PAGE gel illustrating the purification of <i>B. subtilis</i> YkvM.....	121
Figure 18.	The purification and characterization of synthetic preQ ₀	122
Figure 19.	Steady-state kinetic analysis of YkvM.....	123
Figure 20.	Titration of YkvM with preQ ₀	124
Figure 21.	Measurement of the extinction coefficient of the absorbance band at 376 nm.....	125

Figure 39.	Mass spectrum of preQ ₁ generated from unlabeled NADPH.....	143
Figure 40.	Mass spectrum of preQ ₁ generated from <i>pro-S</i> and <i>pro-R</i> stereospecifically deuterium labeled NADPH.....	144
Figure 41.	Proposed mode of substrate binding by the conserved residue Glu ⁹⁷ of YkvM.....	145
Figure 42.	Purification of YkvM Glu ⁹⁷ mutants.....	146
Figure 43.	Steady-state kinetic analysis of YkvM Glu ⁹⁷ mutants for preQ ₀	147
Figure 44.	Stopped-flow spectrometric analysis of formation of the absorbance band at 376 nm.....	148
Figure 45.	Analysis of the kinetics of the formation of the absorbance band at 376 nm.....	149
Figure 46.	Replot of the k_{obs} of thioimide formation versus preQ ₀ concentration data	150
Figure 47.	Single turnover kinetics of YkvM monitoring the loss in absorbance at 340 nm.....	151
Figure 48.	Multiple turnover kinetics of YkvM monitoring the loss in absorbance at 340 nm.....	152
Figure 49.	Substrate analogs with potential structural requirements for YkvM oxidoreductase activity.....	153
Figure 50.	Activity assays of indole-3-nitrile as a substrate for YkvM and the Glu ⁹⁷ mutants.....	154
Figure 51.	Activity assays of 4-aminobenzonitrile as a substrate for YkvM and the Glu ⁹⁷ mutants.....	155
Figure 52.	Activity assays of phenylacetonitrile as a substrate for YkvM and the Glu ⁹⁷ mutants.....	156
Figure 53.	Activity assays of YgcM coupled to FofE.....	157
Figure 54.	Proposed kinetic scheme of YkvM.....	158
Figure 55.	Proposed catalytic mechanism of YkvM.....	159

List of Schemes

Scheme 1.	Retrosynthetic analysis for the total synthesis of epoxyqueuine.....	160
Scheme 2.	Epoxyqueuine pyrrolo[2,3- <i>d</i>]pyrimidine core structure synthesis...	161
Scheme 3.	Proposed elaboration of the ribosyl moiety of oQ	162
Scheme 4.	Synthetic strategy for the coupling of the deazaguanine core with ribosyl moiety.....	163
Scheme 5.	Chemical synthesis of preQ ₀	164
Scheme 6.	Enzymatic synthesis of <i>pro-R</i> deuterium labeled NADPH	165
Scheme 7.	Enzymatic synthesis of <i>pro-S</i> deuterium labeled NADPH.....	166
Scheme 8.	Alternate synthetic scheme for the elaboration of the ribosyl moiety of oQ	167

List of Abbreviations

Adomet S-adenosyl-L-methionine

B. subtilis *Bacillus subtilis*

CD circular dichroism

CFE cell free extract

DMAP 4-N,N-dimethylaminopyridine

DMF dimethylformamide

DMSO dimethylsulphoxide

DNA deoxyribonucleic acid

DTT dithiotreitol

E. coli *Escherichia coli*

EDTA ethylenediaminetetraacetate

ESI-MS electrospray ionization mass spectrometry

FoIE *E. coli* GTP cyclohydrolase I

G* archaeosine, 2-amino-4,7-dihydro-4-oxo-7- β -D-ribofuranosyl-1H-pyrrolo(2,3-*d*)pyrimidine-5-carboximidamide

GAPDH glyceraldehyde-3-phosphate dehydrogenase

GDPMannH guanosine diphosphate-mannose dehydrogenase

GTP guanosine triphosphate

GTPCHI GTP cyclohydrolase I

h hour

his₆ hexahistidine

HMG CoA reductase 3-hydroxy-3-methylglutaryl CoA reductase

HPLC high performance liquid chromatography

Hz Hertz

IAC iodoacetamide

IPTG isopropyl β -D-thiogalactopyranoside

kDa kilodaltons

LB Luria-Bertani

MCE mixed cellulose ester

min minute

mRNA messenger RNA

β -NADPH β -nicotinamide adenine phosphate dinucleotide (reduced form)

β -NADP⁺ β -nicotinamide adenine phosphate dinucleotide (oxidized form)

NHase nitrile hydratase

NMR nuclear magnetic resonance

Ni-NTA nickel-nitrile tetraacetic acid

OD optical density

oQ epoxyqueuosine, 7-((1*S*,2*R*,3*S*,4*R*,5*S*)-1-aminomethyl-2,3-epoxy-4,5-*cis*-dihydroxy-cyclopentane)-7-deazaguanosine

PCR polymerase chain reaction

PMSF phenylmethylsulfonylfluoride

preQ₀ 7-cyano-7-deazaguanine

preQ₁ 7-aminomethyl-7-deazaguanine

PTPS 6-pyruvoyl-tetrahydropterin synthase

Q queuosine, 7-(1*S*,2*R*,3*S*,4*R*,5*S*)-4,5-*cis*-dihydroxy-1-cyclopentene-3-ylaminomethyl)-7-deazaguanosine

QueA S-adenosylmethionine:tRNA ribosyltransferase -isomerase

RNA ribonucleic acid

SAM S-adenosyl-L-methionine

sec second

SDS-PAGE sodium dodecyl sulfate polyacrylamide gel electrophoresis

THF tetrahydrofuran

TGT tRNA-guanine transglycosylase

TLC thin layer chromatography

TMS tetramethylsilane

Tris tris(hydroxymethyl)aminomethane

tRNA transfer ribonucleic acid

tRNA^{Asp} aspartate-specific transfer ribonucleic acid

tRNA^{Asn} asparagine-specific transfer ribonucleic acid

tRNA^{His} histidine-specific transfer ribonucleic acid

tRNA^{Tyr} tyrosine-specific transfer ribonucleic acid

UDPGlcDH uridine diphosphate-glucose dehydrogenase

UDPManNAcDH uridine diphosphate-N-acetylmannosamine dehydrogenase

UDPManDH uridine diphosphate-mannose dehydrogenase

UV-Vis ultraviolet-visible

YkvM *B. subtilis* NADPH:7-cyano-7-deazaguanine oxidoreductase

YqcD *E. coli* NADPH:7-cyano-7-deazaguanine oxidoreductase

INTRODUCTION

Transfer Ribonucleic Acid (tRNA)

Transfer RNAs play a critical role in the biosynthesis of proteins. Accurately aminoacylated tRNAs are required for the translation of the genetic code into a protein sequence (1). Before this event, extensive post-transcriptional processing is required to produce a mature tRNA molecule (1). These post-transcriptional processing events include chemical modification of the genetically encoded bases in tRNA and result in the production of a rich variety of structurally modified nucleosides. Currently, over 107 unique chemical modifications of tRNA nucleosides have been identified (2, 3), many of which are conserved across broad phylogenetic boundaries (4). Nucleoside modifications typically occur in ~10% of the nucleosides of a particular tRNA, but can involve as many as 25% for a specific tRNA (5). An estimated 1% of genomes are dedicated towards encoding genes necessary for tRNA nucleoside modifications (6, 7), indicating the importance of this phenomena for basic cell physiology.

The structures, positions in specific tRNAs, and biosynthetic pathways of many of the modified nucleosides have been elucidated (2) and the growing list of tRNA modifications are currently being catalogued (8). Although the biological roles and the molecular mechanisms by which those roles are performed for many of these nucleosides are still unclear, it is generally believed that modifications outside of the anticodon region help to maintain the structural integrity and overall

tertiary structure of the tRNA, while modifications within and around the anticodon region play a direct role in translation by increasing translational fidelity (5, 9-11).

Chemical Modifications of tRNAs

The nature of nucleoside alterations vary from simple modifications of the base or ribose ring to extensive “hypermodification” of the canonical bases. Simple modifications are defined as those transformations involving a small structural change, and these transformations typically only require a single enzymatic step. Examples of this class of modification include methylations (12), base isomerizations (13), and reduction of the base (14). In contrast, “hypermodified” nucleosides are nucleosides whose biosynthesis involve multiple enzymatic steps and typically result in substantive structural changes. The most structurally complex of these modified nucleosides are the 7-deazaguanine bases archaeosine (G*, 1) [2-amino-4,7-dihydro-4-oxo-7- β -D-ribofuranosyl-1H-pyrrolo(2,3-*d*)pyrimidine-5-carboximidamide] (15) and queuosine (Q, 2) [7-(1*S*,2*R*,3*S*,4*R*,5*S*)-4,5-*cis*-dihydroxy-1-cyclopentene-3-ylaminomethyl)-7-deazaguanosine (15, 16), which in some mammalian tRNA can be further modified by glycosylation with mannose 3 or galactose 4 (17, 18) (Figure 1), or in bacterial systems, acylated with glutamic acid (19, 20). The observation that both bases possess the 7-deazaguanine core structure suggested that, in part, they share a common biosynthetic route. Q is ubiquitous throughout eukarya and bacteria, but it

is inexplicably absent in yeast and mycoplasma. Q and its derivatives occur exclusively at position 34 (the wobble position) in the anticodons of tRNAs coding for the amino acids asparagine, aspartic acid, histidine, and tyrosine (21) (Figure 2). Each of these tRNAs possess the genetically encoded anticodon sequence GUN (where N represents any nucleotide). The presence of Q in the anticodon suggests the modification plays a direct role in translational efficiency and/or fidelity. G* is present exclusively in the archaea, where it is found in the majority of known archaeal tRNAs specifically at position 15 of the dihydrouridine loop (22) (Figure 2). Its position at the interface of the D-loop and the T-stem in the tertiary structure of the tRNA is consistent with a role in maintaining the structural integrity of the tRNA (23).

Physiological Role of Queuosine

Q has been implicated in a number of physiological phenomena, including eukaryotic cell proliferation and differentiation (24, 25), tyrosine biosynthesis in mammals (26), translational frameshifts essential to retroviral protein biosynthesis (27, 28) and bacterial virulence (29, 30). In eukaryotes, Q has been further shown to be important in neoplasm staging (31), and perhaps cellular signaling via the free base (32). Transformed Chinese hamster embryo cells (33) and Ehrlich Ascites tumor cells (34) have a deficiency of Q in their tRNA (hypomodification). In both cases, it was shown that addition of exogenous queuine to the medium returned the tRNA to its normal level of queuine modification and reversed some of the

phenotypes (e.g. low levels of growth) of the transformed state. In a case that demonstrates the ability of Q to serve as a recognition determinant, tRNA^{Asp} containing Q in its anticodon (position 34) has been observed to act as a better substrate for the aspartyl-tRNA synthetase than tRNA^{Asp} containing G in that position (35).

While the above studies imply that there are specific biological functions for the Q modification of tRNA, it is worthy noting that there is also experimental evidence showing that the absence of Q does not always impair the fitness of organisms. Noguchi *et al.* have generated an *E. coli* mutant that is defective in queuine modification (36). This strain of *E. coli* grows as well as a wild type strain under normal conditions; however, when subjected to conditions unfavorable for growth, the mutant strain exhibits a marked reduction in viability compared to wild type. While the previous examples show that Q is clearly central to cellular metabolism, these results also show that the Q modification is not absolutely required for life.

Biosynthesis of Queuosine

Although Q is present in both eukarya and bacteria, only bacteria are capable of *de novo* Q biosynthesis. Eukaryotes utilize a salvage system (37) and so acquire Q as a nutrient factor from the diet and/or intestinal flora, and insert the free base form of Q, queuine, directly into the appropriate tRNAs by the enzyme tRNA-guanine transglycosylase (TGT) (38, 39).

The *de novo* biosynthesis of Q in bacteria is only partially understood. Addition of 2-¹⁴C]-guanine to the growth medium of a *Salmonella typhimurium* guanine auxotroph followed by isolation of Q from tRNA resulted in the incorporation of radioactivity into the modified nucleoside (40). A parallel experiment employing 8-¹⁴C]-guanine found no incorporation of radiolabel into Q. These results led to the proposal that the pyrrolo[2,3-*d*]pyrimidine nucleus of Q arises from guanine (as GTP) in a manner similar to the biosynthesis of toyocamycin (41, 42) or the pterin ring system (43, 44). Through an ill-defined series of steps (Figure 3), unknown enzyme(s) catalyze the expulsion of C8 and presumably N7 to form the first known intermediate in Q biosynthesis, the 7-(cyano)-7-deazaguanine, preQ₀ **5** (36, 40). This intermediate is then converted to 7-(aminomethyl)-7-deazaguanine, preQ₁ **6** (25, 45, 46), by QueF (YkvM is the QueF ortholog in *Bacillus subtilis*), which is subsequently inserted into the appropriate tRNAs by a bacterial TGT in which the genetically encoded base (guanine) is eliminated (47). The remainder of Q biosynthesis occurs at the level of the tRNA. The enzyme S-adenosylmethionine:tRNA ribosyltransferase-isomerase (QueA) catalyzes the penultimate step of Q biosynthesis, the addition of an epoxycyclopentane diol to give the intermediate epoxyqueuosine (oQ) [7-((1*S*,2*R*,3*S*,4*R*,5*S*)-1-aminomethyl-2,3-epoxy-4,5-*cis*-dihydroxy-cyclopentane)-7-deazaguanosine (48-50), which in an apparent vitamin B₁₂ dependent step is then reduced to Q (51). In higher organisms, Q-tRNA can be further modified by a

glycosylation of the cyclopentene diol with either mannose or galactose in some tRNAs (17, 18), or in bacteria, acylated with glutamic acid (19, 20).

Biosynthesis of Archaeosine

The presence of a 7-substituted 7-deazaguanine core structure in both Q and G*, coupled with the similarity of preQ₀ to archaeosine base suggested a parallel biosynthetic pathway in the archaea for archaeosine biosynthesis (15, 22, 52-54). The steps leading to preQ₀ are presumably identical in both archaea and bacteria. The pathways diverge at preQ₀, with preQ₀ serving as the substrate for an archaeal TGT (Figure 4). It has been demonstrated that preQ₀ is the relevant physiological substrate for archaeal TGT (23, 54, 55) since only preQ₀ and guanine were found to be efficient substrates of the enzyme, and archaeosine base proved to be unstable in water, readily losing ammonia to give preQ₀ (23). Following preQ₀ base incorporation into tRNA by archaeal TGT, an enzymatic reaction equivalent to the formal addition of ammonia completes the biosynthesis of archaeosine. The enzyme responsible for this final step in archaeosine biosynthesis is currently unknown.

Early Steps in Q Biosynthesis

As noted earlier, many of the enzymatic steps in Q biosynthesis are still unclear. However, recent work by Valerie de Crecy-Lagard and coworkers have implicated a previously undefined operon harboring genes necessary for Q

biosynthesis (56). Using a comparative genetics approach, whereby phylogenetic occurrence, clustering, and the predicted enzymatic activities based on sequence similarity with known proteins are analyzed, four new enzyme families involved in Q biosynthesis were discovered. This new operon is represented by *ykvJKLM* in *B. subtilis* (Figure 5). The early steps in Q biosynthesis are believed to follow the pathway of pterin synthesis, and the involvement of a GTP cyclohydrolase in the first step is consistent with the loss of C-8 in the radiolabel studies described previously. The gene *ykvK* has been annotated as 6-pyruvoyl-tetrahydropterin synthase (PTPS), an enzyme involved in tetrahydropterin biosynthesis in higher mammals (57). Because BH4 is not found in most bacteria, the function of members of this family in *B. subtilis* and *E. coli* are not clear. Recently, the *ykvK* homolog *E. coli* (*ygcM*) was cloned and expressed and showed to have some PTPS activity (8.7% of the mammalian counterpart) (58), but it was also observed that this protein could convert sepiapterin to 7,8-dihydropterin without any cofactor, thus showing a new activity of sepiapterin C6 side chain cleavage reaction (58). The relevance of this activity in the biosynthetic pathway to preQ₀ remains unclear. The *ykvJ* gene has been annotated as an ATPase conferring aluminum resistance (59); the role and activity of this protein remains unknown, but its role in the initial steps of Q biosynthesis has been confirmed through genetic screening (60). The *ykvL* gene encodes a radical SAM enzyme, the generation of radical species of S-adenosylmethionine through Fe-S centers facilitates a diverse set of reactions including methylations, isomerizations, sulfur insertions, ring formation and protein

radical formation (61). It is notable that an iron dependent enzyme is known to be present in the Q biosynthesis pathway (38). The Iwata-Reuyl lab has recently shown that the *ykvM* gene encodes a nitrile oxidoreductase that carries out the conversion of preQ₀ to preQ₁ (62).

In addition to the identification of the *ykvJKLM* operon (now renamed *queCDEF*) in the early steps of Q biosynthesis, it has been recently shown that in some bacteria, the regulation of the corresponding genes are under the control of a preQ₁ riboswitch (63). It is thought that the binding of the small molecule to the RNA element regulates gene expression by effecting a conformational change that influences the efficiency of transcription termination or translation initiation for the corresponding mRNA (64, 65). The 5' untranslated region of the *B. subtilis* *ykvJKLM* operon selectively binds to, and exhibits a dissociation constant for, preQ₁ in the nanomolar range. In the case of the preQ₁ riboswitch, the RNA motif contains highly conserved sequence and structural elements that differentiates this riboswitch from adenine (66) or guanine sensing (67) riboswitches. Compared to other natural metabolite-binding RNAs, the preQ₁ aptamer appears to have a simple structure, consisting of a single stem-loop and a short tail sequence that together are formed from as few as 34 nucleotides (63). The association of the riboswitch with genes involved in preQ₁ anabolism suggests that it serves to down-regulate gene expression in response to ligand binding. Both preQ₁ and preQ₀ are recognized by the preQ₁ aptamer (measured K_d values of 20 nM and 100 nM, respectively) suggesting that preQ₁ is the primary target of the RNA element, and it seems

reasonable from a gene-control perspective that the final Q biosynthetic intermediate that exists in the free base form would serve as the regulator.

NADPH:7-cyano-7-deazaguanine oxidoreductase

The *queF* gene family, represented by *ykvM* in *B. subtilis* and *yqcD* in *E. coli*, encode an oxidoreductase involved in an early step of Q biosynthesis. The enzyme utilizes two equivalents of the cofactor NADPH for the four electron reduction of the nitrile group of preQ₀ to give the primary amine of preQ₁ (62) (Figure 6).

Homology between *queF* and GTP cyclohydrolase I (GTPCH-I) resulted in the initial functional misannotation of the *queF* gene family as GTPCH-I in genomic databases. The homology score between the two protein families (detected by PSI-BLAST; www.ncbi.nlm.nih.gov/blast) is \approx 25 % sequence identity and 40 % similarity in a 100-aa stretch (Figure 7). Based on this homology, the QueF protein family is predicted to belong to the tunnel fold (T-fold) family of enzymes (62). This class of proteins is named as such because these folds are found as multimeric proteins (Figure 8) crossed by a tunnel (68). In the case of YkvM, the quaternary arrangement has been shown to be a dodecamer and for YqcD, the functional protein exists as a dimer (69). Although YqcD exhibits a low order quaternary form *in vitro*, it is believed that this protein forms a higher order aggregate structure in the cell, possibly a tetramer (V. De Crecy-Lagard, personnel communication). T-fold proteins bind substrates belonging to the purine

or pterin families, and share a fold-related binding site with a glutamate or glutamine residue anchoring the substrate. In GTP cyclohydrolase (Glu152), dihydroneopterin aldolase (Glu74), and 6-pyruvoyl tetrahydropterin synthase (Glu107), the conserved glutamate is positioned such as to serve as an acceptor for the pyrimidine ring of the substrate, hydrogen bonding with the N1 and N2 atoms (GTP numbering) (68). In urate oxidase, the conserved glutamine (Gln228) carries out this function (68). In all of these examples, the conserved Glu/Gln forms two hydrogen bonds to the substrate (Figure 9).

Based on their amino acid sequences, QueF family members are further divided into two structural subfamilies (Figure 10). The YkvM subfamily is comprised of ~160-amino acid unimodular proteins, possessing a single T-fold domain and a characteristic motif (the QueF motif) E(S/L)K(S/A)hK(L/Y)(Y/F/W) (where h is a hydrophobic amino acid) bracketed on the N- and C- terminal sides by an invariant Cys and Glu, respectively. The YqcD subfamily of QueF enzymes is characterized by ~280-amino acid bimodular proteins comprised of tandem T-fold domains in which the QueF motif and the invariant Cys and Glu are located separately in the weakly homologous N- and C- terminal domains of the polypeptide chain, respectively.

QueF proteins are predicted to be closely related to GTPCH proteins. FoIE (the GTPCH in *E. coli*) has been studied extensively, and the crystal structure of FoIE in complex with substrate GTP has been solved (70). FoIE contains several conserved cysteines, and it is shown in the crystal structure that the FoIE cysteine

that aligns universally with the YkvM cysteine is involved in co-ordination and binding of a zinc metal ion. A homology model built by threading the YkvM sequence through the structure of FolE, followed by the docking of preQ₀ in the putative active site and energy minimization (Figure 11), suggested that the assumed cysteine of YkvM, Cys⁵⁵, is present in the active site and resides approximately 2.9 Å from the nitrile of preQ₀ (69). Analysis of the conserved Glu of YkvM, Glu⁹⁷, indicated that this residue plays a similar substrate binding role to that observed for FolE and the other T-fold proteins, the binding of the C₂-NH₂ amine of preQ₀.

The discovery of the QueF activity adds to a small group of enzymes traditionally classified as NAD(P)⁺-dependent four-electron-transfer dehydrogenases (71). These include UDP-glucose dehydrogenase (UDPGlcDH) [and its homologs UDP-N-acetylmannosamine dehydrogenase (UDPManNAcDH) and GDP-mannose dehydrogenase (GDPManDH)], histidinol dehydrogenase and 3-hydroxy-3-methylglutaryl-coenzyme A (HMG-CoA) reductase, all of which have enzymatic activities equivalent to both an alcohol and aldehyde dehydrogenase in a single active site. Notably, these enzymes lack significant sequence homology and these proteins have been found to employ distinctly different chemical mechanisms. In the case of UDPGlcDH, an active site cysteine has been implicated in catalysis similar to that invoked by the glyceraldehyde-3-phosphate dehydrogenase (GAPDH) paradigm of aldehyde-oxidizing enzymes, and a number of studies support the proposal that a covalent enzyme-substrate adduct is formed

through this residue (72, 73). HMG-CoA does not have an active site cysteine as a nucleophile, but the action on the thioester substrate may be thought to resemble the GAPDH archetype in its chemistry of aldehyde oxidation. Histidinol dehydrogenase, although containing two strictly conserved cysteine residues (74), is a Zn^{2+} -dependent metalloenzyme. The x-ray structure of this protein suggests that the reaction mechanism is mediated by an active site histidine (His327) working *via* acid-base catalysis (75, 76).

Most prominently, the QueF activity is a new mode of catalysis for nitrile metabolism (Figure 12). The pathways of nitrile metabolism currently known and characterized involve hydrolysis [nitrile hydratase (NHase), nitrilase], oxidation (oxygenase), and reduction (nitrogenase) (77). QueF may be mechanistically similar to the catalysis invoked by the hydrolytic enzymes. NHase, a metalloenzyme, requires either cobalt (III) or iron (III) to co-ordinate an active site water molecule for catalysis (77). The metal bound hydroxide ion acts as a nucleophile, attacking the nitrile carbon atom to form an imidate intermediate. Rearrangement of the imide group completes the chemical conversion of the nitrile to the amide product before release from the active site. The nitrilase family of enzymes catalyzes the degradation of nitrile substrates to the corresponding carboxylic acid. A strictly conserved cysteine residue in the active site acts as a nucleophile (78); attack of the thiol group on the carbon atom of the nitrile with concomitant protonation of the nitrogen atom forms a thioimide intermediate. This intermediate is then subjected to nucleophilic attack by a water molecule to form a

tetrahedral intermediate. Collapse of the tetrahedral intermediate releases ammonia and leaves the substrate still bound in the active site as the thioester (79). Hydrolysis of this enzyme bound species affords the acid product.

The nitrile oxidoreductase, YkvM, is unique in biology, as the direct transformation of a nitrile to an amine has never been observed and therefore, the QueF protein family presents an interesting and uncharacterized case of protein catalysis. The goal of this work is the biochemical characterization of this novel class of proteins through kinetic, chemical, mutational and structural analysis. Elucidation of these aspects will allow us to explore the utility of this enzyme to carry out the reduction of alternate nitrile substrates, the ultimate goal being the engineering of this protein to selectively and efficiently reduce industrially important nitrile containing compounds.

S-adenosylmethionine:tRNA ribosyltransferase isomerase (QueA)

The enzyme QueA catalyzes the penultimate step in Q biosynthesis. The presence of the QueA activity was discovered after it was observed that *E. coli* cells, when placed under conditions of methionine deficiency, showed an under-modification of all Q-specific tRNAs (80, 81). Furthermore, studies under these conditions showed that a single Q intermediate could be isolated and identified, the preQ₁ nucleoside (45, 81). Accumulation of the precursor preQ₁ was also observed from *E. coli* strain JE10651 (82), a Q deficient mutant that was shown to have a defective *queA* gene. Complementation of this strain with a plasmid harboring an intact *queA* fully restored Q production.

After the *queA* gene was cloned and the protein product was purified, Slany *et al.* showed that oQ-tRNA modification occurred only in the presence of the cofactor S-adenosyl-L-methionine (Adomet) (48), a highly utilized metabolite of methionine. The reaction product was isolated by HPLC and analyzed by mass spectrometry and NMR spectroscopy to identify oQ as the modified nucleoside (49). Radiolabel incorporation studies of methionine or adenine labeled Adomet did not result in any radioactivity incorporated into oQ (48). However, the use of ribosyl labeled Adomet for the QueA reaction and the subsequent isolation of oQ revealed that the ribosyl moiety of Adomet was the precursor to the epoxycyclopentane diol moiety of oQ (50). As a result of these findings, it was concluded that QueA catalyzes the transfer and isomerization of the ribosyl moiety

of Adomet to preQ₁-tRNA, yielding adenine, methionine, and oQ-tRNA as products (Figure 13).

A chemical mechanism was proposed for this reaction in which nucleophilic attack from the primary amine of preQ₁-tRNA takes place at C-1' of Adomet as the initial step (50). The ring opened alkoxide subsequently acts as a nucleophile and displaces methionine leading to an epoxide intermediate. After deprotonation at C-5', ring formation occurs by intramolecular nucleophilic attack on C-1' to expel adenine and form oQ. However, if it is assumed that the *cis*-diol present in AdoMet remains unchanged in the conversion to oQ, then the absolute stereochemistry of oQ and AdoMet renders C-N bond formation via this route untenable (Figure 14). Instead, C-4' of AdoMet is implicated as the site of C-N bond formation (83).

The regiochemistry of C-N bond formation between preQ₁-tRNA and Adomet has been explored through the utilization of [1'-¹³C]AdoMet in the QueA reaction followed by the identification of the isotopically enriched carbon in the oQ nucleoside (83). Since the ¹³C NMR spectrum of oQ is not known, the isolated product was analyzed by observation of the ¹H-¹³C coupling in a difference spectrum of the coupled and uncoupled spectra (Figure 15). The proton directly bonded to the ¹³C atom clearly gave a resonance at 3.77 ppm with a ¹H-¹³C coupling constant of 193 Hz. These results effectively excluded C-1 and C-4 (epoxycyclopentane diol naming) as sites of isotopic enrichment due to the chemical shifts of the corresponding hydrogens being significantly upfield (C-1,

3.37 ppm) and downfield (C-4, 4.29 ppm) from the observed resonance of the hydrogen directly bonded to the ^{13}C -enriched carbon. Of the three remaining carbons with resonances in the immediate vicinity of 3.77 ppm, C-5 was also excluded as the site of enrichment based on the magnitude of the ^1H - ^{13}C coupling which was indicative of a C-H bond with substantial s-character, consistent with an epoxycyclopentane C-H bond but not a hydroxycyclopentane C-H bond. This left the site of isotopic enrichment at one of the epoxide carbons C-2 or C-3 and, based on the substituent effects of the adjacent heteroatoms, the C-2 proton resonance is expected to be the upfield resonance (3.71 ppm), given its position adjacent to the C-1 alkylamine, with the resonance at 3.76 ppm due to the C-3 proton as a result of the more electronegative hydroxyl at C-4. Therefore, the NMR data supports C-3 as the site of enrichment, implicating C4' of Adomet as the site of C-N bond formation, but does not rigorously rule out C-2 (83).

Chemical mechanisms to either $[3\text{-}^{13}\text{C}]\text{oQ}$ or $[2\text{-}^{13}\text{C}]\text{oQ}$ from $[1\text{-}^{13}\text{C}]\text{Adomet}$ may be envisioned, but when keeping mechanistic economy in mind, the route to $[3\text{-}^{13}\text{C}]\text{oQ}$ is more reasonable as this does not require any reorganization of the diol moiety in the conversion of AdoMet to oQ. Presented in Figure 16 is a mechanism which is consistent with the data implicating C-3 of oQ as the site of enrichment (83). Initial enzyme-catalyzed deprotonation of AdoMet at C-5' generates a sulfonium ylide which collapses to the vinyl sulfonium with ring opening and the concomitant elimination of adenine. Addition of the preQ₁-tRNA primary amine to the *re*-face of C-4' then generates the new sulfonium ylide, which

can subsequently attack the *si*-face of the C-1' aldehyde to give the alkoxy-carbocycle. Intramolecular S_N^2 attack of the alkoxy oxygen on the adjacent carbon results in the elimination of methionine, and gives the final product, oQ-tRNA.

To gain further insight into the chemical mechanism in the QueA reaction, a total synthesis of oQ is proposed. Full ^1H and ^{13}C NMR assignments, followed by NMR analysis of the specifically enriched [^{13}C]-oQ, will allow correlation of the regiochemistry of the new C-N bond between preQ₁-tRNA and the ribosyl moiety of AdoMet.

Retrosynthetic Analysis of the Epoxyqueuine Base

Epoxyqueuine **7** [7-((1*S*,2*R*,3*S*,4*R*,5*S*)-1-aminomethyl-2,3-epoxy-4,5-*cis*-dihydroxy-cyclopentane)-7-deazaguanine] serves as a satisfactory reference for assignment of the NMR resonances of the cyclopentane ring of oQ, and Scheme 1 illustrates the retrosynthetic strategy that will be employed to obtain epoxyqueuine. Hoops *et al.* (84) reported a versatile and efficient synthesis of a variety of 5-substituted pyrrolo[2,3-*d*]pyrimidines *via* displacement of the quaternary ammonium salt of 2-amino-5-(*N,N*-dimethylaminomethyl)-pyrrolo[2,3-*d*]pyrimidin-4-one **8**. We envision using this strategy to acquire the protected form of epoxyqueuine by coupling **8** with the isopropylidene protected stereospecific (1*S*,2*R*,3*S*,4*R*,5*S*)-1-amino-2,3-epoxy-4,5-*O*-isopropylidene-cyclopentane **9**. The elaboration of **9** can be accessed from stereospecific cyclopentenone **10**.

The route to the dimethyl analog of preQ₁ involves 7 synthetic steps. The deazaguanine core is accessible (Scheme 2) following the work of Davoll in three steps (**11-13**) (85). Upon protection of the C₂-NH₂ amine as the octanoyl **14**, the fully protected form of preQ₁ **15** is prepared in high yield *via* Mannich reaction with dibenzylamine and formaldehyde (86). Amine exchange of **15** with dimethylamine and subsequent C₂-NH₂ deprotection under basic conditions provides compound **8**. The synthesis is thus reduced to the preparation of the (1*S*,2*R*,3*S*,4*R*,5*S*)-1-aminomethyl-2,3-epoxy-4,5-O-isopropylidene-cyclopentane **9**. The key intermediate towards the elaboration of this compound is the synthesis of stereospecific 4,5-O-isopropylidene-cyclopent-2-en-1-one **10**. Cyclopentenone **10** has previously served as an intermediate in the syntheses of prostaglandins (87) and carbocyclic nucleosides such as neplanocin A (88, 89). While many routes to enantiopure **10** have been reported (90-95), their syntheses are generally lengthy and inefficient. Ali *et al.* (96) have reported a three step synthesis of **10** in an overall yield of 45% from D-ribose, therefore this route was selected to acquire **10**. Scheme 3 details the synthetic route proposed to furnish **9**. D-ribose is protected as the methyl riboside **16** followed by oxidation to the lactone **17**. Wittig rearrangement of this product provides the stereospecific cyclopentenone **10**. Access to stereospecific **9** relies on two essential transformations; the stereoselective reduction of **10**, and the introduction of the epoxide moiety *trans* to the protected diol. The selective reduction of **10** from the *Si* face of the carbonyl to give the 4,5-O-isopropylidene-cyclopent-2-ene-1-ol **18** with the desired *R*

configuration has been reported (97, 98), consistent with the expected inaccessibility of the *Re* face of the carbonyl due to the steric bulk of the isopropylidene group. Given the known directing effects of hydroxyl groups in epoxidation reactions (99) and the presence of the acetonide, an exclusively *trans* epoxidation of **18** is predicted to occur (100), providing 2,3-epoxy-4,5-O-isopropylidene-cyclopentan-1-ol **19**. Activation of the alcohol (98, 101-103) to 2,3-epoxy-4,5-O-isopropylidene-1-tosyl-cyclopentane **20** followed by azide displacement (102-104) resulting in inversion of stereochemistry at C1 to give 1-azido-2,3-epoxy-4,5-O-isopropylidene-cyclopentane **21** completes the stereochemical requirements of the cyclopentane portion of epoxyqueuine. Treatment of **21** under reducing conditions (102-104) gives fully elaborated 1-amino-2,3-epoxy-4,5-O-isopropylidene-cyclopentane **9**.

Coupling of 2-amino-5-(*N,N*-dimethylaminomethyl)-pyrrolo[2,3-*d*]pyrimidin-4-one **8** with the ribosyl moiety **9** is carried out following the method described by Hoops *et al.* (84). Compound **8** is treated with methyl iodide to form the ammonium salt; substitution by **9** gives oQ base protected as the acetonide **22**. Deprotection (105) completes the synthesis and furnish epoxyqueuine **7** (Scheme 4).

Queuosine biosynthesis is clearly marked with unprecedented enzyme chemistry, and the overall focus of this dissertation is the study of the enzymes QueF and QueA in the Q pathway. In addition to work proposed previously for the characterization of the novel nitrile oxidoreductase, investigations of QueA are

described. The mechanism of the QueA reaction, specifically the regiochemistry of ribosyl addition from AdoMet to preQ₁-tRNA remains unclear, and this work presents progress towards a total synthesis of oQ to complement the isotope studies already performed in the Iwata-Reuyl laboratory.

EXPERIMENTAL PROCEDURES

Chemicals

Buffers and salts of highest quality grade available were purchased from Sigma unless otherwise noted. Dithiothreitol (DTT), isopropyl β -D-thiogalactopyranoside (IPTG), and kanamycin sulfate were from US Biologicals. β -NADPH and β -NADP⁺ were from Research Products International Corp. Sulfhydryl reagent iodoacetamide (IAc) was from Alfa Aesar. Sepharose CL-6B, bromophenol blue, and Blue Dextran 2000 were from Sigma. L(+)-selenomethionine, isopropanol-*d*₈ (99+%) and deuterium oxide were from Acros. Plasmid Mini Kits and Ni²⁺-NTA agarose were from Qiagen. Amicon Ultra YM-10 and YM-5 units were from Amicon. Dialysis was performed in Slide-A-Lyzer™ cassettes from Pierce. Oligonucleotides were from Integrated DNA Technologies. The linearized vector pET30 Xa/LIC was provided as a part of the cloning kit from Novagen. DNA from restriction digests and PCR reactions were purified using the UltraClean DNA Purification Kit from MoBio. Protein concentrations were based on the Bradford dye-binding procedure (BioRad) using bovine serum albumin (Sigma) as a standard. For wild-type YkvM, the protein concentration was determined using the extinction coefficient at $\epsilon_{280\text{ nm}}$ (23,660 M⁻¹) experimentally determined as described by Gill and Von Hippel (106). Genomic DNA from *E. coli* was a generous gift from Dr. David Boone, Portland State University.

Instrumentation

PCR was carried out on the GeneAmp PCR system 2400 from PerkinElmer Life Sciences. An Amersham Biosciences Typhoon 9200 variable mode imager with ImageQuant 5.2 software was used for fluorescence detection of ethidium bromide stained agarose gels. UV-vis spectrophotometry was performed with either a Varian Cary 100 Bio equipped with a circulating water bath or a Beckman DU-520 General Purpose Spectrophotometer. Rapid-scanning kinetic measurements were made using a HI-TECH Scientific SF-61 stopped flow spectrophotometer equipped with a M300 monochromator and connected to a RTE7 Digital-One circulating water bath from Thermo-NesLab. The hardware was interfaced with a HI-TECH Scientific IS-2 software suite v2.3b6 for data acquisition and analysis. Fluorescence measurements were made using a QM3 spectrofluorimeter from Photon Technology International. Circular dichroism spectra were recorded on an Aviv 202 spectropolarimeter (at Oregon Health and Sciences University (OHSU), Portland, OR) using a Peltier thermostatted cell holder and a 1-mm path length rectangular cell (Starna Cells Inc.). Centrifugation was performed with an Avanti J-20 XP centrifuge using a JA-25.50 and JA-10 rotor and a Model TJ-6 swinging bucket centrifuge, both from Beckman Coulter, Inc, and a Spectrafuge 16M tabletop centrifuge from Labnet. High performance liquid chromatography (HPLC) was done with a Hitachi L-7100 with an L-4500A

photodiode array detector and controlled via the Hitachi ConcertChrome HPLC software. Size exclusion chromatography was performed on a BioSep-SEC-S4000 column, semi-preparative HPLC was performed on a Luna C18 column (250 × 10 mm, 5 μm), and analytical HPLC was conducted on a Bondclone C18 column (300 × 3.90 mm, 10 μm), all from Phenomenex. Cells were lysed using a French press from American Instruments Company, Inc. or by sonication using the Microson Ultrasonic Cell Disruptor XL from Misonix (Farmington, New York). Sodium dodecyl sulfate polyacrylamide gel electrophoresis (SDS-PAGE) was carried out with a Mini Protean III from BioRad. Small molecule mass spectrometry was done on a LCQ Advantage ion-trap mass spectrometer (Thermo Electron, San Jose, CA) equipped with an electrospray ionization (ESI) source at the BioAnalytical Shared Resource/Pharmacokinetics Core Facility in the Department of Physiology and Pharmacology at OHSU, Portland, Oregon. Whole protein mass spectrometry was performed on a quadrupole time-of-flight mass spectrometer (QSTAR XL, Applied Biosystems/MDS Sciex, Foster City, CA) equipped with a standard ion source (MDS Sciex, Concord, Canada) at the Proteomics Shared Resource facility at OHSU, Portland, Oregon. DNA sequencing was done using Big Dye Terminator sequencing protocols and was performed at the Portland State University-Keck Genomics Facility.

Bacterial Strains and Enzymes

E. coli strain DH5 α (F⁻ Φ 80dlacZ Δ M15 Δ (lacZYA-argF)U169 *deoR* *recA1endA1* *hsdR17*(r_K⁻,m_K⁻) *phoA* *supE44* λ -*thi-1* *gyrA96* *relA1*) was from Gibco BRL Life Technologies. *E. coli* strain BL21 (DE3) (F⁻ *dcm* *ompT* *hsdS*(r_B⁻, m_B⁻) *gal* λ) was from Stratagene. Lysozyme was from MP Biomedicals. Restriction enzymes and their appropriate reaction buffers were from MBI Fermentas and New England Biolabs, Inc. PfuTurbo® Polymerase and PfuUltra™ Polymerase were from Stratagene. Bovine Factor Xa was from Promega or USB. *Pro-R* specific alcohol dehydrogenase (*Thermoanaerobium brockii*) and glucose-6-phosphate dehydrogenase type VII from *Saccharomyces cerevisiae* were from Sigma. Gel filtration standards ovalbumin, bovine serum albumin, alcohol dehydrogenase, apo-ferritin and rabbit muscle pyruvate kinase type II were from Sigma. Bovine thyroid thyroglobulin was from Amersham Biosciences.

Expression and Purification of his₆-YkvM.

A 10 μL aliquot of *E. coli* BL21(DE3) cell stock containing the pET30-*ykvM* plasmid was used to inoculate 3 mL of LB media containing 30 $\mu\text{g mL}^{-1}$ kanamycin. After 8 h of incubation at 37°C and 250 rpm, a 1 mL aliquot was removed and used to inoculate 100 mL of LB medium containing 30 $\mu\text{g mL}^{-1}$ kanamycin. The cultures were incubated at 37°C and 250 rpm for 12 h, at which point 5 mL of this culture was added to 500 mL LB medium supplemented with 30 $\mu\text{g mL}^{-1}$ kanamycin. When the OD₆₀₀ reached 0.8, the cell cultures were induced with 0.5 mM IPTG. The cultures were allowed to grow for an additional 4 h at which time the cells were harvested by centrifugation (6,000 x g, 10 min at 4°C) and flash frozen in liquid nitrogen. Typically, 20 g of cells were obtained from 3 L of media.

Cells were suspended to a density of 250 mg mL⁻¹ in 100 mM Tris (pH 8.0), 100 mM KCl, 2 mM β -mercaptoethanol, and 1 mM PMSF. The cells were lysed by two passes through a French Press at 20,000 psi. After removal of cell debris by centrifugation (15,000 x g, 20 min), streptomycin sulfate was added to a final concentration of 3%. The mixture was chilled on ice for 1 h before the nucleic acids were pelleted by centrifugation (20,000 x g, 20 min). The supernatant was filtered through a 0.45 μm MCE syringe filter and loaded onto a column containing 10 mL of Ni²⁺-NTA agarose equilibrated in 100 mM Tris (pH 8), 100 mM KCl, 2 mM β -mercaptoethanol, 1 mM PMSF, and 1% Triton X-100 (Buffer A). The column was washed consecutively in the following manner: 5 column volumes of

Buffer A, 5 column volumes of Buffer A containing 20 mM imidazole (Buffer B), 5 column volumes of Buffer B without Triton X-100 or PMSF (Buffer C), 5 column volumes of buffer C except with 50 mM imidazole (Buffer D), and then 5 column volumes of Buffer C except with 100 mM imidazole (Buffer E). The fusion protein was eluted with 5 column volumes of Buffer C except with 200 mM imidazole (Buffer F). The eluant was collected in 10 mL fractions and analyzed by SDS-PAGE, and fractions containing his₆-YkvM were pooled, concentrated to ~ 1 mL using Amicon Ultra YM 10,000 and dialyzed overnight against 4 L of 100 mM Tris (pH 8.0), 100 mM KCl, and 1 mM DTT. Following dialysis, the fusion protein was directly treated with Factor Xa.

Purification of Recombinant Wild-Type YkvM.

Factor Xa (10 µg) was added to a mixture of 20 mg his₆-YkvM in 100 mM Tris (pH 7.5), 100 mM KCl, and 1 mM CaCl₂. After 20 h, the reaction was loaded onto a Ni²⁺-NTA agarose column (2 mL) equilibrated in 100 mM Tris (pH 8.0), 100 mM KCl, and 1 mM β-mercaptoethanol (Buffer G). The cleaved wild-type protein was eluted with 5 column volumes of Buffer G. The eluant was collected and analyzed as described above, and fractions containing wild-type YkvM were pooled and concentrated to ~1 mL using Amicon Ultra YM 10,000. An equal volume of 50 % glycerol was added, and after determination of the resulting protein concentration, the wild-type protein in 25 % glycerol was stored at -80°C.

Preparation of the Selenomethionine Incorporated YkvM for Structure Studies

A 10 μL aliquot of *E. coli* BL21(DE3) cell stock containing the pET30-*ykvM* plasmid was used to inoculate 3 mL of LB media containing 30 $\mu\text{g mL}^{-1}$ kanamycin. After 8 h of incubation at 37°C and 250 rpm, a 1 mL aliquot was removed and used to inoculate 100 mL of LB medium containing 30 $\mu\text{g mL}^{-1}$ kanamycin. The cultures were incubated at 37°C and 250 rpm for 12 h, after which the cells were pelleted by centrifugation, and washed twice with M9 media (107). The cells were resuspended in 50 mL M9 and then 5 mL of the cell suspension was added to 500 mL M9 media containing 0.2 % glucose, 2 mM MgSO_4 , 100 μM CaCl_2 , 5×10^{-5} % thiamine, 5×10^{-5} % biotin, 1.65×10^{-5} % guanosine, thymine and uracil, 90 $\mu\text{g mL}^{-1}$ of each amino acid except methionine, 30 $\mu\text{g mL}^{-1}$ kanamycin, essential micronutrients (108) (2 mM $\text{FeSO}_4 \cdot 7\text{H}_2\text{O}$, 1 $\mu\text{g mL}^{-1}$ riboflavin, 1 $\mu\text{g mL}^{-1}$ niacinamide, 1 $\mu\text{g mL}^{-1}$ pyridoxine monohydrochloride), and 60 $\mu\text{g mL}^{-1}$ of L(+)-seleno-methionine (Acros, 99+% e.e.). The cells were grown to an $\text{OD}_{600} = 0.5\text{-}0.6$, followed by the addition of a solution containing lysine, phenylalanine, threonine (each to a final concentration of 45 $\mu\text{g mL}^{-1}$), leucine, and valine (each to a final concentration of 45 $\mu\text{g mL}^{-1}$). The media was further supplemented with 80 $\mu\text{g mL}^{-1}$ L(+)-seleno-methionine and allowed to grow for 15 min before the addition of IPTG to a final concentration of 0.5 mM. The cells were grown overnight, collected by centrifugation and stored at -80°C until further use.

The purification of the selenomethionine incorporated derivative of YkvM was performed in the same manner as described for the wild type protein.

Following purification, β -mercaptoethanol (1 mM) was added to prevent the oxidation of selenomethionine to the selenoxide.

Expression and Purification of YqcD.

A 10 μ L aliquot of *E. coli* BL21(DE3) cell stock containing the pET30-*yqcD* plasmid was used to inoculate 3 mL of LB media containing 30 μ g mL⁻¹ kanamycin. After 8 h of incubation at 37°C and 250 rpm, a 1 mL aliquot was removed and used to inoculate 100 mL of LB medium containing 30 μ g mL⁻¹ kanamycin. The cultures were incubated at 37°C and 250 rpm for 12 h, at which time 5 mL this culture was added 0.5 L LB medium supplemented with 30 μ g mL⁻¹ kanamycin. When the OD₆₀₀ reached 0.8, the cell cultures were induced with 0.5 mM IPTG. The cultures were allowed to grow for an additional 4 h at which time the cells were harvested by centrifugation (6,000 \times g, 10 min at 4°C) and flash frozen in liquid nitrogen. Typically, 20 g of cells were obtained from 3 L of medium.

Cells were suspended to a density of 250 mg mL⁻¹ in 100 mM Tris (pH 8.0), 100 mM KCl, 2 mM β -mercaptoethanol, and 1 mM PMSF. The cells were subjected to lysis by two passes through a French Press at 20,000 psi. After removal of cell debris by centrifugation (15,000 \times g, 20 min), streptomycin sulfate was added to a final concentration of 3%. The mixture was chilled on ice for 1 h before the nucleic acids were pelleted by centrifugation (20,000 \times g, 20 min). The supernatant was filtered through a 0.45 μ m MCE syringe filter and loaded onto a

column containing 10 mL of Ni²⁺-NTA agarose equilibrated in Buffer A. The column was washed consecutively in the following manner: 5 column volumes of Buffer A, 5 column volumes of Buffer B, 5 column volumes of Buffer C, 5 column volumes of Buffer D, and then 5 column volumes of Buffer E. The fusion protein was eluted with 5 column volumes of Buffer F. The eluant was collected in 10 mL fractions and analyzed by SDS-PAGE, and fractions containing his₆-YqcD were pooled, concentrated to ~ 1 mL using Amicon Ultra YM 10,000 and dialyzed overnight against 4 L of 100 mM Tris (pH 8.0), 100 mM KCl, and 1 mM DTT. Following dialysis, the fusion protein was treated directly with Factor Xa.

Purification of Recombinant Wild-Type YqcD.

Factor Xa (10 µg) was added to a mixture of 20 mg his₆-YqcD in 100 mM Tris pH 7.5, 100 mM KCl, and 1 mM CaCl₂. After 20 h, the reaction was loaded onto a Ni²⁺-NTA agarose column (2 mL) equilibrated in Buffer G. The cleaved wild-type protein was eluted with 5 column volumes of Buffer G. The eluant was collected and analyzed as described above, and fractions containing wild-type YqcD were pooled and concentrated to ~1 mL using Amicon Ultra YM 10,000. An equal volume of 50 % glycerol was added, and after determination of the resulting protein concentration, the wild-type protein in 25 % glycerol was stored at -80°C.

Determination of the Kinetic Parameters K_m and k_{cat} .

NADPH and NADP^+ concentrations were determined at pH 7 using $\epsilon_{340} = 6,220 \text{ M}^{-1}$ and $\epsilon_{260} = 18,000 \text{ M}^{-1}$, respectively. For the determination of the NADPH kinetic parameters, the assay contained 100 mM Tris (pH 7.5), 100 mM KCl, 1 mM DTT, 20 μM preQ₀ and NADPH was varied between 5-140 μM . The reaction was monitored by following the oxidation of NADPH at 340 nm for 120 sec at 30°C. The reported data are the means of three replicate determinations. For the determination of the preQ₀ kinetic parameters, the progress of the reaction was monitored by fluorescence detection of the alkaline degradation product of NADP^+ as described (109-111). The reaction mixture contained 100 mM phosphate (pH 7.5), 100 mM KCl, 1 mM DTT, 400 μM NADPH, and variable preQ₀, 0.066-2 μM , at 30°C. At the time specified, aliquots of 50 μL were transferred to an equivalent volume of 0.3 M HCl and incubated for 10 min at room temperature. Fifty microliters of the HCl-treated sample was then removed and added to 200 μL of 9 M NaOH, mixed thoroughly, and placed in the dark. The product was left to develop in the dark for 2.5 h before analysis. Prior to analysis, 100 μL of the resulting alkaline solution was added to 2.5 mL of water for measurement. Fluorescence was measured with an excitation wavelength of 360 nm and an emission wavelength of 455 nm. The excitation and emission slit widths were set to 10 nm. A control assay was performed in the absence of preQ₀ and product concentrations were determined from a NADP^+ standard curve. The reported data are the means of four replicate determinations and the reactions were initiated by the addition of enzyme unless otherwise noted.

Data Analysis.

The kinetic constants V_{\max} and K_m were obtained after fitting the initial velocity data to the rate equation describing a bi-uni-uni-bi ping-pong ter-ter kinetic mechanism (112) as has been shown for other NAD(P)⁺-dependent four-electron-transfer dehydrogenases. In this analysis, it is assumed preQ₀ is the leading substrate and both equivalents of NADPH exhibit equal binding affinity ($K_{mB} = K_{mC}$).

$$\frac{v}{V_{\max}} = \frac{[A][B][C]}{K_{ia}K_{mb}[C] + K_{mc}[A][B] + K_{mb}[A][C] + K_{ma}[B][C] + [A][B][C]} \quad (1)$$

When two of the substrates are the same (NADPH binds and reacts twice, therefore B=C), the system reduces to the following equations:

For A (preQ₀):

$$\frac{v}{V_{\max}} = \frac{[A]}{K_{mA} \left(1 + \frac{K_{ia}K_{mB}}{K_{mA}[B]} \right) + [A] \left(1 + \frac{2K_{mB}}{[B]} \right)} \quad (2)$$

For B (NADPH):

$$\frac{v}{V_{\max}} = \frac{[B]}{K_{mB} \left(2 + \frac{K_{ia}}{[A]} \right) + [B] \left(1 + \frac{K_{mA}}{[A]} \right)} \quad (3)$$

Plots were constructed using Kaleidagraph software package (Synergy Software, Reading, PA). The data reported are the averaged values of the kinetic parameters obtained from the steady-state kinetic plots plus/minus the standard error.

Substrate Titration Studies.

Titration of YkvM with preQ₀ was monitored in the absence of NADPH. PreQ₀ (1 μ L aliquots from a stock solution of 500 μ M or 3 mM in DMSO) was titrated into a solution of YkvM (20 μ M) or the C55S/C55A mutants (50 μ M) containing 100 mM Tris (pH 7.5), 100 mM KCl, and 1 mM DTT while monitoring the absorbance from 230-450 nm. The addition of substrate was continued until there was no further increase in absorbance or the ratio of substrate to enzyme reached 4. The concentration of DMSO did not exceed 4 % of the total volume.

Extinction Coefficient Determination for the Absorbance Band at 376 nm.

A standard curve was generated by monitoring the absorbance band at 376 nm. Dilutions of a reaction mixture containing 10 mM phosphate (pH 7.5), 10 mM KCl, 1 mM DTT, 100 μ M preQ₀, and 50 μ M YkvM were made with a buffer of 10 mM phosphate (pH 7.5), 10 mM KCl, and 1 mM DTT. A two-fold excess of preQ₀ was used to ensure saturation of the protein active sites. The final protein concentrations were 0, 6.25, 12.5, 25, 37.5, and 50 μ M. The resulting solutions were scanned between 230-450 nm, and the absorbance values at 376 nm were replotted against the YkvM concentrations. Linear regression analysis of the data from triplicate determinations indicate the extinction coefficient of the band at 376 nm is 4353 M⁻¹

Inactivation and Protection Studies of YkvM.

Inactivation of YkvM with iodoacetamide was monitored following the oxidation of NADPH at 340 nm. Inactivation of the enzyme was measured in the absence of dithiothreitol to prevent the reaction of the inhibitor with added thiols. The reaction was carried out as follows; enzyme (to a final concentration of 5 μ M) was added to a solution of 100 mM Tris (pH 7.5), 100 mM KCl, and 50 μ M iodoacetamide. At specific times, aliquots (10 μ L) were removed and diluted into a standard assay solution containing 100 mM Tris (pH 7.5), 100 mM KCl, 100 μ M preQ₀, and 100 μ M NADPH, and the reaction monitored by UV-Vis spectroscopy (6 min) at 30°C. Enzyme protection assays were performed following this method except the inactivation mixture also contained 100 μ M preQ₀.

Preparation of YkvM Mutants.

Mutagenesis was carried out with the QuikChange XL kit (Stratagene). The sequences of the primers used for the construction of the mutant plasmids were as follows: C55A, sense, 5'-CCGGAATTCACATCTTTAGCTCCTAAAACAGGC-3' and antisense, 5'-CTGGCCTGTTTTAGGAGCTAAAGATGTGAATTCCGG-3'; C55S, sense, 5'- CCGGAATTCACATCTTTATCTCCTAAAACAGGC-3' and antisense, 5'-CTGGCCTGTTTTAGGAGATAAAGATGTGAATTCCGG-3'; E97A, sense, 5'-GTGACTTCCACGCGGACTGCATGAATATCATCATGAAC-3' and antisense, 5'-GTTTCATGATGATATTCATGCAGTCCGCGTGGAAGTCAC-3'; E97L,

sense, 5'-GTGACTTCCACCTGGACTGCATGAATATCATCATGAAC-3' and antisense, 5'-GTTTCATGATGATATTCATGCAGTCCAGGTGGAAGTCAC-3'; E97K, sense, 5'-GTGACTTCCACAAGGACTGCATGAATATCATCATGAAC-3' and antisense, 5'-GTTTCATGATGATATTCATGCAGTCCTTGTGGAAGTCAC-3'; E97Q, sense, 5'-GGTGACTTCCACCAGGACTGCATGAATATCATCATGAACG-3' and antisense, 5'-CGTTCATGATGATATTCATGCAGTCCTGGTGGGAAGTCACC-3'; E97D, sense, 5'-GGTGACTTCCACGACGACTGCATGAATATCATCATGAACG-3' and antisense, 5'-CGTTCATGATGATATTCATGCAGTCGTCGTGGGAAGTCACC-3'. The *ykvM* gene in the pET-30Xa vector was used as template to generate the single mutants. The PCR protocol consisted of an initial hold at 94°C for 45 sec, followed by 18 cycles of 94°C for 45 sec, 55°C for 60 sec, and 68°C for 8 min. After 18 cycles, the reaction mixtures were kept at 4°C. *DpnI* (1 µL, 10U/µL, Fermentas) was added and the reaction mixture was incubated at 37°C for 1 h before the plasmid was transformed into ultracompetent *E. coli* (DH5α) cells. Single colonies grown overnight on kanamycin containing (30 µg mL⁻¹) agar plates were selected and cultured in 3 mL LB media containing 30 µg mL⁻¹ for 7 h. The plasmid DNA was purified using the Qiagen miniprep kit, and the mutated genes sequenced to verify the mutation and the otherwise unaltered DNA sequence. For protein expression, the mutant plasmids were transformed into the *E. coli* BL21(DE3) cell line. The

expression and purification of the YkvM mutant proteins were carried out as described for the wild-type protein.

Mass Spectrometry Analysis of C55S and C55A.

The concentrated sample (typically 50 μM of protein) was dialyzed into 5 mM phosphate buffer (pH 7.5), 5 mM KCl, and 1 mM DTT, then diluted to approximately 1 pmol μL^{-1} with 50% methanol/0.1% formic acid and analyzed by a quadrupole time-of-flight mass spectrometer (QSTAR XL, Applied Biosystems/MDS Sciex, Foster City, CA) equipped with a standard ion source (MDS Sciex, Concord, Canada). The instrument was externally calibrated in the positive ion mode using two fragment ion peaks (m/z 175.1190 and m/z 1285.5444) from the tandem mass spectrum of Glu-fibrinopeptide (Sigma). The samples were directly infused into the ion source using a 500 μL syringe at a flow rate of 5 μL min^{-1} . The following parameter settings were used to acquire mass spectra from m/z 900-1600 in the positive ion TOF/MS mode: spray voltage, 5500V; curtain gas, 20; GS1 gas, 15; declustering potential (DP), 85 V; declustering potential 2 (DP2), 15 V; focusing potential (FP), 265 V; accumulation time, 1 s. Spectra were summed over a minimum of 120 scans, and the series of multiply charged ion peaks were deconvoluted by the Bayesian protein reconstruct tool (Bioanalyst QS 1.1 software package) to determine the zero charge masses of the intact proteins.

Detection of a Covalent Enzyme-Substrate Complex.

Native YkvM purified as described above was dialyzed into 5 mM phosphate buffer (pH 7.5), 5 mM KCl and 1 mM DTT. Following concentration of the protein to 2 mg mL⁻¹, the enzyme was portioned into 50 μ L aliquots, flash frozen in liquid nitrogen and stored at -80°C. PreQ₀ was prepared in water, and concentrated ammonium hydroxide was then added in small amounts (25 μ L at a time) until the solid was dissolved. The concentration of preQ₀ in the resultant solution was determined at pH 7 in 100 mM Tris buffer (pH 7.0). For experiments with preQ₀, samples of thawed protein and variable amounts of substrate (0 – 10 equivalents) were mixed and incubated at room temperature for 5 min before acidification with an equal volume of 50% methanol/0.1% formic acid and injection onto the mass spectrometer. The conditions for MS analysis were identical to those described above.

Activity Assays of C55S and C55A.

Activity of C55S and C55A were determined by measuring both the oxidation of NADPH at 340 nm and the formation of the fluorescent alkaline degradation product of NADP⁺. For the UV-vis spectroscopic method, the assay solution contained 10 mM Tris (pH 7.5), 10 mM KCl, 1 mM DTT, 35 μ M preQ₀, 100 μ M NADPH and protein (270 μ M C55S or 650 μ M C55A) at 30 °C. For the fluorescence method, the assay solution contained 10 mM phosphate (pH 7.5), 10 mM KCl, 1 mM DTT, 60 μ M preQ₀, 400 μ M NADPH and protein (250 μ M C55S or 300 μ M C55A) at 30°C. The workup and analysis of the alkaline NADP⁺

product was performed as described above. The data presented are the means of two replicate determinations.

Circular Dichroism (CD) Spectroscopy.

Prior to analysis, YkvM, C55S, and C55A were dialyzed into 20 mM phosphate buffer (pH 7.5) and 20 mM NaF. The CD spectra were obtained at a protein concentration of 2 mg mL⁻¹ in the far-UV region (180-260 nm, wavelength step, 0.10 nm, averaging time, 5.0 s) under a nitrogen atmosphere at 25°C. Two scans were completed consecutively and the signal was averaged. Following completion of the scans, the sample was removed from the cell and subjected to amino acid analysis (Dr. H. P. Bächinger Lab, Shriner's Hospital, OHSU) before calculation of delta epsilon values. The equation used was as follows:

$$\Delta\varepsilon = \frac{\theta}{c \times l \times 3,298} \quad (4)$$

where: $\Delta\varepsilon$ is the molar circular dichroism in M⁻¹ cm⁻¹, θ is the measured circular dichroism, c is the concentration of the protein and l is the cell path length (0.1 cm).

Molecular Weight Determination of YkvM Mutants.

Size exclusion chromatography was performed on a BioSep-SEC-S4000 column (Phenomenex). The mobile phase was 50 mM phosphate (pH 7.2) at a flow rate of 1 mL min⁻¹. The void volume (V_0) and the total bead volume (V_T) were measured with blue dextran (2,000 kDa) and DNP-aspartate (300 Da),

respectively. Calibration of the column was conducted with the following protein standards: thyroglobulin (670 kDa), apo-ferritin (443 kDa), pyruvate kinase (237 kDa), alcohol dehydrogenase (150 kDa), bovine serum albumin (66 kDa), and ovalbumin (44 kDa). K_D values were calculated according to the equation $(V_e - V_0)/(V_T - V_0)$, where V_e is the elution volume of the protein of interest, and then plotted versus log MW to generate the standard curve.

Enzymatic Synthesis of (4R)-[4-²H]NADPH and (4S)-[4-²H]NADPH.

(4R)-[4-²H]NADPH was synthesized following the method of Jeong (113) with some modifications (Scheme 6). A total of 8 mg of NADP⁺ (8.7 mM final concentration), 0.1 mL of *d*₈-isopropanol (99+% %, Aldrich, 0.131 M final concentration), and 100 units of alcohol dehydrogenase (*Thermoanaerobium brockii*) were dissolved in 1 mL of 100 mM phosphate pH 8.0, 100 mM KCl, and 100 mM EDTA. The reaction was allowed to proceed at 37°C, and the formation of (4R)-[4-²H]NADPH was monitored by following the increase in absorbance at 340 nm. When no further increase in the OD₃₄₀ was observed, the enzyme was separated from the reaction mixture using a 10 kDa molecular weight cutoff filter (Centriprep YM10, Amicon Bioseparations, Bedford, MA). (4R)-[4-²H]NADPH was purified on a semipreparative Luna C18 column (250 × 10 mm, 5 μm) from Phenomenex. The products were separated during a 20-min run of isocratic 75 mM NaCl buffered with MTEN (5 mM 4-morpholineethanesulfonic acid, 2.5 mM Tris base, 2.5 mM ethanolamine, and an additional 10 mM NaCl) adjusted to pH 8.2

(114). The flow rate was 3 mL min⁻¹. The NADPH was collected into a tube containing 200 µL of 200 mM Tris pH 9.5 so that the final pH of the eluted NADPH was 9.0-9.3 before lyophilization. The product was freeze-dried three times from deuterium oxide and dissolved in deuterium oxide for ¹H-NMR analysis (115).

(4S)-[4-²H]NADPH was synthesized following the method of Pollack (116) (Scheme 7). The reaction contained 10 mg NADP⁺ (9.8 mM final concentration), 4 mg [1-²H]-glucose (97%, Aldrich, 18.2 mM final concentration), 0.73 mL of 83 mM phosphate pH 8.0, 0.486 mL DMSO (40 % final concentration), and 30 units of glucose-6-phosphate dehydrogenase. The reaction was allowed to proceed at 37°C until a maximum absorbance at 340 nm was achieved (1 h). The protein was removed by filter concentration and (4S)-[4-²H]NADPH was purified and analyzed for the correct stereoisotopic label as described above.

Determination of the Primary and Alpha Secondary Kinetic Isotope Effects.

YkvM assays were performed in 10 mM Tris (pH 7.5), 10 mM KCl, 1 mM DTT, 20 µM preQ₀, 1 µM YkvM and variable (10-120 µM) (4S)-[4-²H]NADPH, (4R)-[4-²H]NADPH, or unlabelled NADPH. The reaction was monitored by following the oxidation of NADPH at 340 nm at 30°C. Assays were performed in triplicate. The data was fitted to the rate equation describing NADPH (equation 3) using Kaleidagraph to extract the kinetic parameters.

Cofactor Stereospecificity Determination.

A reaction mixture containing 4 mM (4S)-[4-²H]NADPH, (4R)-[4-²H]NADPH or unlabeled NADPH and 2 mM preQ₀ in 10 mM phosphate (pH 7.5), 10 mM KCl, and 1 mM DTT was incubated with 50 μM YkvM or YqcD at 30°C. To allow for the complete consumption of NADPH and maximum formation of preQ₁, the reaction was allowed to proceed for 3 h before removal of the protein by filtration. The reaction products were loaded onto a semi-preparative HPLC column (Luna C18, 250 x 10 mm, 5 μm from Phenomenex) equilibrated in 20 mM ammonium acetate (pH 6.0) and the column was developed with an isocratic run of 20 mM ammonium acetate (pH 6.0) at a flow rate of 5 mL min⁻¹ to elute preQ₁ at 18 min. Fractions containing the product were pooled, frozen, and lyophilized to dryness. The precipitated residue was dissolved in 0.6 mL of deuterium oxide and a ¹H-NMR spectrum was acquired.

Another sample of preQ₁ was dissolved in 20 mM ammonium acetate (pH 9.0) and 50% methanol and infused directly into an LCQ Advantage ion-trap mass spectrometer (Thermo Electron, San Jose, CA) equipped with an electrospray ionization (ESI) source. The ion interface was operated in the negative mode using the following settings: needle voltage 4.5 kV, sheath and auxiliary gas flow rates of 25 and 3.0 psi, respectively, tube lens voltage 50 V, capillary voltage 3.0 V, and capillary temperature 275 °C. The mass range between *m/z* 50-1100 was scanned.

Activity Assays of YkvM-Glu⁹⁷ Mutants.

Measurements of the specific activities of the YkvM-Glu⁹⁷ mutants (Glu97Ala, Glu97Gln, Glu97Leu, Glu97Lys, and Glu97Asp) were conducted following the oxidation of NADPH to NADP⁺ at 340 nm. The reactions were performed under V_{\max} conditions for wild-type YkvM (100 μ M preQ₀, 100 μ M NADPH) in 10 mM phosphate buffer (pH 7.5), 10 mM KCl, and 1 mM DTT at 30°C. A solution of protein prepared as described above was added to initiate the reaction, and the reaction was monitored for 10 min. The reported specific activities are the mean of three trials.

Steady-kinetic analysis of the Glu97Ala, Glu97Gln, and Glu97Asp mutants was performed by following the formation of the fluorescence NADP⁺ alkaline degradation product. The assay solution contained 10 mM phosphate buffer (pH 7.5), 10 mM KCl, 1 mM DTT, 200 μ M NADPH, and variable preQ₀ (20-600 μ M) at 30°C. The reactions were initiated with enzyme (8.9 μ M of Glu97Ala, 13 μ M of Glu97Gln, 2 μ M of Glu97Asp). At the specified times up to 2 h, aliquots were removed and subjected to the 0.3 M HCl and 9 M NaOH workup steps as described previously. The data was fitted to equation (2) to obtain the kinetic parameters for preQ₀.

PreQ₀ Binding and Formation of the Putative Covalent Adduct.

The kinetics for the formation of the thioimide covalent adduct was measured by stopped-flow spectrophotometry. Equal volumes of enzyme solution (to a final concentration of 20 μ M) and substrate solution containing variable

concentrations of preQ₀ (to a final concentration of 0-200 μM) were mixed and monitored at 376 nm for 20 s. For each substrate concentration, the data from at least five replicates were averaged and fit to either single-exponential or double-exponential equations.

$$y = A \exp(-k_{obs}t) + a \quad (5)$$

$$y = A_1 \exp(-k_{obs1}t) + A_2 \exp(-k_{obs2}t) + a \quad (6)$$

Where y is the absorbance signal, A , A_1 , and A_2 are the amplitudes, a is the intercept, and k_{obs} , k_{obs1} , and k_{obs2} are the apparent rate constants.

Transient Kinetics of Substrate Turnover

For stopped-flow turnover experiments, the change in the absorbance signal of NADPH at 340 nm was monitored upon rapid mixing of equal volumes of premixed enzyme-preQ₀ solution from one syringe and NADPH from a second syringe.

For single turnover experiments, the enzyme-preQ₀ solution contained a fixed concentration of YkvM (50 μM) and a substoichiometric concentration of preQ₀ (45 μM), and the cofactor solution contained NADPH at varying concentrations (0-50 μM). For each concentration of the cofactor that was used, the averaged reaction traces from at least three replicates were fit to either single-exponential or double-exponential functions. Similarly, single-turnover experiments were carried out by substituting *pro-R* deuterium labeled NADPD for NADPH.

For stopped-flow multiple-turnover experiments, the enzyme solution contained a fixed concentration of YkvM (2 μM) and excess preQ₀ (20 μM), and the cofactor solution contained NADPH at concentrations in the range of 0-160 μM . For each concentration of the cofactor that was used, the averaged reaction traces from at least three replicates were fit to either the linear (7) or “burst” (8) equation.

$$y = k_{obs}t + a \quad (7)$$

$$y = A \exp(-k_{obs1}t) + k_{obs2}t + a \quad (8)$$

Where k_{obs} and k_{obs2} are the second-order rate constants of the linear steady-state phase and k_{obs1} is the pseudo-first-order rate constant of the exponential phase.

Substrate Analogs

The ability of YkvM to bind to and turn-over alternate substrates was examined with a series of aromatic nitrile compounds. To assay this activity, the fluorescence method for the detection of the alkaline degradation product of NADP⁺ was utilized. Screens for activity with the substrate analogs were conducted with wild-type YkvM and selected Glu⁹⁷ mutants described above. The reactions contained 10 mM phosphate buffer (pH 7.5), 10 mM KCl, 1 mM DTT, 100 μM NADPH, 50 μM enzyme, and nitrile (100 μM). A control reaction containing no substrate was carried out throughout the workup steps, and the rate of NADP⁺ formation was calculated from a NADP⁺ standard curve.

Cloning of E. coli ygcM.

The *E. coli* gene *ygcM* was amplified from genomic DNA by PCR and inserted into the pET30Xa vector using ligation-independent cloning as described by Novagen. PCR amplification was performed using PfuUltra™ DNA polymerase (1 μ L of 50 U μ L⁻¹), the supplied buffer, 200 μ M dNTPs, 20 ng *E. coli* genomic DNA, and 250 ng of each primer. The sense and antisense primer were 5'-GGTATTGAGGGTCGCATGATGTCCACCACG-3' and 5'-AGAGGAGAGTTAGAGCCTCATTCGCC-3', respectively. The PCR program included an initial hold for 45 sec at 94°C, followed by 35 cycles of 95°C for 45 sec, 60°C for 45 sec, and 72°C for 2 min. The amplified PCR product was purified from a 1% agarose gel before annealing into the pET30Xa expression vector (according to manufacturer's instructions) and transformation into the *E. coli* DH5 α cell line. A single colony was used to inoculate 3 mL of LB medium supplemented with 30 μ g mL⁻¹ kanamycin. After 12 h of incubation at 37°C and shaking, the cultures were pelleted by centrifugation at 3,000 x g for 15 min. The plasmid pET30-*ygcM* was isolated and analyzed by restriction digests. The reaction mixture contained 80 ng pET30-*ygcM* plasmid, 1 U *Xba*I, 1 U *Hind*III, bovine serum albumin (BSA), and the recommended buffer. The reaction was incubated for 1 h for 37°C and analyzed by 1% agarose gel electrophoresis to confirm the insertion of the *ygcM* gene. The integrity of *ygcM* gene in the pET30Xa plasmid was confirmed Big Dye terminator sequencing (PSU-Keck Genomics Facility).

Expression and Purification of His₆-YgcM

E. coli BL21(DE3) was transformed with 50 ng of pET30-*ygcM* plasmid and plated on LB medium plates containing 30 $\mu\text{g mL}^{-1}$ kanamycin. Single colonies were used to inoculate 3 mL of LB medium containing 30 $\mu\text{g mL}^{-1}$ kanamycin. After 12 h of incubation at 37°C with shaking, a 1 mL aliquot was removed and used to inoculate 100 mL of LB medium containing 30 $\mu\text{g mL}^{-1}$ kanamycin. The cultures were incubated at 37°C with shaking for 12 h, at which time 5 mL of the culture was added to 3 L Erlenmeyer flasks containing 500 mL LB medium with 30 $\mu\text{g mL}^{-1}$ kanamycin. When the OD₆₀₀ reached 0.8, the cell cultures were induced with 0.5 mM IPTG. The cultures were allowed to grow for an additional 4 h at which time the cells were harvested by centrifugation (6,000 g, 10 min at 4°C) and flash frozen in liquid nitrogen. Typically, 30 g of cells were obtained from 3 L of medium.

The following steps were performed at 4°C unless otherwise noted. Cells were suspended at 250 mg mL⁻¹ in 100 mM Tris/HCl, (pH 8.0), 100 mM KCl, 2 mM 2-mercaptoethanol, and 1 mM PMSF. The cells were lysed by two passes through a French Press at 20,000 psi. After removal of cell debris by centrifugation (15,000 g, 20 min), streptomycin sulfate was added to a final concentration of 3%. The mixture was chilled on ice for 1 h before the nucleic acids were pelleted by centrifugation (20,000 g, 20 min). The supernatant was filtered through a 0.45 μm MCE syringe filter and loaded onto a column containing 10 mL of Ni²⁺-NTA agarose equilibrated in Buffer A. The column was washed consecutively in the

following manner: 5 column volumes of Buffer A, 5 column volumes of Buffer B, 5 column volumes of Buffer C, 5 column volumes of buffer D, and then 5 column volumes of Buffer E. The fusion protein was eluted with 5 column volumes of Buffer F. The eluant was collected in 10 mL fractions and analyzed by SDS-PAGE, and fractions containing his₆-YgcM were pooled, concentrated to ~ 1 mL using Amicon Ultra YM 10,000 and dialyzed overnight against 4 L of 100 mM Tris (pH 8.0), 100 mM KCl, and 1 mM DTT. An equal volume of 50 % glycerol was added, and after determination of the resulting protein concentration, the wild-type protein in 25 % glycerol was stored at -80°C.

Activity Assays of YgcM

The YgcM activity to produce 6-pyruvoyltetrahydropterin (PPH4) from dihydroneopterin triphosphate (H₂-NTP) was measured in coupled assays with FolE, a Type I cyclohydrolase. The reaction mixture was as follows: 100 mM Tris/HCl (pH 7.5), 10 mM MgCl₂, 3 mM GTP, and aliquots of enzymes (FolE, to a final concentration of 20 μM, and YgcM, to a final concentration of 50 μM) in a total volume of 50 μL. The mixture was incubated at 37°C for 1 h and treated with 50 mM EDTA and 1.4 U of alkaline phosphatase. After a further incubation for 1 h at 37°C, an equal volume of an acidic iodine solution (2% KI and 1% I₂ in 1 M HCl) was added and the resulting mixture was stored for 1 h in the dark. After centrifugation to remove the precipitated protein, the supernatant was reduced with ascorbic acid and analyzed by HPLC with a Bondclone 10 C18 column

(Phenomenex, 300 x 3.9 mm) equilibrated in 25 mM ammonium acetate (pH 6.0) at a flow rate of 1 mL min⁻¹ using the following gradient (time, % acetonitrile): 0 min, 0%; 10 min, 0%; 30 min, 4%; 35 min, 50%; and 40 min, 0%.

Cloning of E. coli YbaX.

The gene *ybaX* was amplified from *E. coli* genomic DNA by PCR and inserted into the pET30Xa vector using ligation-independent cloning as described by Novagen. PCR amplification was performed using PfuUltraTM DNA polymerase (1 μL of 50 U μL⁻¹), the supplied buffer, 200 μM dNTPs, 20 ng *E. coli* genomic DNA, and 250 ng of each primer. The sense and antisense primer were 5'- GGTATTGAGGGTCGCATGAAACGTGC-3' and 5'- AGAGGAGAGTTAGAGCCTTACTTCAACCC -3', respectively. The PCR program included an initial hold for 45 sec at 94°C, followed by 35 cycles of 95°C for 45 sec, 60°C for 45 sec, and 72°C for 2 min. The amplified PCR product was purified from a 1% agarose gel before annealing into the pET30Xa expression vector (according to manufacturer's instructions) and transformation into the DH5α cell line. Transformants were selected from kanamycin (30 μg mL⁻¹) supplemented agar plates and a single colony was used to inoculate 3 mL of LB medium supplemented with 30 μg mL⁻¹ kanamycin. After 12 h of incubation at 37°C with shaking, the cultures were pelleted by centrifugation at 3,000 g for 15 min. The plasmid pET30-*ybaX* was isolated and analyzed by restriction digests. The reaction mixture contained 80 ng pET30-*ybaX* plasmid, 1 U *Xba*I, 1 U *Hind*III, bovine

serum albumin, and the recommended buffer. The reaction was incubated for 1 h for 37°C. *Bss*III (1 U) was then added and the mixture was incubated for 1 h at 50°C. The restriction digest products were analyzed by 1% agarose gel electrophoresis to confirm the insertion of the *ybaX* gene. The integrity of *ybaX* gene in the pET30 plasmid was confirmed Big Dye terminator sequencing (PSU-Keck Genomics Facility).

Expression and Purification of His₆-YbaX

E. coli BL21(DE3) was transformed with 50 ng of pET30-*ybaX* and plated on LB medium plates containing 30 µg mL⁻¹ kanamycin. Single colonies were used to inoculate 3 mL of LB medium containing 30 µg mL⁻¹ kanamycin. After 12 h of incubation at 37°C with shaking, a 1 mL aliquot was removed and used to inoculate 100 mL of LB medium containing 30 µg mL⁻¹ kanamycin. The cultures were incubated at 37°C with shaking for 12 h, at which time 5 mL of the culture was added to 3 L Erlenmeyer flasks containing 500 mL LB medium with 30 µg mL⁻¹ kanamycin. When the OD₆₀₀ reached 0.8, protein production was induced with 0.5 mM IPTG. The cultures were allowed to grow for an additional 4 h at which time the cells were harvested by centrifugation (6,000 x g, 10 min at 4°C) and flash frozen in liquid nitrogen. Typically, 25 g of cells were obtained from 3 L of medium.

Cells were suspended to a density of 250 mg mL⁻¹ of 100 mM Tris/HCl, (pH 8.0), 100 mM KCl, 2 mM 2-mercaptoethanol, and 1 mM PMSF. Lysozyme

and DNase I were added to a final concentration of $250 \mu\text{g mL}^{-1}$ and $10 \mu\text{g mL}^{-1}$ of cell suspension, respectively, and the solution was gently rotated at 37°C for 1 h. After the removal of cell debris by centrifugation ($15,000 \text{ g}$, 20 min), the mixture was chilled on ice for 10 min before the CFE was filtered through a $0.45 \mu\text{m}$ MCE syringe filter and loaded onto a column containing 10 mL of Ni^{2+} -NTA agarose equilibrated with Buffer A. The column was washed consecutively in the following manner: 5 column volumes of Buffer A, 5 column volumes of Buffer B, and then 5 column volumes of Buffer C. The fusion protein was eluted with 5 column volumes of Buffer F. The purified protein was concentrated to $\sim 1 \text{ mL}$ using Amicon Ultra YM 10,000 and dialyzed overnight against 4 L of 100 mM Tris/HCl (pH 8.0), 100 mM KCl, and 1 mM DTT. An equal volume of 50 % glycerol was added, and after determination of the resulting protein concentration, the wild-type protein in 25 % glycerol was stored at -80°C .

Chemical Synthesis

General.

Chemicals of the highest grade available were purchased from Acros Organics (Fisher). Deuterated solvents were from Cambridge Isotopes, Inc., and NMR tubes were from Wilmad Glass. ¹H-NMR was performed with a Tecmag-Libra modified NM-500 MHz NMR spectrometer or with a Bruker AMX-400 MHz NMR spectrometer. NMR data analysis was performed with the SwanNMR software package (117). Chemical shifts are reported in ppm from the internal standard tetramethylsilane (TMS, δ 0.00) and the following abbreviations are used to report the spectral data: s, singlet, d, doublet, t, triplet, q, quartet, dd, doublet of doublets, m, multiplet, br, broad, J, coupling constant, and Hz, hertz. Silica gel flash column chromatography was performed on silica gel 60 (230-400 mesh) from Acros. Thin layer chromatography (TLC) was performed on Whatman Al-Si G/UV F₂₅₄ plates. Compounds on developed TLC plates were detected with a UVP Model UVGL-58 ultraviolet lamp (254 nm) from Upland (CA). Tetrahydrofuran was distilled from sodium benzophenone ketyl immediately prior to use. Benzene and pyridine were distilled from calcium hydride and stored over activated molecular sieves (3 Å). Methanol was distilled from magnesium and iodine and stored over activated molecular sieves (3 Å). Dimethyl formamide was distilled from calcium oxide under reduced pressure. Removal of solvent *in vacuo* was performed on a rotary evaporator at 30°C and 20 mm Hg (aspirator) or 1 mm Hg (vacuum pump) unless otherwise specified. Drying of solids was performed at

50°C under reduced pressure (1 mm Hg) to a constant mass. Reactions performed under a dry atmosphere were conducted in flasks equipped with a drying tube filled with Drierite™. All anhydrous reactions were conducted in oven-dried glassware and under a nitrogen atmosphere. Other solvents and reagents were used as received.

Synthesis of 7-aminomethyl-7-deazaguanine (PreQ₁) (Scheme 2).

Ethyl 2,2-diethoxyethylcyanoacetate (11).

A mixture of bromoacetal (5 g, 25.3 mmol), ethyl cyanoacetate (14 g, 123.8 mmol), anhydrous potassium carbonate (3.5 g, 25.3 mmol), and sodium iodide (0.25 g, 1.7 mmol) was stirred under reflux in an oil-bath at 145-150°C until the vigorous reaction (evolution of carbon dioxide) had subsided, and then for a further 4 h at 140-145°C. After allowing the reaction to cool to room temperature, the mixture was separated between water (30 mL) and ether (30 mL). The ether layer was washed with water, the aqueous portions were again extracted with ether, and the combined ether solutions were dried (MgSO₄). Evaporation of the ether and fractionation of the residue through a 6" copper sponge column under reduced pressure gave the ester (1.84 g, 46%) as a clear liquid. B.p. 111-115°C/2 mm Hg; IR (neat, cm⁻¹): 2980.0, 2251.7, 1748.3, 1445.7, 1373.4, 1262.1, 1128.0, 1062.8 (Appendix D). ¹H-NMR (CDCl₃): 1.22 (6H, m), 1.33 (3H, t), 2.25 (2H, dm), 3.46 (1H, t), 3.52 (2H, m), 3.66 (2H, m), 4.27 (2H, q), 4.7 (1H, t).

2,4-Diamino-5(2,2-diethoxyethyl)-6-hydroxypyrimidine (12).

Sodium ethoxide was first formed *in situ* by the addition of sodium metal (1.2 g, 52.1 mmol) to anhydrous ethanol (15 mL). Guanidine thiocyanate (1.03 g, 8.73 mmol) was added in one portion and the mixture was heated to reflux. The ester **11** (2 g, 8.73 mmol) was then added dropwise and the reaction was further refluxed for 4 h. After cooling, the ethanol was removed by rotary evaporation, the remaining residue was dissolved in a minimal amount of water and washed with ether. The addition of an equivalent of acetic acid to the aqueous solution and rotary evaporation results in the formation of a yellow precipitate which separates either directly or upon evaporation. The resultant precipitate was collected by filtration and converted to its potassium salt with 5 M KOH. Reprecipitation of the salt with concentrated HCl furnished the pyrimidine product as a yellow solid (1.16 g, 55 %). IR (KBr, cm^{-1}): 3464.6, 3374.4, 2977.1, 1637.9, 1594.8, 1563.2, 1422.1, 1373.6. $^1\text{H-NMR}$ (d_6 -DMSO): 1.08 (6H, t), 2.42 (2H, d), 3.59 (4H, m), 4.43 (1H, t), 5.89 (2H, s), 6.00 (2H, s), 9.88 (1H, br s). m.p. 157-158°C (Appendix D).

2-Amino-pyrrolo[2,3-d]pyrimidin-4-one (13).

The pyrimidine **12** (1 g, 4.1 mmol) was stirred in 0.5 M HCl (1.5 equivalents) for 3 h at room temperature. The product was isolated by precipitation with aqueous ammonia to give a white solid that was collected by filtration and dried under vacuum (590 mg, 95 %). IR (KBr, cm^{-1}): 3446.6, 3374.4, 2932.0,

1653.5, 1621.9, 1540.6, 1423.3, 1373.6. ¹H-NMR (*d*₆-DMSO): 6.26, (1H, d), 6.69 (1H, d), 10.79 (1H br s), 11.25 (1H, br s), m.p. > 250°C (Appendix D).

*2-Octanoyl-pyrrolo[2,3-*d*]pyrimidin-4-one (14).*

A vigorously stirred and chilled suspension of 2-aminopyrrolo[2,3-*d*]pyrimidin-4-one **13** (2 g, 0.013 mmol) in dry pyridine (20 mL) was treated with octanoyl chloride (6.34 g, 0.039 mmol) and catalytic dimethylaminopyridine at 85°C for 1 h. After cooling, the mixture was neutralized with 6.5% NH₃ in EtOH (60 mL) in an ice-bath. The resulting solution was filtered to isolate a brown precipitate which was washed successively with EtOH and ether. The crude product was recrystallized from EtOH to give the product as a light brown solid (3.13 g, 85%). IR (KBr, cm⁻¹): 3204.4, 2959.1, 1653.5, 1640.2, 1635.4, 1563.2, 1400.7. ¹H-NMR (*d*₆-DMSO): 0.89 (3H, t), 1.29 (8H, s), 1.75 (2H, m), 2.47 (2H, t), m.p. > 250°C (Appendix D).

*2-Octanoyl-5-(*N,N*-dibenzylaminomethyl)pyrrolo[2,3-*d*]pyrimidin-4-one (15).*

A solution of 2-octanoyl-pyrrolo[2,3-*d*]pyrimidin-4-one **14** (1 g, 3.6 mmol), 37% formalin solution (7.2 mmol) and dibenzylamine (7.2 mmol) in 80% aqueous acetic acid (25 mL) was warmed at 60°C for 20 h inside a pressure vessel. The reaction mixture was cooled, carefully opened, diluted with 0.5 M HCl (25 mL), and left at room temperature for 2 h. After neutralization with aqueous ammonia, the mixture was thoroughly extracted with CH₂Cl₂ and the combined extracts were

evaporated to dryness. The residue was chromatographed on a silica gel column using 5-20% MeOH/ CH₂Cl₂ as eluent. The desired fractions were combined and concentrated under reduced pressure. The resulting brown solid was recrystallized from EtOH to afford **15** as a white solid (1.37 g, 78%). IR (KBr, cm⁻¹): 3238.0, 2932.0, 1653.5, 1621.9, 1576.7, 1563.2, 1527.1, 1436.8, 1251.7, 741.7, 698.5. ¹H-NMR (*d*₆-DMSO): 0.85 (3H, t), 1.26 (8H, br s), 1.57 (2H, m), 2.44 (2H, m), 3.56 (4H, s), 3.76 (2H, s), 6.88 (1H, d), 7.21-7.42 (10H, m) (Appendix D).

2-amino-5-(N,N-dimethylaminomethyl)pyrrolo[2,3-d]pyrimidin-4-one (8).

The protected preQ₁ compound, 2-octanoyl-5-(N,N-dibenzylaminomethyl)pyrrolo[2,3-*d*]pyrimidin-4-one (1 g, 2.06 mmol) was added to a solution of dimethylamine (1.5 mL, 22.6 mmol) and MeOH-THF (1:1, 10 mL). The resulting mixture was allowed to react in a sealed tube at 75°C for 24 h. The reaction was cooled to room temperature, the vessel was carefully opened, and 5 M KOH (0.1 mL) was added. The mixture was allowed to further react for 60 h at room temperature with stirring. Diethyl ether (20 mL) was added and the resulting product mixture was incubated for 12 h at -20°C to deposit a precipitate. The product was collected by filtration and dried *in vacuo* at room temperature in a dessicator to afford 175 mg (41%) of **8**. ¹H-NMR (*d*₆-DMSO): 2.1 (6H, s), 3.5 (2H, s), 5.9 (2H, s), 6.4 (1H, s), 10.2 (1H, s), 10.8 (1H, s).

2-amino-5-(aminomethyl)pyrrolo[2,3-d]pyrimidin-4-one (PreQ₁) (6).

2-octanoyl-5-(dibenzylaminomethyl)pyrrolo[2,3-*d*]pyrimidin-4-one (200 mg, 0.412 mmol) was added to a solution of ammonia saturated methanol-THF (1:1, 2 mL), and the resulting mixture was allowed to react in a sealed tube at 75°C for 24 h. The reaction mixture was cooled to room temperature and 5 M KOH (50 μ L) was added. It was then stirred at 60 h at room temperature and evaporated to dryness. The residue was purified by chromatography on a silica gel column using 5-20% MeOH/ CH₂Cl₂. The desired fractions were combined and concentrated under reduced pressure. The resulting red solid was recrystallized from EtOH to give preQ₁. For enzymological work, preQ₁ was further purified by reverse-phase HPLC, Luna C18, 250 \times 10 mm, 5 μ m, (Phenomenex). PreQ₁ eluted at 17 min during an isocratic run of 20 mM ammonium acetate (pH 6.0). Fractions containing the desired compound were collected, frozen and lyophilized to dryness to afford the product as a white powder. ¹H-NMR (*d*₄-MeOH): 4.13 (2H, s), 6.81 (1H, s) (Figure 37).

Synthesis of 7-cyano-7-deazaguanine (preQ₀). (Scheme 5)

Chloro(formyl)acetonitrile.

While maintaining a temperature of 0°C, methyl formate (4.38 g, 77 mmol) was added to a stirred mixture of sodium methoxide (3.57 g, 66 mmol) in 60 mL of THF. This was followed by the dropwise addition of chloroacetonitrile (5 g, 66 mmol) over a 1 h period. The mixture was allowed to stir for an additional 3 h, and

then 100 mL of 12 M HCl was added dropwise, while maintaining the temperature below 10°C. This resultant solution was reduced *in vacuo* at 40°C to 15 mL and then placed in an addition funnel to be used in the synthesis of PreQ₀.

2-amino-5-cyanopyrrolo[2,3-d]pyrimidin-4-one (PreQ₀) (5).

NaOAc·3H₂O (14 g, 110 mmol) was dissolved in 110 mL of distilled H₂O. 2,6-Diaminopyrimidin-4-one (6.66 g, 53 mmol) was added and the mixture was heated to 50°C, at which time chloro(formyl)acetonitrile (prepared as described above) was added over a 1 h period. The solution was allowed to stir for 12 h and then heated to first remove the THF, and then heated at reflux for 1 h. The mixture was allowed to cool to room temperature and then filtered. The solid was washed with copious amounts of water and acetone. Crude preQ₀ was purified by conversion to the potassium salt with 50 mL of 5 M KOH, treatment of the resultant solution with charcoal, filtering, and then bringing the pH to 6 with 30% HCl. The resultant solid was collected by filtration and dried under vacuum for 24 h to yield 6.47 g (70%) of product. PreQ₀ was further purified by recrystallization from methanol followed by treatment with charcoal; subsequent removal of the charcoal by filtration, evaporation of the solvent, and drying as before yielded a pure white solid. Prior to enzymological work, preQ₀ was subjected to C18 reverse-phase HPLC with a semipreparative Luna C18 column (250 x 10 mm, 5 μm, Phenomenex). A series of linear gradients was developed from 4% acetonitrile in 20 mM ammonium acetate (pH 6.0) to 50% acetonitrile in 20 mM ammonium

acetate (pH 6.0) (time, % acetonitrile): 0-10.0 min, 4%; 10.0-20.0 min 5%; 20.0-22.0, 50%; 22.0-30.0 min, 100%; and 30.0-31.0 min, 4%. The flow rate was kept constant at 6 mL min⁻¹ and the elution was monitored at A₂₆₀. Samples containing preQ₀ (14-16 min) were pooled and lyophilized to dryness. UV-Vis spectroscopy and proton NMR were performed to confirm the structure of preQ₀. ¹H-NMR (d₆-DMSO): 6.38 (2H, s), 7.61 (1H, s), 10.70 (1H, s), 11.97 (1H, s) (Appendix D).

Synthesis of the oQ Ribosyl Moiety (Scheme 3)

Methyl 2,3-O-Isopropylidene-D-ribofuranoside (16).

A mixture of dry D-ribose (1 g, 6.7 mmol) and 2,2-dimethoxypropane (2 mL) in acetone (8 mL) was cooled in an ice bath and perchloric acid (0.4 mL of 70%) was slowly added. The ice bath was then removed and the contents stirred at room temperature for 2 h followed by addition of methanol (1.4 mL) and the reaction was further stirred for 2 h. The mixture was again cooled down in an ice bath and neutralized with cold sodium carbonate (0.32 g in 1 mL H₂O). The precipitate was removed by filtration and the filtrate was concentrated. The concentrated residue was dissolved in ether (20 mL) and washed with brine and water. The aqueous portion was extracted with ether (2 x 15 mL) and the combined ether fractions were dried (Na₂SO₄). The evaporation of solvent yielded a yellow residue which was purified by flash column chromatography (hexanes/ether 5:1) to afford protected ribose (1.25 g, 92%) as an oil. IR (neat, cm⁻¹

¹): 3446.3 (OH), 2938.1, 1373.7, 1273.0, 1211.6, 1093.3, 1045.1. ¹H-NMR (CDCl₃): 1.32 (3H, s, CCH₃), 1.48 (3H, s, CCH₃), 3.2 (1H, s, OH), 3.44 (3H, s, OCH₃), 3.67 (2H, d, J=3.7 Hz, H-5), 4.41 (1H, t, J=3.7, H-4), 4.71/4.85, (2H, ab pair, J=6.3 Hz, H-2/H-3), 5.00 (1H, s, H-1) (Appendix D).

2,3-O-Isopropylidene-4-methoxy-erythrofuranoside (17).

To a stirred solution of protected sugar (5 g, 24.5 mmol) in benzene (250 mL) in a round bottomed flask fitted with a Dean-Stark apparatus and a condenser was added vacuum dried pyridinium chlorochromate (21 g, 97.4 mmol). The mixture was refluxed overnight on a heating mantle. The benzene contents were decanted and the residue was washed three times with ether. The combined fractions were passed through a pad of Celite, and then through a short column of silica gel to give crude lactone which was crystallized from hexane-ether to furnish pure lactone **17** (2.4 g, 52%) as fine white crystals. IR (KBr, cm⁻¹): 2999.6, 1784.8, 1459.4, 1385.1, 1283.3, 1215.6, 1188.6, 1125.4, 1075.7, 1044.1 980.9, 935.8, 863.5. ¹H-NMR (CDCl₃): 1.38 (3H, s, CH₃), 1.46 (3H, s, CH₃), 3.53 (3H, s, OCH₃), 4.55 (1H, d, J=5.37 Hz, H-3), 4.80 (1H, d, J=5.37 Hz, H-2), 5.34 (1H, s, H-1) (Appendix D).

2,3-O-Isopropylidene-4-cyclopentenone (10).

A round bottom flask fitted with a septum was charged with dimethyl methylphosphonate (0.33 g, 2.66 mmol) in dry THF (20 mL) and cooled to -78°C.

n-butyllithium (1.06 ml, 2.5 M solution, 2.66 mmol) was added dropwise from a syringe to the stirred phosphonate solution (15-20 min) and stirring was continued for 30 min. Lactone **17** (500 mg, 2.66 mmol) was dissolved in THF (2.5 mL) and the mixture was added in one portion. After stirring for an additional 2 h at -78°C , the reaction mixture was allowed to warm to room temperature (45 min). The solution was poured into a mixture of ether (50 mL) and water (10 mL) and the layers were separated quickly. The aqueous layer was extracted with ether (10 mL) and the combined organic phase was washed with brine, dried over Na_2SO_4 and concentrated at room temperature. The residue was purified by flash chromatography with 5:1 hexanes/ether to yield cyclopentenone **10** (296 mg, 80%) as a white powder. $^1\text{H-NMR}$ (CDCl_3): 1.43 (6H, s, $2\times\text{CH}_3$), 4.48 (1H, d, $J=5$ Hz, H-2), 5.29 (1H, dd, $J_1=5\text{Hz}$, $J_2=2$ Hz, H-3), 6.22 (1H, d, $J=6\text{Hz}$, H-5), 7.60 (1H, dd, $J_1=6\text{Hz}$, $J_2=2\text{Hz}$, H-4) (Appendix D).

2,3-O-isopropylidene-4-cyclopenten-1-ol (18).

The cyclopentenone (200 mg, 1.30 mmol) and $\text{CeCl}_3\cdot 7\text{H}_2\text{O}$ (483 mg, 1.30 mmol) were added to 15 mL of MeOH and cooled to 0°C . NaBH_4 (98.3 mg, 2.60 mmol) was added (foamed) and the mixture was allowed to stir for 1 h at 0°C . The pH was then adjusted to ~ 7 with 1 N HCl, 20 mL ether was added, and the organic layer was washed with a small amount of brine. The ether layer was dried over Na_2SO_4 , filtered, and concentrated to a yellow liquid. The liquid was dissolved in a small amount of CH_2Cl_2 and added to the top of a silica gel column (3 g). The

product was eluted with 1:2 ether/hexanes to give 172 mg (85%) of the alcohol **18** as a colourless liquid. ¹H-NMR (CDCl₃): 5.88 (2H, s, H-4 and H-5), 5.01 (1H, d, J=6 Hz, H-1), 4.74 (1H, t, J=6 Hz, H-3), 4.55 (1H, dd, J=6 Hz, H-2), 2.71 (1H, d, J= 6 Hz, OH), 1.43 (3H, s, CH₃), 1.41 (3H, s, CH₃) (Appendix D).

2,3-epoxy-4,5-isopropylidene cyclopentan-1-ol (19).

To an acetonitrile solution (50 mL) of protected cyclopentenol **18** (1.479 g, 9.48 mmol) was added an aqueous Na₂EDTA solution (20 mL), 4 x 10⁻⁴ M). The resulting homogeneous solution was cooled to 0-1°C, followed by the addition of trifluoroacetone (10 mL) *via* a precooled syringe. To this homogenous solution was added in portions a mixture of sodium bicarbonate (6.5 g, 76 mmol) and Oxone (7.5 g, 49 mmol) over a period of 1 h (pH ~ 7). The reaction was complete in 2 h as shown by TLC. The reaction mixture was then poured into water (30 mL), extracted with methylene chloride (4 x 60 mL), and dried over anhydrous sodium sulfate. After removal of the solvent under reduced pressure, the residue was subjected to silica gel flash column chromatography and eluted (1:2 ether/hexanes) to give the epoxide alcohol **19** (1.63 g, 81%) as a liquid. ¹H-NMR (CDCl₃): 1.42 (3H, s, CH₃), 1.57 (3H, s, CH₃), 2.9 (1H, d, J=5 Hz, OH), 3.65 (1H, d, J=2 Hz, H-3), 3.67 (1H, d, J=2 Hz, H-2), 4.14 (1H, t, J=6 Hz, H-1), 4.55 (1H, t, J=6 Hz, H-5), 4.7 (1H, d, J=5 Hz, H-4) (Appendix D).

2,3-epoxy-4,5-isopropylidene-1-tosyl-cyclopentane (20).

To a homogenous solution of epoxy-alcohol **19** (1.233 g, 7.17 mmol) and dry pyridine (6 mL) was added tosyl chloride (2.73 g, 14.3 mmol) and catalytic DMAP. The mixture was stirred overnight at room temperature and then 30 mL of water was added. The mixture was extracted with CH₂Cl₂ (4 x 50 mL) and the organics dried over MgSO₄. The dried extracts were concentrated under reduced pressure and the resulting residue was purified by silica gel flash column chromatography (1:2 ether/hexanes) to give 2.10 g (90%) of the tosyl-epoxide **20**. ¹H-NMR (CDCl₃): 1.42 (3H, s, CH₃), 1.57 (3H, s, CH₃), 2.45 (3H, s, CH₃), 3.63 (1H, s, H-3), 3.71 (1H, d, J=2 Hz, H-2), 4.45 (1H, t, J= 6 Hz, H-1), 4.64 (1H, d, J=5 Hz, H-5), 4.70 (1H, d, J=5 Hz, H-4), 7.35 (2H, d), 7.84 (2H, d) (Appendix D).

1-azido-2,3-epoxy-4,5-isopropylidene-cyclopentane (21).

A solution of tosyl-epoxide **20** (60 mg, 0.307 mmol) in dry DMF (4 mL) in the presence of lithium azide (26 mg, 0.613 mmol) was heated at 140°C for 2 h with stirring. After the reaction was completed, the reaction mixture was concentrated, diluted with ethyl acetate (20 mL) and then washed successively with water (10 mL), saturated NaCl (10 mL), and water (10 mL). The organic layer was dried (MgSO₄), filtered, and concentrated. The resulting oil was purified by silica gel flash column chromatography (1% ethyl acetate in hexanes) to give the azide product (1%, only enough for NMR). ¹H-NMR (CDCl₃): 1.32 (3H, s, CH₃), 1.47 (3H, s, CH₃), 3.69 (1H, d, J=2Hz, H-3), 3.75 (1H, s, H-2), 3.85 (1H, s, H-1), 4.37 (1H, d, J=6 Hz, H-5), 4.75 (1H, d, J=6 Hz, H-4).

RESULTS

Expression and Purification of YkvM

The QueF homolog from *Bacillus subtilis*, YkvM, was expressed in *E. coli* from plasmid pET30Xa-*ykvM* and the his₆-fusion protein was purified by affinity chromatography (Figure 17). The majority of the desired protein is retained on the column and was eluted with 200 mM imidazole to afford pure protein (Lane 6). Cleavage of the N-terminal fusion tag with Factor Xa followed by an additional elution of the native protein through Ni²⁺-NTA agarose resin to remove residual fusion protein provided YkvM purified to good homogeneity (Lane 7) as judged by SDS-PAGE.

Synthesis of preQ₀

PreQ₀ was synthesized in two steps (Scheme 5, 70% yield) as described (118); treatment of the crude product by differential acid-base precipitation and Soxhlet extraction, followed finally by HPLC (Figure 18A), using an isocratic mobile phase of 4% acetonitrile in ammonium acetate (elution time 22 min), gave preQ₀ purified as a white powder after lyophilization. Characterization of the product was made by ¹H-NMR (118), and analysis of the product for its characteristic UV-vis chromophore (Figure 18B) was used to confirm the structure of preQ₀.

Steady State Kinetic Analysis

The full QueF reaction involves the binding and reaction of one molecule of preQ₀ and two molecules of NADPH. For initial velocity analysis of the reaction we assumed a bi-uni-uni-bi ping-pong ter-ter kinetic mechanism (112), with preQ₀ binding first and both equivalents of NADPH exhibiting equal binding affinity.

Kinetic assays to monitor YkvM activity were performed by two methods. First, a fluorescence assay based on the detection of the degradation product of NADP⁺ in alkaline solution was used to monitor YkvM activity at low (nanomolar) concentrations of preQ₀. At the specified time, aliquots were removed from the reaction mixture and treated with HCl for 10 min to destroy unreacted NADPH; it is known that the reduced form can be completely destroyed in acid without affecting the oxidized form (110). After incubation, treatment with NaOH followed by 2.5 h incubation in the dark developed the fluorescent alkaline NADP⁺ product. Excitation of this product at 360 nm results in an emission band that shows a maximum at 455 nm. The kinetic constants k_{cat} and K_m were obtained (Table 1) after fitting the initial velocity data to rate equation (2) (Figure 19). This analysis gave the kinetic parameters for preQ₀, $K_m = 0.237 \pm 0.045 \mu\text{M}$, $k_{\text{cat}} = 0.66 \pm 0.04 \text{ min}^{-1}$, and $k_{\text{cat}}/K_m = 4.6 \times 10^4 \text{ M}^{-1} \text{ s}^{-1}$. Kinetic assays were also carried out using a continuous assay following the loss of absorbance at 340 nm due to the oxidation of NADPH to NADP⁺ was utilized when measurement of YkvM under the condition of saturating preQ₀ was required. Analysis of the steady state kinetics

for NADPH and application of the appropriate velocity equation gave the kinetic constants $K_m = 19 \pm 2 \mu\text{M}$, $k_{\text{cat}} = 0.69 \pm 0.02 \text{ min}^{-1}$, and $k_{\text{cat}}/K_m = 6.1 \times 10^2 \text{ M}^{-1} \text{ s}^{-1}$.

Substrate Titration Studies.

To probe the binding of preQ₀ to the protein, titrations of substrate into enzyme were monitored by UV-vis. While preQ₀ and YkvM do not show any significant absorbance beyond 320 nm (Figure 20A), titrations of enzyme with substrate results in the formation of a new peak at 376 nm. The titration was continued until a maximal absorbance was reached, and a replot of the absorbance values at 376 nm versus the concentration of preQ₀ (Figure 20B) shows that the absorbance reaches a maximum when substrate becomes stoichiometric with enzyme. A standard curve was generated by recording the absorbance value at 376 nm for YkvM saturated with preQ₀ (two-fold, Figure 21); linear regression analysis of the data indicates the extinction coefficient of the new band is $4,353 \pm 89 \text{ M}^{-1}$.

Detection of a Covalent Intermediate by Mass Spectrometry

YkvM was analyzed in the absence and presence of preQ₀ by ESI-MS in order to detect the putative YkvM-preQ₀ covalent adduct. The mass spectrum obtained for the native protein of YkvM showed the expected parental mass peak at 19,373 Da, and the associated potassium ion adducts (in ascending order), 19,411 Da; 19,450 Da; 19,489 Da; 19,525 Da; 19,564 Da; 19,601 Da (Figure 22). A 5-fold excess of preQ₀ was incubated with YkvM for 5 min at room temperature before

acidification and injection onto the mass spectrometer. The resulting spectrum showed, in addition to the parent peaks, a minor peak at 19,547 Da. This molecular mass is consistent with the covalent attachment of one molecule of preQ₀ (M.W. 175 Da). The additional series of peaks in this spectrum, 19,585 Da, and 19,625 Da are attributed to the potassium adducts of the protein-preQ₀ complex (Figure 23).

Inactivation and Protection Studies.

To assess whether a cysteine residue is important for the catalytic activity of YkvM, investigations of enzyme activity in the presence of the thiol alkylating reagent iodoacetamide were performed. Incubations of YkvM with iodoacetamide showed a time-dependent inactivation of the enzyme (Figure 24A) and the protein was rendered essentially inactive after 8 min. When preQ₀ was included at saturating concentration in the pre-incubation mixture, significant attenuation of protein inactivation was observed (Figure 24B). In this series of reactions, activity by the protein was observed even after 20 minutes of incubation time with iodoacetamide/preQ₀.

C55S, C55A Mutant Preparation.

The Cys⁵⁵ point mutations were generated using the Quikchange kit (Stratagene) and the *ykvM* gene in the pET30Xa vector as template. Amplification of the desired mutant plasmid by PCR was conducted with the appropriate sense

and antisense primers, and after digestion of the parental DNA with *DpnI*, the mutant plasmids were transformed into *E. coli* DH5 α ultra-competent cells. Isolated colonies grown on kanamycin containing agarose plates were used to inoculate LB media. Recovery of the mutant plasmid followed by DNA sequencing confirmed the desired point mutations.

For expression of the Cys⁵⁵ mutants, the mutant plasmids were transformed into *E. coli* BL21(DE3). Proteins were expressed as N-terminal his₆ fusion proteins and purification by Ni²⁺-NTA agarose affinity chromatography afforded pure proteins as judged by SDS-PAGE (Lanes 2 and 3, Figure 25). The recombinant proteins were analyzed by ESI-MS (Proteomics Shared Resource, Oregon Health and Sciences University), and the parent molecular mass of C55S (M+H⁺ = 24,342 Da) and C55A (M+H⁺ = 24,327 Da) are consistent with the values of his₆-YkvM (calculated M+H⁺. 24,358 Da) containing only the desired mutation (Figure 26). Prior to activity assays, the his₆ sequence was removed using Factor Xa proteolysis to provide native mutant proteins (Lanes 4 and 5, Figure 25).

Activity Assays of the Cys⁵⁵ Mutants.

Both the C55S and C55A mutants exhibited low activity (< 0.001 %, Table 2) when examined by both the UV-vis (Figure 27) and the alkaline NADP⁺ detection assays (Figure 28) under conditions of saturating substrates (35 μ M preQ₀, 100 μ M NADPH for the UV-vis method, and 60 μ M preQ₀, 400 μ M NADPH for the fluorescence method) and high enzyme concentration (250 μ M and

300 μ M each of C55S and C55A, respectively). Substrate titration studies of these proteins with preQ₀ (up to a four-fold excess) did not result in a new absorbance band at 376 nm as observed for wild-type YkvM (Figure 29).

Circular Dichroism Spectroscopy.

To determine whether the loss of activity observed from the Cys⁵⁵ mutants was the result of the enzymes' inability to catalyze chemistry and not due to significant structural changes associated with the point mutation, circular dichroism spectra of the wild-type protein, C55A, and C55S were obtained. To eliminate the absorbance of chloride ions below 200 nm, potassium fluoride was exchanged for potassium chloride in the buffer. CD measurements were made with the proteins at a concentration of 2 mg mL⁻¹ and the proteins were scanned from 260-180 nm. Following data acquisition, the protein concentration of the analyzed sample was determined by amino acid analysis. The spectrum of the wild type protein suggests significant β -sheet character as predicted from structural sequence analysis (62) and the classification of this protein as a member of the T-fold superfamily (62). The overlay spectra of YkvM and the Cys⁵⁵ mutants (Figure 30) indicate that these proteins all exhibit identical secondary structures.

Size Exclusion Chromatography

To evaluate whether the Cys55 mutants were compromised in their ability to oligomerize to the homododecameric structure exhibited by the wild-type

enzyme, the native molecular weights of the Cys⁵⁵ mutant proteins were determined using analytical size exclusion chromatography. A standard curve was generated using thyroglobulin (670 kDa), apo-ferritin (443 kDa), pyruvate kinase (237 kDa), alcohol dehydrogenase (150 kDa), bovine serum albumin (66 kDa), and ovalbumin (44 kDa) as protein standards (Figure 31, Table 3). The mutant proteins C55S and C55A eluted with a calculated K_D of 0.580 and 0.577 (Table 4), respectively, consistent with a native molecular weight of 235 kDa and a quaternary structure consistent with a dodecamer. These results show that even though the active site of YkvM is predicted to be found at the monomer-monomer interface, the Cys⁵⁵ mutations do not alter the oligomerization pattern of YkvM. To confirm the integrity of the column and standard curve, an injection with wild-type YkvM was performed and the resulting trace was compared with the mutant proteins (Figure 32).

Preparation of Stereospecifically Deutero-labelled Cofactor

Isotope labeling studies were performed in order to elucidate the stereospecificity of hydride transfer from cofactor to substrate (Figure 33). NADPH specifically deuterated in the *pro-R* position at C-4 of the nicotinamide ring was prepared by the reduction of NADP⁺ in the presence of deuterated isopropanol using the alcohol dehydrogenase of *T. brockii*, which is known to be *pro-R* specific (Scheme 6). The *pro-S* stereoisomer was generated from NADP⁺ and D-[1-²H]-glucose by glucose-6-phosphate dehydrogenase in the presence of

40% DMSO (Scheme 7), following a protocol first described by Cleland (119). The reduced nucleotides were purified by HPLC (Figure 34), identified by the characteristic chromophore at 340 nm, and used as substrates in the YkvM reaction (Figure 35). Both the *pro-R* and *pro-S* deuterium labeled cofactors were suitable substrates in the YkvM reaction, but when compared to unlabeled NADPH, the activity of these isotopically-substituted substrates were appreciably lower than that observed for the unlabeled material.

Kinetic Isotope Effects

To understand the effect of the stereoisotopic substitution on the hydride transfer reaction, steady-state analysis for both the *pro-R* and *pro-S* deuterium labeled cofactors and unlabelled NADPH was carried out (Figure 36). Comparison of the steady-state kinetic parameters obtained for (4*R*)-[4-²H]NADPH and unlabeled NADPH indicate a 2.6 fold deuterium kinetic isotope effect on k_{cat} with (4*R*)-[4-²H]NADPH ($k_{\text{H}}/k_{\text{D}} = 2.59$) (Table 5). The magnitude of the KIE measured here indicates that YkvM catalyzes the transfer of the *pro-R* hydride of NADPH in the enzymatic reaction, and that the isotope effect observed is due to the cleavage of the C-D bond in NADPH. The magnitude of the primary kinetic isotope effect reported here also suggests that these chemical steps are at least partially rate-determining on the overall k_{cat} of YkvM. Steady-state analysis of (4*S*)-[4-²H]NADPH compared to unlabeled NADPH indicates that substitution with

deuterium at the geminal position imparts a small alpha secondary kinetic isotope effect ($k_H/k_D = 1.11$).

NMR Spectroscopy of Deuterium Labeled preQ₁.

In order to confirm the transfer of the appropriate hydride from NADPH to preQ₀, a preparative scale reaction of YkvM using (4*R*)-[4-²H]NADPH, (4*S*)-[4-²H]NADPH, or unlabeled NADPH was performed. PreQ₁ from these reactions was purified by HPLC using an isocratic mobile phase of ammonium acetate to elute the product at 18 min (Figure 37). This material was collected and lyophilized twice from deuterium oxide to recover a white powder that was analyzed by ¹H-NMR. The proton spectrum of preQ₁ (in deuterium oxide) recovered from the unlabeled reaction is characterized (Figure 38, bottom) by a one proton singlet at 6.88 ppm (C₈-H), a two proton singlet at 4.20 ppm (C₁₀-H₂), and a three proton singlet at 1.90 ppm (preQ₁ was recovered as the ammonium acetate salt) (86). The product of the reaction using *pro-S* labeled cofactor (Figure 38, middle) is identical to that of the unlabelled reaction, and this is consistent with the kinetic isotope effect measurements described above. The spectrum of preQ₁ generated using (4*R*)-[4-²H]NADPH (Figure 38, top) shows the presence of the C₈-H at 6.88 ppm and the acetate peak at 1.90 ppm, but the peak due to the C₁₀-H₂ methylene is notably absent. This is evidence that preQ₁ resulting from the utilization of (4*R*)-[4-²H]NADPH in the YkvM reaction is the doubly deuterium labeled product.

Mass Spectrometry Analysis

To further examine the preQ₁ generated from these isotopically enriched reactions, the enzymatic products were subjected to ESI-MS. Mass spectral data were obtained when the mass spectrometer was operating in the negative mode (M⁻H⁻). The parent molecular mass of preQ₁ (calculated MW 179 Da) produced from unlabeled NADPH (Figure 39) and (4*S*)-[4-²H]NADPH (Figure 40A) were *m/z* 178.2 Da, and *m/z* 178.3 Da, respectively, and these isotope labeling results are consistent with the NMR studies shown above. The mass spectrum of the (4*R*)-[4-²H]NADPH derived product (Figure 40B) was marked by a 2 Da shift in the mass signal (*m/z* 180.1 Da) attributed to presence of the doubly deuterated product.

Stereospecificity of Hydride Transfer Catalyzed by the YqcD Class of QueF.

The hydride stereospecificity experiments described above were performed using YqcD, the QueF homolog in *E. coli*. YqcD represents the second structural subclass of this protein family. YqcD was expressed *E. coli* and purified by nickel chelation affinity chromatography as the his₆ fusion protein. Treatment with FactorXa provided native YqcD that was homogenous as judged by SDS-PAGE. PreQ₁ generated from the YqcD reaction using (4*R*)-[4-²H]NADPH, (4*S*)-[4-²H]NADPH, or unlabeled NADPH was analyzed by ¹H-NMR. The results were identical to those obtained using YkvM as catalyst; therefore, YqcD also carries out the QueF reaction in a *pro-R* specific manner. These results also imply that

although the QueF family exhibits structural diversity, the mechanism of hydride transfer across the two subclasses is conserved.

Preparation and Characterization of Glu⁹⁷ Mutants.

To test the prediction that the role of the conserved Glu⁹⁷ involves substrate binding (Figure 41) as observed for other T-fold enzymes and as suggested by the homology model of the YkvM active site, site-directed mutagenesis of this residue and the characterization of the resulting protein products was performed. The preparation of the YkvM Glu⁹⁷ mutants Glu97Ala, Glu97Gln, Glu97Asp, Glu97Leu, and Glu97Lys was carried out using Quikchange kit protocols in an analogous manner as described for the preparation of the Cys⁵⁵ mutants. DNA sequencing on all mutant plasmids was performed to confirm the structure and desired mutation in the *ykvM* gene. The expression and purification of the recombinant YkvM-Glu⁹⁷ mutants was performed as described for the wild-type protein, and following removal of the his₆ leader sequence with Factor Xa, Glu⁹⁷ mutants were purified to > 98 % homogeneity as judged by SDS-PAGE (Figure 42). Biophysical characterization of these mutants was performed, and size exclusion chromatography indicated mutations at Glu⁹⁷ did not affect the oligomerization of YkvM (Table 4). For each mutant, the protein eluted from the column at a native molecular weight ~238 kDa (dodecameric structure). Substrate titration studies did not show the formation of a new band at 376 nm, but HPLC performed on reaction assays from each of the mutants confirmed preQ₁ as the

enzymatic product. Activity assays were conducted following the oxidation of NADPH at 340 nm to measure the specific activities of these mutant proteins; for each of the Glu⁹⁷ mutants, activity was significantly reduced upon substitution of this residue; with specific activities between 1-6% that of wild-type YkvM (Table 6). Steady-state kinetic analysis of the alanine mutant (following production of the fluorescent alkaline NADP⁺ product) (Figure 43A) indicated the K_m of preQ₀ for this mutant was 30 μ M, approximately 120-fold greater than the Michaelis constant of preQ₀ to the wild-type protein (0.237 μ M). This is consistent with the prediction that Glu⁹⁷ functions in preQ₀ binding and positioning in the active site. Furthermore, the 15-fold reduction in the measured k_{cat} (0.7 min⁻¹ for the wild-type protein and 0.045 min⁻¹ for the Glu97Ala mutant), suggests that substitution of the glutamate residue also impacts the chemical steps during the reaction. Similar kinetic results were obtained for the Glu97Gln mutation (Figure 43B). The K_m of preQ₀ ($K_m = 67 \mu$ M) for this enzyme form was increased 280-fold compared to wild-type, and the measured k_{cat} of 0.036 min⁻¹ is 20-fold lower than YkvM. Interestingly, kinetic analysis of the Glu97Asp mutant gave similar results. Although this mutation only removes one methylene group from the natural residue, the specific activity of this mutant was 5.2 % that of the wild-type. Steady-state kinetic data for this protein indicates a 14-fold reduction in k_{cat} (0.053 min⁻¹) and a K_m value of 7.6 μ M, 25-fold higher than wild-type (Figure 43C). Mutation to the cationic side chain (Glu97Lys) resulted in a specific activity 3.1 % that of the wild-type.

PreQ₀ Binding and Formation of the Putative Covalent Adduct.

The kinetics for the formation of the absorbance band at 376 nm were determined by stopped flow spectroscopy. The rapid kinetic studies were performed in the absence of NADPH. The plots (Figure 44) show that the rate of formation of the putative thioimide is concentration dependent, and the rate of peak formation plateaus at concentrations of preQ₀ in excess (> 2 fold) of the concentration of YkvM in the solution (20 μM). The data were fit to either the single exponential or double exponential equations; in both cases, the quality of the curve fits deteriorates for the data collected beyond 80 μM preQ₀ (Figure 45). However, a replot of the k_{obs} values obtained for those curves that displayed a sufficient fit to the single exponential (Figure 46) shows a hyperbolic response consistent with saturation kinetics.

Transient Kinetics of Substrate Turnover

Single turnover experiments of YkvM was performed using protein pre-incubated with substoichiometric preQ₀ in one syringe, and the progress of the reaction was monitored immediately after introduction with NADPH from a second syringe. The data shows a rapid consumption of NADPH upon mixing. However, the quantity of NADPH oxidized does not correspond to the amount expected if all preQ₀ was preloaded on YkvM as the thioimide (Figure 47). Based on the approximate difference in absorbance values at time zero and when the reaction

enters the linear phase, only 10-20 % of the preQ₀ in the solution was subjected an immediate first reductive cycle. The data were fit to either the single exponential or double exponential equations, and as before, deviation of the curve fit was observed at the high end of the concentrations tested.

Multiple turnover experiments of YkvM were also performed by stopped flow spectroscopy. In these cases, a small burst phase associated with the immediate mixing of YkvM and preQ₀ from one syringe and NADPH from another was observed (Figure 48). The data were fit to the burst phase equation (eq 8), and the replot of the $k_{\text{obs}2}$ obtained here provided a k_{obs} comparable to k_{cat} obtained for the steady-state kinetic analysis of NADPH ($k_{\text{obs}2}$ is effectively $k_{\text{steady-state}}$ under these conditions, and this experiment confirms the overall $k_{\text{cat}} = 0.7 \text{ min}^{-1}$).

Substrate Analogs.

The reduction of alternate nitrile-containing substrates was analyzed by following the production of the fluorescent alkaline degradation product of NADP⁺. A series of aromatic nitriles that, by appearance, are closely related to the natural substrate, preQ₀ were studied (Figure 49). These were indole-3-nitrile, phenylacetonitrile, and 4-aminobenzonitrile. The substrate analogs were screened for NADP⁺ production with wild-type YkvM and the Glu97Ala and Glu97Leu mutants. We envisioned these aliphatic side-chain containing mutants would present a complementary hydrophobic binding site for the unsubstituted nitrile analogs. Assays were conducted at high concentrations (100 μM, prepared in

DMSO) of nitrile and enzyme (50 μM), and at 5-times the K_m concentration of NADPH (100 μM). A control reaction was carried out in the absence of substrate, and this showed high precision; minimal variability in this control sample was observed over the 1 h reaction period (Figure 50A). Incubation with indole-3-nitrile clearly shows the production of NADP^+ in a time-dependent fashion (Figure 50B), consistent with the YkvM catalyzed reduction of indole-3-nitrile to indole-3-aminomethyl. Using a NADP^+ standard curve, the rate of formation of NADP^+ from this reaction was 0.020 $\mu\text{M min}^{-1}$. The calculated specific activity of YkvM for the indole analog (0.041 $\mu\text{M min}^{-1} \text{mg}^{-1}$) is 4400-fold lower ($< 0.001\%$ observed activity) than that of YkvM for the natural substrate, preQ₀ (Table 6). Similar NADP^+ production was observed with Glu97Ala (Figure 50C), but the time course assay of indole-3-nitrile with Glu97Leu showed lower levels of NADP^+ formation (Figure 50D). Examination of 4-aminobenzonitrile with YkvM showed this compound results in detectable levels of alkaline NADP^+ product formation (at a rate of 0.006 $\mu\text{M min}^{-1} \text{mg}^{-1}$) but as predicted from active-site side-chain interactions, this is a poorer substrate for both Glu97Ala and Glu97Leu mutants (Figure 51). Reactions containing phenylacetoneitrile showed low but detectable levels of NADP^+ production with all proteins tested (measured rate 0.003 $\mu\text{M min}^{-1}$, specific activity 0.005 $\mu\text{M min}^{-1} \text{mg}^{-1}$) (Figure 52), but comparison of activity between phenylacetoneitrile and preQ₀ turnover by the wild-type protein indicate a considerable reduction in activity ($>3.0 \times 10^4$ -fold).

Cloning, Expression, Purification and Activity Assays of YgcM and YbaX, Two Enzymes Involved in Q Biosynthesis.

The *E. coli* genes *ygcM* and *ybaX* were individually cloned using ligation-independent cloning and inserted into the pET30Xa vector. DNA sequencing confirmed the integrity of the construct. The plasmid bearing these genes were transformed to *E. coli* BL21(DE3) cell line, and the protein products was expressed as the hexa-histidine tagged recombinant protein. Purification by affinity chromatography afforded pure proteins as judged by SDS-PAGE, and the fusion proteins were used without further purification.

The 6-pyruvoyltetrahydropterin synthase (PTPS) activity of YgcM was shown by observation of the formation of 6-pyruvoylpterin from neopterin triphosphate, the later produced from GTP by FolE in an enzyme coupled reaction. The enzyme products were subjected to dephosphorylation with alkaline phosphatase and an acidic iodine oxidation treatment to develop the characteristic pterin chromophore, and then analyzed by HPLC (Figure 53). Reactions containing GTP and FolE showed only the expected neopterin product (Figure 53A). When YgcM was included, a new peak eluting at ~11 min was observed (Figure 53B). Comparison of the chromophore of this peak suggested the pterin-like structure. Since the PTPS enzyme is a magnesium dependent protein, the reaction was supplemented with 10 mM magnesium chloride, and the result was an increase in intensity of the peak at 11 min with a corresponding decrease in

intensity of the neopterin peak consistent with greater flux through the two enzyme pathway in the presence of the stimulating metal ion.

QueA: Towards the Total Synthesis of Epoxyqueuine.

Synthesis of the 7-deazaguanine Core.

The 7-deazaguanine core structure of oQ, 2-amino-5-(N,N-dimethylaminomethyl)pyrrolo[2,3-*d*]pyrimidin-4-one **8** was synthesized in six steps as previously described (85, 86) in an overall yield of 18 %. Ethylcyanoacetate was first condensed with diethoxybromoacetal in the presence of potassium carbonate to give ethyl 2,2-diethoxyethylcyanoacetate **11** (46% yield) after purification by distillation under reduced pressure. Ethyl 2,2-diethoxyethylcyanoacetate was then cyclized with guanidine thiocyanate to generate 2,4-diamino-5(2,2-diethoxyethyl)-6-hydroxypyrimidine **12** (55% yield) which was purified by differential acid-base precipitation. Treatment of this product under mild acid conditions (0.5 M HCl) afforded 7-deazaguanine **13** (quantitative yields) after neutralization of the solution. This material was dried and the C₂-NH₂ amine was protected as the octanoyl group using octanoyl chloride, freshly distilled pyridine, and catalytic amounts of dimethylaminopyridine. The octanoyl protected analog **14** of 7-deazaguanine was obtained (85% yield) after recrystallization with ethanol. The C-7 exocyclic aminomethyl moiety was added *via* the Mannich reaction of the octanoyl-protected deazaguanine with formalin and

dibenzylamine to generate the fully protected form of preQ₁ **15**. This material was obtained in good yield (75%) after purification by flash column chromatography and recrystallization from ethanol. Amine exchange of the dibenzyl group with dimethylamine, followed by deprotection of the octanoyl group with KOH gave the N,N-dimethyl analog of preQ₁ **8** after treatment with cold ether to precipitate the product and recrystallization with ethanol (70% yield).

Construction of the Stereospecific Ribosyl Moiety.

Cyclopentenone **10** was synthesized in three steps (overall yield 38%) from D-ribose following the scheme provided by Ali *et al.* (96). The isopropylidene protected methyl riboside **16** was obtained in high yields (92%) after purification by flash column chromatography. Oxidation of this product in the presence of excess (4-fold) pyridinium chlorochromate gave the isopropylidene protected 4-methoxy-buturyl- δ -lactone **17** at 52% yields after recrystallization. Wittig rearrangement of the lactone product provided the stereospecific cyclopentenone **10** after flash column chromatography (80% yield). The reduction of **10** under the Luche (97, 120) conditions (NaBH₄, cerous chloride dihydrate) gave stereospecific **18** as an oil and in good yields (85%) after flash column chromatography. Epoxidation was carried out utilizing a novel dioxirane epoxidation system (121, 122) to afford **19** as a colorless oil after purification by flash column chromatography (82% yield). The epoxide proton resonances were observed as a pair of doublets at 3.67 ppm and 3.65 ppm, and the associated coupling constant

($J=2$ Hz) is consistent with that of neighboring epoxide protons. Structural assignments were made by 2D-COSY-NMR (Appendix D), and stereochemistry was determined by nuclear Overhauser effect (NOE) measurements (Appendix D). NOEs were observed between the epoxide protons H2-H3, and also between isopropylidene protons H4-H5. The absence of an NOE between proton sets H1-H2 and H3-H4 indicate that these sets of protons lie on opposite planes of the cyclopentane ring. This stereochemistry was also indicated by the COSY spectrum where an absence of coupling between H1-H2 and H3-H4 was observed. Given that the epoxide and the isopropylidene groups occupy opposite faces of the ring, the presence of these groups *trans* orient the H2-H3 epoxide protons and the H4-H5 isopropylidene protons in an orthogonal arrangement, resulting in no coupling between the *trans* protons. Activation of the alcohol **19** as the tosylate proceeded smoothly and the product **20** was isolated in 95% yield after silica gel flash column chromatography.

DISCUSSION

Queuosine biosynthesis is clearly marked with unprecedented enzyme chemistry, and the overall focus of this work is the study of two enzymes in the queuosine biosynthetic pathway. The QueF protein family encodes an NADPH-dependent oxidoreductase, and is responsible for the four-electron reduction of preQ₀ to preQ₁. The fundamental chemical conversion carried out by this protein is the reduction of a nitrile functional group to an amine. While the reduction of the nitrile group to an amine is a common reaction in organic chemistry, it is a process that has not been previously observed in biology. The goal of this work is the chemical and kinetic characterization of this new class of protein.

Steady-state kinetic analysis of QueF using YkvM, the *B. subtilis* ortholog, was carried out using the continuous assay following the loss of absorbance at 340 nm due to the oxidation of NADPH to NADP⁺. This work provided the steady state kinetic parameters for NADPH after fitting the initial velocity data to the rate equation describing the bi-uni-uni-bi ping-pong ter-ter kinetic mechanism ($K_m = 19 \pm 2 \mu\text{M}$, $k_{\text{cat}} = 0.69 \pm 0.02 \text{ min}^{-1}$ and $k_{\text{cat}}/K_m = 6.1 \times 10^2 \text{ M}^{-1} \text{ s}^{-1}$). The value of K_m is consistent with the values of K_m for NADPH in other bacterial NADPH-dependent oxidoreductases (123, 124). The measured k_{cat} is comparable with the two subsequent enzymes in the pathway (125, 126). Measurement of the kinetic parameters for preQ₀ following the loss of absorbance at 340 nm was hampered by the low signal to noise at low concentrations of preQ₀ turnover ($< 1 \mu\text{M}$). To

determine the enzyme velocity at low concentrations of preQ₀, a number of assay methods were tested for measurement of the YkvM reaction. These included monitoring the formation of the amine product by derivatization of preQ₁, the fluorescent labeling of preQ₁ nucleoside with dansyl chloride (127), and fluorescamine (128-131). These methods were complicated by the observation that the excitation and emission bands of the modified preQ₁ species (ex. 360 nm and em. 465 nm) overlapped with the excitation and emission bands of NADPH (ex. 340 nm and em. 440). This in turn led assay development towards an investigation of NADPH/NADP⁺ fluorescence for the measurement of YkvM activity. The activity of NAD(P)⁺ linked enzymes have been monitored by measuring changes in cofactor concentration by fluorescence (132, 133). In addition, this method has been reported to provide ~ 10³ greater signal to noise compared to absorbance measurements (134). Therefore, measurement of the oxidation of NADPH by YkvM by fluorescence was investigated, but it was determined that the turnover number was slower than the rate of NADPH quenching in the sample, thereby excluding this assay from the possible methods of YkvM measurement.

To measure the initial velocity kinetics at nanomolar concentrations of preQ₀ turnover, a fluorescence assay based on the detection of the alkaline degradation NADP⁺ product was ultimately optimized. This method has been recently applied for the high-throughput screening of cytochrome P450 substrates and mutants (109). Analysis of the initial velocity data using rate equation for the single substrate provided the kinetic parameters for preQ₀, $K_m = 0.237 \pm 0.045 \mu\text{M}$,

$k_{\text{cat}} = 0.66 \pm 0.04 \text{ min}^{-1}$ and $k_{\text{cat}}/K_m = 4.6 \times 10^4 \text{ M}^{-1} \text{ s}^{-1}$. The Michaelis constant of preQ₀ for this enzyme is comparable to the K_m value of preQ₁ for TGT, the next enzyme in the queuosine biosynthetic pathway ($K_m = 0.39 \text{ }\mu\text{M}$) (84).

Sequence analysis of YkvM has shown that Cys⁵⁵ is strictly conserved over all members in this family of proteins (62) and also aligns with a universally conserved Cys residue in the structurally related GTPCH family, where it serves as a ligand for an active-site Zn²⁺ metal ion. Furthermore, a homology model of the YkvM active site indicates the Cys⁵⁵ is positioned in close proximity to the substrate, suggesting that this residue may be important in catalysis (69).

To examine the role of the putative active site cysteine, inactivation studies using the thiol alkylating agent iodoacetamide were carried out. Incubations of YkvM with iodoacetamide indicated a rapid time-dependent inactivation of the enzyme, while inactivation was significantly attenuated in the presence of preQ₀; the results are consistent with the hypothesis that a catalytically important Cys residue, presumably Cys⁵⁵, is present in the active-site where it can react with iodoacetamide, and the presence of the substrate protects this residue from reaction with iodoacetamide.

Given the predicted proximity of Cys⁵⁵ to the nitrile of preQ₀, we reasoned that its role might be to serve as a catalytic nucleophile in the reaction, reacting with the nitrile to form a covalent thioimide intermediate which might then be the relevant species for reduction. Such an intermediate has precedence in the nitrilase catalyzed hydrolysis of nitriles (78, 79), and in a papain mutant engineered to

catalyze nitrile hydrolysis (135). A thioimide intermediate can also be considered analogous to a thioester intermediate; the formation of a thioester in catalytic mechanisms is well-documented in a variety of enzymatic mechanisms, and in particular is observed with both the GAPDH archetype of aldehyde oxidizing enzymes and catalysis employed by a similar nicotinamide-dependent 4-electron redox process, UDP-glucose dehydrogenase (72, 73). Titrations of substrate into enzyme resulted in a new peak at 376 nm consistent with the expected UV-vis absorption of thioimide group conjugated into extended π systems (136). The observation that this absorbance band reaches a maximum when the substrate becomes stoichiometric with enzyme (ie. saturation of the enzyme active sites) further supports the theory that a covalent intermediate is present on the reaction path of YkvM, and the active site Cys⁵⁵ is implicated as the covalent nucleophile.

To further investigate the catalytic role of Cys⁵⁵, serine and alanine point mutations of this residue were generated. Mutations of this type for the catalytic thiol (Cys260) in the active site of UDP-glucose dehydrogenase resulted in protein forms that showed less than 0.01% remaining activity (73, 137). These mutations rendered YkvM essentially inactive (for both mutants, less than 0.001 % activity remained), and substrate titration experiments with the mutant proteins resulted in no observable band at 376 nm, even at high preQ₀/enzyme ratios. This is consistent with the inability of these proteins to form the putative covalent thioimide intermediate observed for the wild-type protein with preQ₀. Furthermore, circular dichroism of the wild type, C55S, and C55A were identical, indicating that no

significant changes in secondary structure were associated with these mutations. To detect whether this mutation affected the oligomerization pattern of dodecameric YkvM, size-exclusion chromatography was performed, and the results show that C55S and C55A both retain relative molecular weights consistent with the wild-type dodecameric structure. The biophysical data indicate that, at the secondary and quaternary structure levels, the loss of activity for the Cys⁵⁵ mutants is due solely to the loss of the catalytic thiol, not gross structural perturbations of the enzyme.

To observe the putative adduct formed between preQ₀ and YkvM, ESI-MS was utilized to detect the covalent complex. This method has been successful in detecting the intermediate formed between a series of aromatic nitriles with nitrilase (78). This family of enzymes contains a catalytically essential thiol in the active site, and it has been shown that the reaction mechanism proceeds by nucleophilic attack of the thiol to give a substrate bound species in the form of a thioimidate (77, 79). Mass spectral data of YkvM showed the expected parent molecular mass (19,373 Da) and the associated potassium salt adducts. Although the signal in the mass spectrum is weak, the spectrum obtained for YkvM which had been pre-incubated with preQ₀ prior to analysis shows the formation of a new family of peaks consistent with the attachment of a molecule of substrate to the protein (19,547 Da) and the corresponding potassium adducts of this species. The observation of the low signal intensity was surprising given that saturation of these active sites with preQ₀ occurs at stoichiometric ratios of protein and substrate.

However, since native YkvM is organized as a dodecameric structure with the active sites present at the intersubunit interfaces, and since that structure is destroyed under electrospray conditions, the covalent adduct may be especially prone to breakdown, leading to poor resolution of the covalent complex in the mass spectrum. Despite the lack of a direct observation of this intermediate, the evidence of the role of Cys⁵⁵ provided by the spectroscopic, mutational, kinetic, and biophysical data strongly supports covalent catalysis by YkvM.

Four-electron reduction of a nitrile group to an amine has never before been observed in biology, and while this protein family represents a new class of enzymatic activity, the discovery also adds to a small group of enzymes traditionally classified as NAD(P)⁺-dependent four-electron-transfer dehydrogenases (71). Bentley's first rule states that all dehydrogenases acting on a given substrate, regardless of the source of the enzyme, possess a common stereospecificity of hydrogen abstraction to NAD(P)⁺ (138). UDP-glucose dehydrogenases from all organisms carry out the two-fold oxidation of UDP-glucose to UDP-glucuronic acid with concomitant *pro-S* reduction of NAD⁺ (139) while histidinol dehydrogenase from all organisms oxidize L-histidinol to L-histidine through two sequential hydride transfers to the *pro-R* side of NAD⁺ (140). Interestingly, hydroxymethylglutaryl-CoA (HMG-CoA) reductases from different organisms have been shown to exhibit different stereospecificity for the oxidation of NADPH (141) and this enzyme class is generally reported as one of the exceptions to Bentley's first rule (142). Since the QueF family comprises two

subclasses, exemplified by *B. subtilis* YkvM and *E. coli* YqcD, the details of the stereospecificity of hydride transfer for these enzymes was investigated.

Isotope labeling studies was utilized to determine the stereospecificity of hydride transfer catalyzed by the QueF family. The experiment was run in parallel using YkvM, a member of the dodecameric subclass, and YqcD, a member of the dimer subclass. Stereospecifically deuterium-labeled NADPH was enzymatically synthesized and purified by published protocols, and these substrates were utilized in the QueF reactions. After recovery of the enzymatically generated preQ₁, the products were characterized by mass spectrometry and ¹H-NMR. Using YkvM as catalyst, it was shown that hydride transfer was facilitated from the *Re* face of the nicotinamide ring of NADPH; evidence for this mechanism included a 2 Da shift in the mass spectrum and the loss of the C₁₀-H₂ signal in the proton spectrum owing to the presence of the doubly deuterated product when *pro-R* deuterium labeled NADPH was used as cofactor. Analysis of preQ₁ generated from *pro-S* deuterium-labeled NADPH showed no difference from the proton and mass spectrum obtained for preQ₁ generated from unlabeled NADPH.

To assess the mechanistic conservation of hydride transfer across the two subclasses of QueF, the isotope labeling studies were also performed with YqcD, and the ¹H-NMR spectra of the resulting preQ₁ products generated with deuterium labeled NADPH were identical to spectra obtained using YkvM. The enzymes YkvM from *B. subtilis* and YqcD from *E. coli* both utilize the *pro-R* hydride of NADPH during the two-fold reduction of the nitrile to the primary amine. We

conclude that this mode of catalysis is conserved within the QueF protein family and therefore consistent with Bentley's first rule.

The data collected here also provides insight into structural aspects and orientation of the reduced cofactor in addition to the mechanistic determination of the hydride transfer. Since the *pro-R* hydride of NADPH is transferred in the QueF reaction, it suggests the reduced nicotinamide ring is positioned in the "anti" conformation in the active site. The basis of distortion by the ring into the boat conformation is the "reverse anomeric effect"⁽¹⁴³⁾; this orientation allows for optimal donation of electron density from the lone pair of the nicotinamide ring into the adjacent antibonding orbital of the sugar oxygen-carbon bond. This makes the *pro-R* hydrogen at the 4-position axial, and based on the principles of orbital overlap, more easily transferred.

Steady-state kinetic isotope measurements of *B. subtilis* QueF indicated a primary kinetic isotope effect (k_H/k_D) of 2.59 for the hydride transfer step; this suggests that the chemical step of QueF (bond breaking of C-H bond in NADPH and transfer and formation of the new C-H bond of preQ₁) is at least partially rate-determining on the overall k_{cat} of the reaction. It is worth noting that although these implications can be made by this measured value of the primary KIE, this value does not reveal or imply whether the rates of the first or second hydride transfer are equal, or if one of these chemical steps is "faster" than the other. Furthermore, during the reaction course, a singly deuterium labeled intermediate resulting from the first reduction must be present, and as the transfer of the second deuterium

hydride takes place, an additional α -secondary deuterium isotope effect is encountered on the expected $sp^2 \rightarrow sp^3$ transition of the reaction intermediate. Transitions of this type typically lead to an inverse KIE at the carbon center. Therefore, the recorded steady-state primary KIE is presumably the sum of the isotope effects at the active site, and the information gained here cannot be interpreted to exclusively represent the two hydride transfer steps of YkvM.

Steady-state kinetic analysis using the *pro-S* deuterium-labeled NADPH revealed that isotopic substitution at the *pro-S* position imparts an alpha secondary kinetic isotope effect ($k_H/k_D = 1.11$). Since the α -carbon undergoes a $sp^3 \rightarrow sp^2$ transition during the course of the reaction, the magnitude of the kinetic isotope effect is expected to be greater than one (144). An intuitive explanation for this effect is based on the coupled motion of the two hydrogens. The primary hydrogen is lost and while the secondary hydrogen moves through a 54° arc during the reaction, the motion of the primary hydrogen is slowed somewhat by a heavier atom in the α -secondary position (145).

As noted previously, the QueF family likely belongs to the tunnel fold (T-fold) family of enzymes (62). T-fold proteins bind substrates belonging to the purine or pterin families and share a fold-related binding site with a glutamate or glutamine residue anchoring the substrate. The residue (Glu⁹⁷ in *B. subtilis* YkvM and Glu¹⁵² in *E. coli* YqcD) is strictly conserved over all QueF sequences, and the homology model of the putative active site predicts that this residue functions in an analogous manner as described for the other members of the T-fold family (69).

For YkvM, Glu⁹⁷ is predicted to form hydrogen bonds with the N²-amine moiety and the N³-hydrogen of the pyrimidine ring of preQ₀.

To assess the role of Glu⁹⁷ on the catalytic activities of YkvM, the Glu97Ala, Glu97Gln, Glu97Asp, Glu97Lys, and Glu97Leu mutants were made by site-directed mutagenesis. Assays of these proteins indicated a significant reduction in activity upon substitution at this residue, and this observation is consistent with the prediction that Glu⁹⁷ resides in the YkvM active site and plays an important role in the catalytic cycle. Mutational studies of the analogous active site glutamate in GTP cyclohydrolase I to aspartate, glutamine, and lysine show, 0.07%, 0.1%, and 0.06% remaining cyclohydrolase activity, respectively (62, 146, 147). However, biophysical analysis indicate that substitution of the conserved glutamate disrupts the oligomerization pattern for GTP cyclohydrolase I (147). In the case of the GTPCHI-Glu152Lys mutant, size exclusion chromatography indicated complete dissociation of the native decamer complex. Interestingly, examination of the protein in the presence of GTP revealed that the mutant is capable of reassociating into the decamer form, and it was concluded that GTP stabilized the native decameric structure by playing the role of a linker between monomer units. In contrast, size exclusion chromatography showed that all YkvM Glu⁹⁷ mutants obtained elute with a native molecular mass consistent with a dodecamer. Thus, mutations of Glu⁹⁷ does not compromise the quaternary structure of the protein and the loss or reduction of activity displayed by the YkvM

mutants is apparently due to the loss of specific protein-substrate interactions when Glu⁹⁷ is replaced by another residue.

For each of YkvM Glu⁹⁷ mutants, the relative specific activity compared to wild-type (determined under nominal V_{\max} conditions for YkvM) was in the range of 1-6 %. Steady-state kinetic analysis of Glu97Ala, Glu97Gln and Glu97Asp indicated that for these mutants, the K_m for preQ₀ was $30 \pm 5 \mu\text{M}$, $67 \pm 4 \mu\text{M}$, and $7.6 \pm 1.3 \mu\text{M}$ respectively. The measured values of K_m are 120-fold (Glu97Ala), 280-fold (Glu97Gln), 25-fold (Glu97Asp) greater than the measured Michaelis constant of preQ₀ for wild-type YkvM ($0.237 \mu\text{M}$), suggesting this residue does indeed participate in substrate binding, and presumably, positioning of the planar preQ₀ in the active site. The measured reduction in k_{cat} (15-fold for Glu97Ala, 20-fold for Glu97Gln, 13-fold for Glu97Asp) for these proteins indicates substitution at the glutamate residue also impacts the chemical steps during the reaction. The measured reductions in k_{cat}/K_m , (2000-fold decrease for Glu97Ala, 5000-fold decrease for Glu97Gln, and 400-fold for Glu97Asp) suggests these mutant protein forms cannot efficiently bind to and turnover preQ₀ in the absence of Glu⁹⁷. During the enzymatic conversion of preQ₀ to preQ₁, a series of mandatory intermediates, such as the imine product generated from the first reductive cycle of YkvM are present. Removal of the active site glutamate, in addition to its' observed effects on the initial binding of preQ₀ to the active site, likely results in diminished binding and positioning of these intermediates during the reaction course of the enzyme, and the reductions in k_{cat} and k_{cat}/K_m reflects the hampered inability of the protein

to carry out chemistry on these poorly situated intermediates efficiently in the absence of the stabilizing residue.

The abundance of optical signals and the ability to monitor the formation of putative intermediates and consumption of substrates in the YkvM reaction spectrophotometrically has allowed us a strategy to attempt to understand the kinetics of this reaction on the microscopic level. Based on the predicted Bi-Uni-Uni-Bi Ter-Ter Ping Pong kinetic mechanism, the putative kinetic scheme for the two-fold reduction is presented in Figure 54. Rapid scanning kinetics was performed by stopped flow spectrophotometry, and data describing the pre-steady state kinetics of thioimide formation was collected. Once analyzed, this data will allow for an approximation of the kinetics of preQ₀ association to YkvM (k_1) and release (k_{-1}), and also give a measure of the kinetics of the first chemical step for the formation (k_2) and the breakdown of the thioimide (k_{-2}). In addition, YkvM was monitored by stopped-flow spectrophotometry under single turnover and multiple turnover conditions in the presence of NADPH and *pro-R* deuterium-labeled NADPH. Analysis of this data, in combination with the restrictions imposed by the limiting kinetics of thioimide transient formation, will allow for a more focused estimate of the later kinetic constants. Once these values are obtained, analysis of the data where *pro-R* deuterated NADPH is used as cofactor will allow for a more refined estimation of the hydride transfer steps of the reaction, as all other NADPH binding and dissociation steps should, in theory, be identical to the values obtained using unlabeled material. The goal of this work is the determination of the intrinsic

rate constants governing the YkvM reaction. To achieve this goal, the complete dataset is currently being subjected to global analysis using DYNAFIT.

The studies presented here have focused on the elucidation of the mechanistic details involved in the two-fold reduction of preQ₀ to preQ₁ by the QueF protein family. The results, taken together, have allowed the following proposal to describe the active site chemistry and chemical mechanism of YkvM (Figure 55). PreQ₀ is recognized, bound and positioned in the active by Glu⁹⁷; this is consistent with recognition and binding of planar purine/pterin substrates in other T-fold enzymes. We propose that, in analogy to nitrilases, the thiol of Cys⁵⁵ (*B. subtilis* numbering) attacks the nitrile of preQ₀ to form a covalent thioimide intermediate. Formation of this adduct can be monitored by UV-vis as a new absorbance band at 376 nm. The delivery of the *pro-R* hydride from the first equivalent of NADPH gives an imine intermediate bound as a thiohemiaminal. Release of the oxidized cofactor is followed by binding of the second molecule of NADPH, collapse of the thiohemiaminal and reduction by the *pro-R* hydride from the second equivalent of NADPH to give preQ₁. Formation of a bound intermediate prevents the hydrolysis of the necessary imine intermediate and allows for the quantitative conversion of preQ₀ to preQ₁. This overall process, whereby the reaction intermediate is sequestered in the active site during the two-fold reduction, is reminiscent of the UDP-glucose dehydrogenase, an enzyme which carries out the net-four electron oxidation of UDP-glucose (72, 73, 137).

The discovery of nitrile reductase activity in the QueF family prompted us to explore the utility of this enzyme for more widespread applications. Nitrile reduction is a ubiquitous chemical transformation in the pharmaceutical, specialty, and commodity chemicals industries. The reduction of nitriles to amines has traditionally been carried out by hydrogenation over various transition metal catalysts. Typical of many industrial chemical processes, nitrile reduction is associated with high-energy demands (temperature and pressure), low selectivity, and results in the generation of hazardous waste. The QueF activity presents an opportunity to introduce an environmentally benign method into the industrial biocatalysis fold. This method offers the ability to conduct the transformation of the nitrile group to an amine under very mild conditions (room temperature, neutral pH and ambient pressure) with minimal generation of hazardous by-products.

To probe the substrate specificity and tolerance of the QueF active site, we assessed the activity of YkvM with a series of nitrile analogs using the UV-vis method to follow the consumption of NADPH. In particular, indole-3-nitrile, 4-amino-benzonitrile, and phenylacetonitrile were incubated with wild-type YkvM and two of the Glu⁹⁷ mutants, Glu97Ala and Glu97Leu at a variety of substrate and enzyme concentrations. These compounds were chosen because of their structural similarity to preQ₀. None of the reactions showed any activity, at least to the detection limits of the UV-vis assay method. We therefore opted to utilize the fluorescence assay to detect the enzymatic production of NADP⁺. Using this assay, the ability of YkvM to turnover the nitrile analogs was reinvestigated. Incubations

of indole-3-nitrile clearly showed the time dependent production of NADP⁺ in the presence of wild-type YkvM. The activity displayed by this analog is not surprising considering that indole-3-nitrile and preQ₀ both present planar aromatic structures to the active site. The homology model of YkvM predicts π - π stacking interactions between preQ₀ and Phe⁹⁵, and this interaction can be easily envisioned with the indole substrate. The model of the active site also suggests that Ser⁸⁸ hydrogen bonds to the N-9 of preQ₀, and this binding interaction is also available for indole-3-nitrile via N-1. The specific activity was measured to be 0.041 $\mu\text{M min}^{-1} \text{mg}^{-1}$, 4400-fold lower than the specific activity measured for preQ₀ turnover by YkvM. NADP⁺ production was also observed in assays containing indole-3-nitrile with Glu97Ala and to a lesser degree, the Glu97Leu mutant. The substrate tolerance exhibited by these mutants may be explained by the increased hydrophobic contacts of the active site afforded by the aliphatic substitutions. The reduced activity of the leucine mutant compared to the alanine may result from the steric effects of the larger side chain in the active site. To examine the substrate tolerance of YkvM for analogs that present an exocyclic amine for the active site, activity screens of YkvM, Glu97Ala, and Glu97Leu were conducted with 4-aminobenzonitrile. Although activity was still significantly decreased given the loss of the majority of substrate recognition determinants when this substrate was incubated with YkvM, measurable NADP⁺ production at a rate of 0.006 $\mu\text{M min}^{-1} \text{mg}^{-1}$ was observed. Measurable turnover with the amino-group containing analog is consistent with the role of Glu⁹⁷ in binding and anchoring of the substrate in the

active site. As demonstrated previously for preQ₀ with the Glu⁹⁷ mutants, reduced levels of NADP⁺ formation (ie. turnover) was detected in assays containing preQ₀ and either the Glu97Ala or Glu97Leu.

The above studies demonstrate that YkvM exhibits some level of substrate promiscuity (low levels of turnover by substrate analogs) and activity of these alternate substrates can be measured using the NADP⁺ fluorescence assay. However, the results of these preliminary screens for activity shows the active site is highly specific for preQ₀, and less than 0.001% activity is observed even for the best substrate analog tested, the indole-3-nitrile. It also remains to be determined whether the product formed from these reactions is indeed the corresponding amine, but based on these preliminary findings, this system is positioned to apply the concepts of directed evolution/rational design on YkvM with the goal of engineering a mutant enzyme with altered substrate selectivity and increased catalytic efficiency. An ideal mutant enzyme of this type would be capable of reducing the nitrile group of a small organic molecule that is not the natural substrate. The current focus of this work is the development of an engineered enzyme to catalyze the reduction of phenylacetonitrile to phenylethylamine. The activity screens showed the time-dependent production of NADP⁺ but at an activity less than 0.001% of wild-type NADP⁺ production in the presence of preQ₀. This number will serve as the baseline figure for the directed evolution of YkvM as a biocatalyst.

Progress towards the Total Synthesis of Epoxyqueuine.

This work also involved an attempted synthesis of epoxyqueuine, the nucleobase portion of the epoxyqueuosine product, to be used in analyzing spectroscopic data obtained from ^{13}C -labeled oQ produced in the QueA reaction. Retrosynthetic analysis suggested that this could be achieved by a convergent synthesis, the final steps involving the coupling of the deazaguanine core portion of epoxyqueuine with the carbocyclic moiety. The 7-dimethylamine-7-deazaguanine core was synthesized in six steps as previously described (85, 86) in an overall yield of 18 %. Stereospecific O-isopropylidene protected cyclopentenone was synthesized in three steps in good yields, and elaboration of the ribosyl moiety (stereospecific reduction, stereospecific epoxidation and tosylation) as proposed gave the tosyl-epoxide cyclopentene in excellent yields (85 %, 82 %, and 95 % yields). However, due to the possibility of a Payne rearrangement leading to a diastereomer of **20**, single crystal x-ray crystallography will be required to confirm the structure of tosylate **20**. If tosylate **20** with the desired stereochemical requirements cannot be obtained by this route, an alternate pathway to stereospecific **9** is proposed (Scheme 8). Since the epoxide moiety confers additional reactivities which may lead to multiple diastereomeric products, we propose to delay the addition of this group until the end of the synthesis. In the alternate synthetic scheme to elaborate ribosyl moiety **9**, stereospecific **18** is still acquired in 4 steps as described, and this intermediate is taken directly to activation of the alcohol **21**, followed by displacement with azide to **25**, and then reduction to

give the amine **26**. Epoxidation of this compound will then give **9**, and a complete 1-D, and 2-D NMR analysis will be carried out to confirm the desired stereochemistry. Coupling with the pyrrolo[2,3-*d*]pyrimidine **8** will then be carried out as shown in Scheme 4, and deprotection of the acetonide will afford epoxyqueuine.

Table 1. Steady-state kinetic parameters of YkvM.

	Kinetic Parameters		
	K_m (μM)	k_{cat} (min^{-1})	k_{cat}/K_m ($\text{M}^{-1} \text{s}^{-1}$)
preQ ₀	0.237 ± 0.045	0.66 ± 0.04	$(4.6 \pm 1.4) \times 10^4$
NADPH	19 ± 2	0.69 ± 0.02	$(6.1 \pm 0.2) \times 10^2$

Values are means \pm standard error

Table 2. Activity of YkvM and Cys55 mutants measured by UV-vis and fluorescence

Protein	Activity (UV-vis)	Activity (fluorescence)
YkvM	100%	100%
Cys55Ser	0%	< 0.0025%
Cys55Ala	0%	< 0.0004%

Mutant activity was measured as specific activity relative to the wild-type protein.

Table 3. Size exclusion chromatography protein standards

Protein	Molecular Weight (kDa)	K_D
Ovalbumin	44	0.910
Bovine serum albumin	66	0.830
Alcohol dehydrogenase	150	0.647
Pyruvate kinase	237	0.574
Apo-ferritin	443	0.454
Thyroglobulin	670	0.380

K_D values were calculated according to the equation $K_D = (V_e - V_0)/(V_T - V_0)$, where V_e is the elution volume of the protein of interest and determined with blue dextran (2,000 kDa), and V_T is the total bead volume and was determined with DNP-aspartate (300 kDa).

Table 4. Native molecular weight determination of YkvM and YkvM mutants

Protein	K_D	Estimated Molecular Weight kDa (number of subunits)
YkvM	0.573	239 (12.3)
C55S	0.580	231(11.9)
C55A	0.577	237 (12.2)
E97A	0.574	239 (12.3)
	0.569	244 (12.6)
E97Q	0.580	231 (11.9)
	0.581	230 (11.9)
E97D	0.578	237 (12.2)
	0.575	238 (12.3)
E97L	0.577	237 (12.2)
	0.569	244 (12.6)
E97K	0.573	239 (12.3)
	0.567	246 (12.7)

Table 5. Steady-state kinetic constants for the YkvM catalyzed reaction with stereospecifically deuterium labeled NADPH

	K_M (μM)	V_{max} ($\mu\text{M}/\text{min}$)	k_{cat} (min^{-1})	k_H/k_D
Unlabelled NADPH	18 ± 2	0.29 ± 0.02	0.70 ± 0.05	
(4 <i>S</i>)-[4- ^2H]NADPH	20 ± 3	0.26 ± 0.02	0.63 ± 0.05	1.11 ± 0.10
(4 <i>R</i>)-[4- ^2H]NADPH	19 ± 2	0.11 ± 0.02	0.27 ± 0.05	2.59 ± 0.10

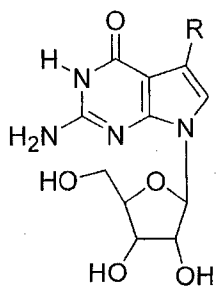
Values are means \pm S.E.

Table 6. Kinetic characterization of the YkvM Glu⁹⁷ mutants

Protein	Specific Activity ($\mu\text{M min}^{-1} \text{mg}^{-1}$)	Relative Activity (%)	K_m (preQ ₀) (μM)	k_{cat} (min^{-1})	k_{cat}/K_m ($\text{M}^{-1} \text{s}^{-1}$)
YkvM	180.9	100	0.237 ± 0.045	0.66 ± 0.04	$(4.6 \pm 1.4) \times 10^4$
Glu97Ala	7.76	4.3	30 ± 5	0.045 ± 0.003	25 ± 1
Glu97Gln	3.38	1.9	67 ± 4	0.036 ± 0.002	9.0 ± 0.8
Glu97Asp	9.32	5.2	7.6 ± 1.3	0.051 ± 0.002	110 ± 4
Glu97Leu	11.21	6.2	N.D.	N.D.	N.D.
Glu97Lys	5.54	3.1	N.D.	N.D.	N.D.

Specific activity was measured based on NADPH oxidation

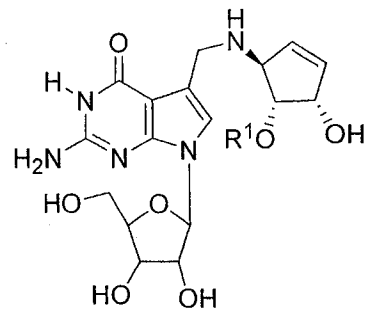
N.D. Not Determined



1 R = $\text{—}\overset{\text{NH}}{\text{C}}\text{—NH}$ Archaeosine

R = —CN preQ₀ nucleoside

R = $\text{—CH}_2\text{—NH}_2$ preQ₁ nucleoside



2 R¹ = H, queuosine

3 R¹ = $\beta\text{-D-mannose}$

4 R¹ = $\beta\text{-D-galactose}$

Figure 1. Structures of the 7-deazaguanosine bases present in tRNA.

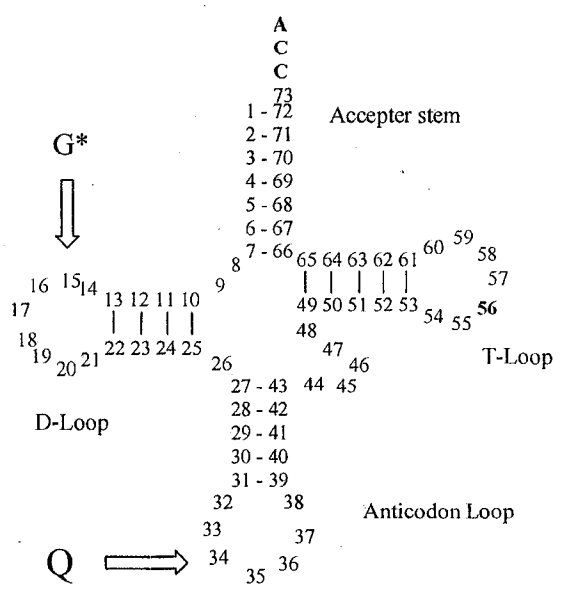


Figure 2. Physiological occurrence of the 7-deazaguanosine modifications in tRNA.

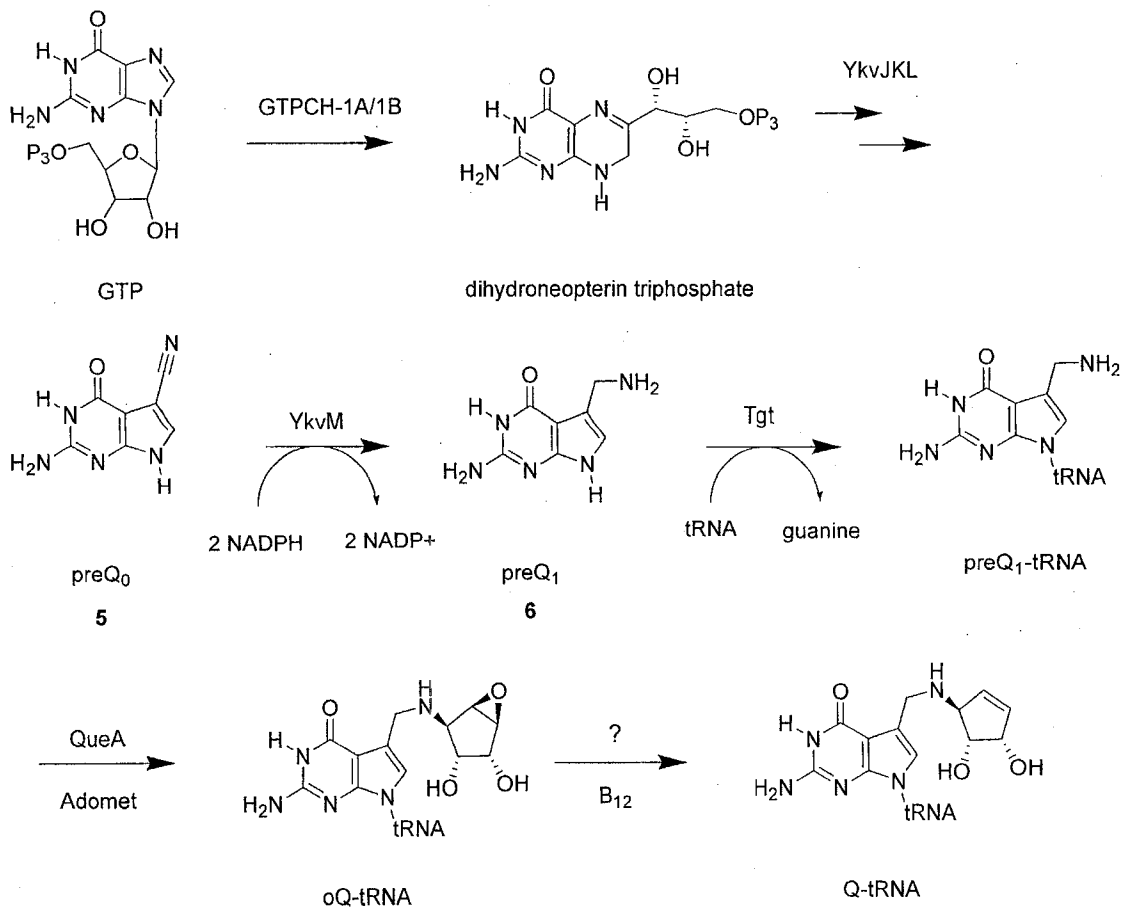


Figure 3. The *de novo* biosynthesis of queuosine in bacteria.

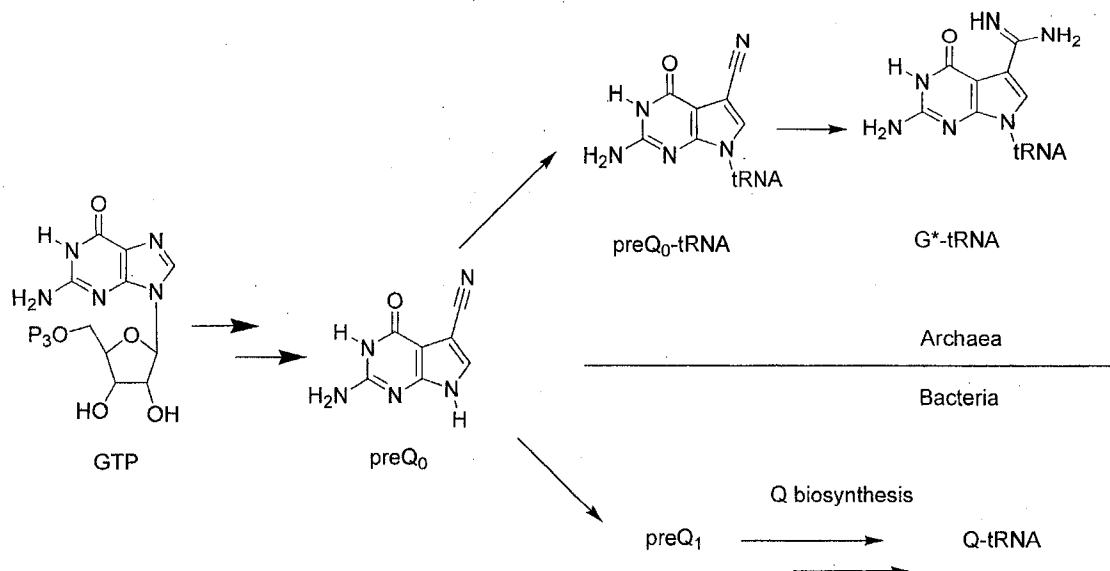


Figure 4. The biosynthesis of archaeosine and the phylogenetic distribution of G* and Q in archaea and bacteria.

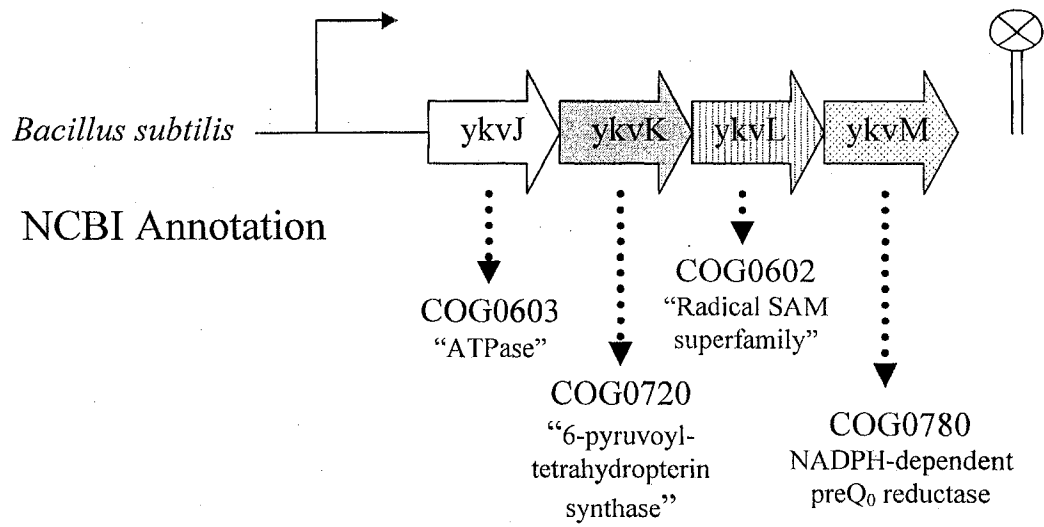


Figure 5. Uncharacterized operon involved in Q biosynthesis.

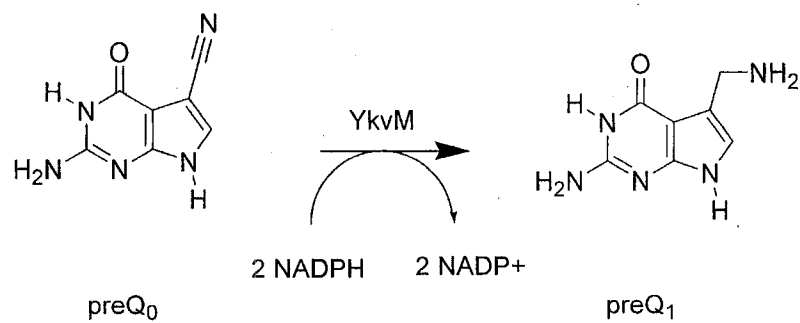


Figure 6. The reaction catalyzed by *Bacillus subtilis* YkvM. YkvM is a NADPH-dependent oxidoreductase and catalyzes the two-fold reduction of the nitrile group of preQ₀ to give preQ₁.

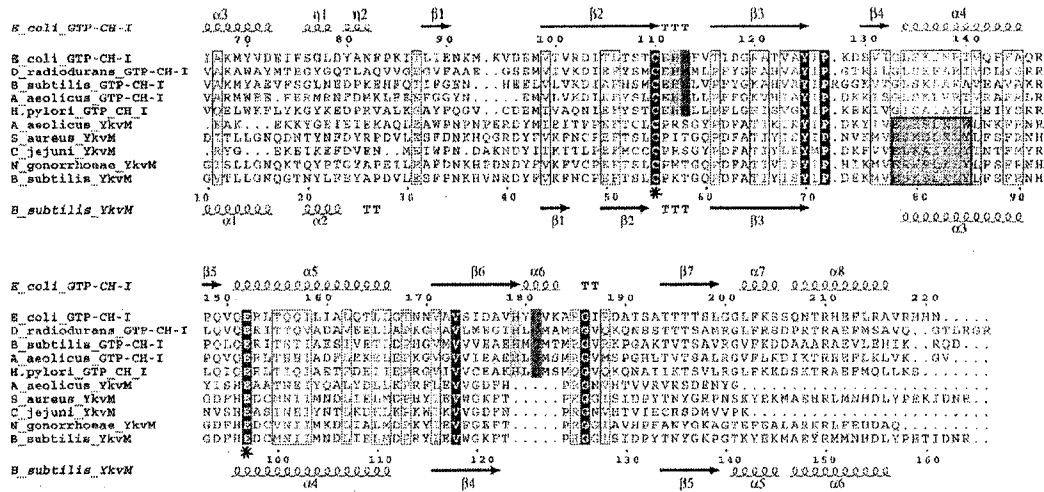


Figure 7. Sequence alignment of GTP-cyclohydrolase I and QueF. The conserved Cys and Glu found in the substrate binding pocket of both protein families are indicated by asterisks. The QueF motif, specific for the QueF family, is highlighted in green. The zinc binding His and Cys residues found in FoliE and not in QueF are highlighted in blue. Other catalytic residues in FoliE not found in QueF are highlighted in yellow.

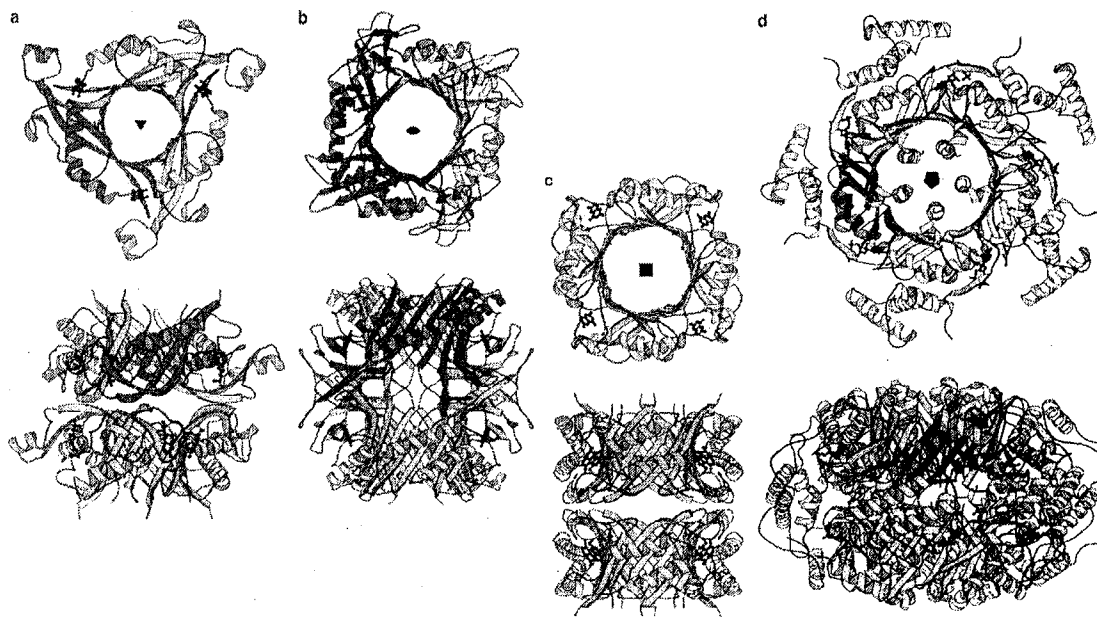
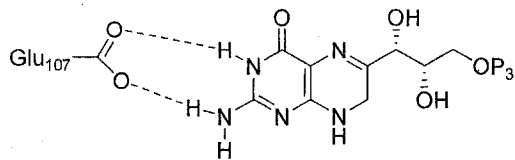
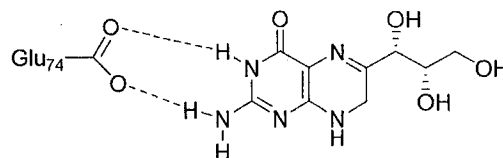


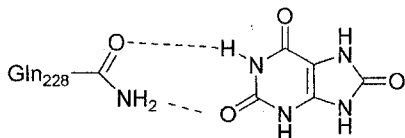
Figure 8. Multimeric barrels generated by T-folds for four functionally different enzymes. The T-fold monomer units are shown in color, and the location of the active sites are shown. a. The barrel of PTPS is built from three T-folds related by a three-fold axis. b. The barrel of UOX is built from two monomers (four T-folds) with the two barrels superimposed face to face. c. The monomer of DHNA is composed of one T-fold and the barrel is built from four T-folds. d. The monomer of GTPCHI has a C-terminal T-fold followed by a helix. The barrel is built from five monomers (five T-folds). The enzymes are comprised of two barrels superposed face to face (Colloc'h, N. *et al. Proteins* (2000) 39, 142-154).



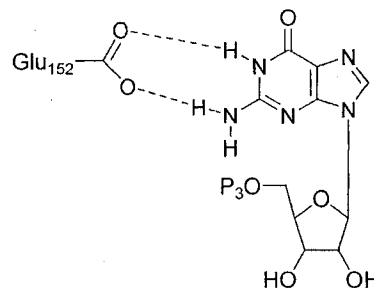
6-pyruvoyltetrahydropterin synthase



dihydroneopterin aldolase



urate oxidase



GTP cyclohydrolase

Figure 9. The role of the universally conserved glutamate/glutamine in T-fold proteins. The conserved residues are present in the active site of the proteins where it forms two hydrogen bonds to the substrate and is positioned to serve as an acceptor for the pyrimidine ring.

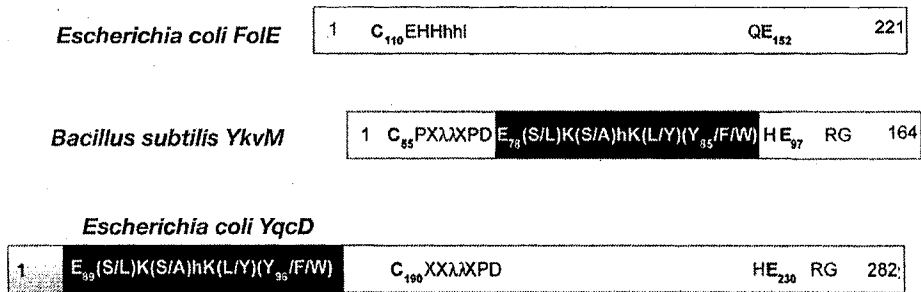


Figure 10. Primary structure organization of the YqcD and YkvM subfamilies of QueF. *B. subtilis* YkvM and the QueF type I proteins are comparable in size with bacterial and mammalian FolE and exist in solution in dodecameric form, whereas *E. coli* YqcD and the QueF type II proteins are larger and are present in solution as dimers.

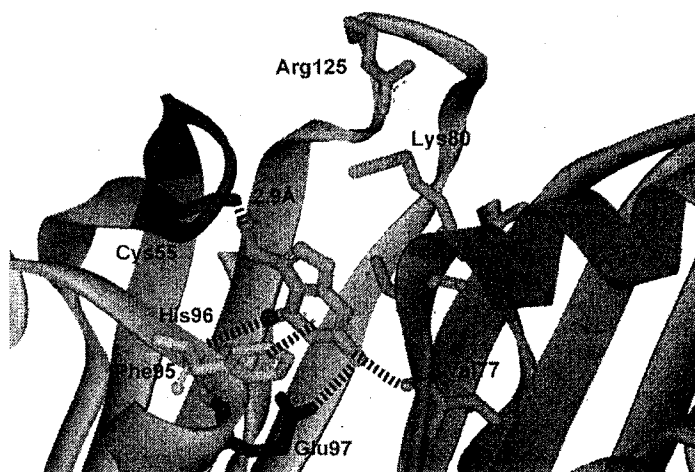


Figure 11. Homology model of the putative YkvM active site. The homology model was built by threading the YkvM sequence through the crystal structure of *E. coli* GTP cyclohydrolase. The active site is located at the interface between two monomers shown in light and dark grey. Potential active-site interactions are indicated. Cys⁵⁵ is positioned 2.9 Å from the nitrile of preQ₀ and is implicated in catalysis. Glu⁹⁷ is shown forming a salt bridge with the N²-amine of preQ₀. The conserved QueF motif is highlighted in green.

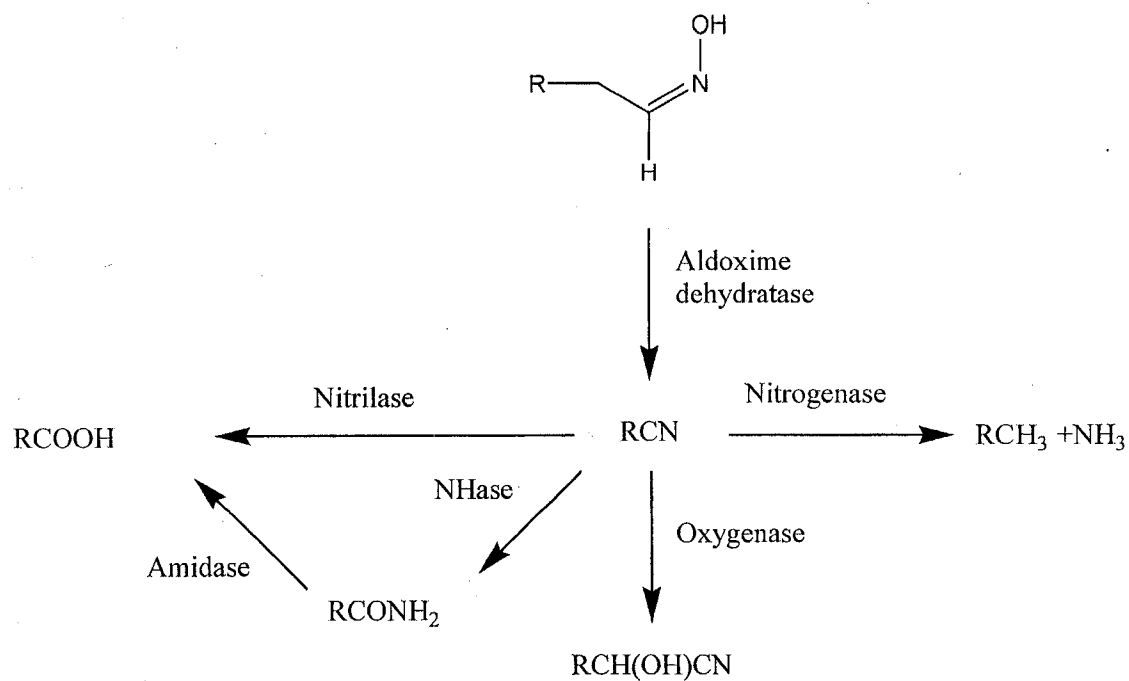


Figure 12. Different pathways of nitrile metabolism.

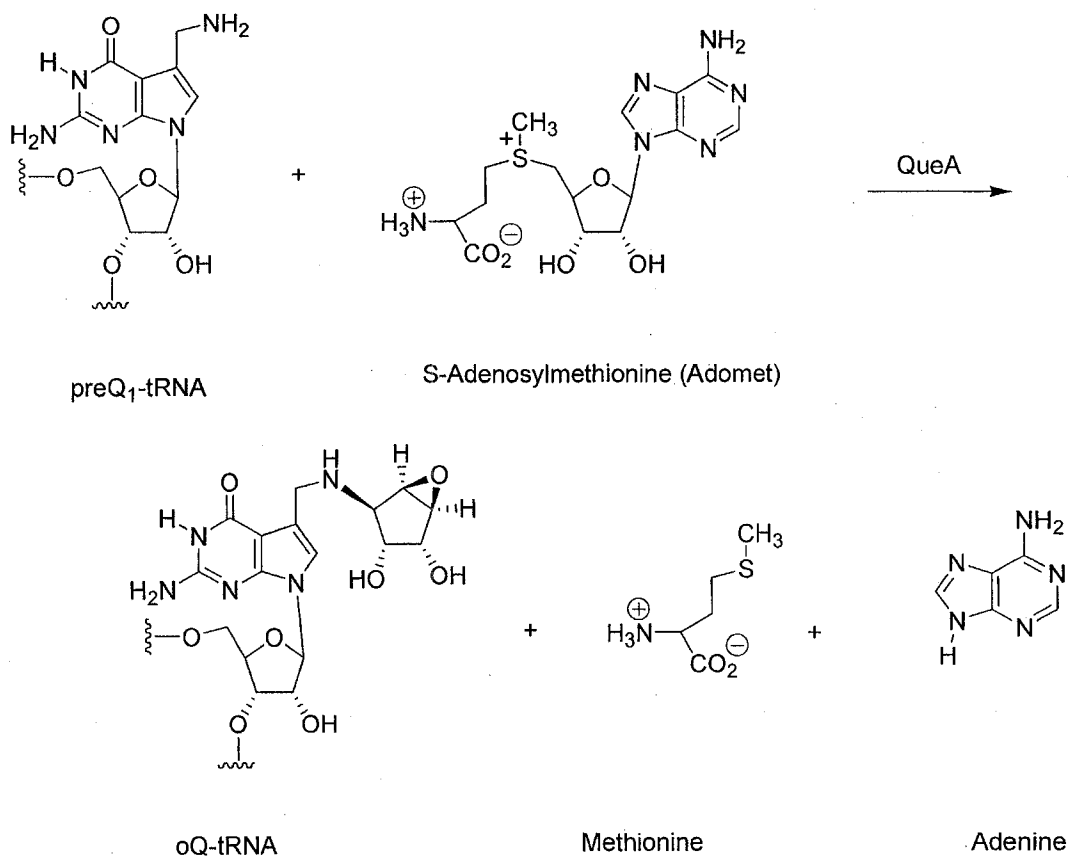


Figure 13. The reaction catalyzed by QueA. The QueA catalyzed reaction promotes the transfer and isomerization of the ribosyl moiety of S-adenosylmethionine to preQ₁-tRNA. The products are methionine and adenine and oQ-tRNA.

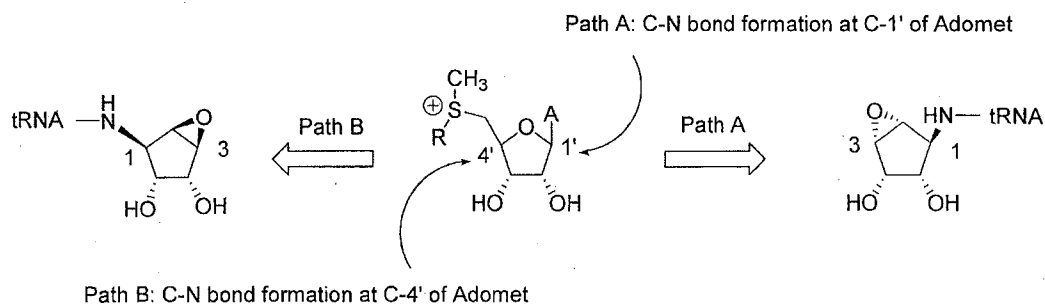


Figure 14. Regiochemistry of C-N bond formation catalyzed by QueA. Chemical constraints of C-N bond formation between preQ₁-tRNA and Adomet. Path A implicates C-N bond formation at C-1' of Adomet leading to the diol syn to the epoxide. In Path B, the primary amine of preQ₁-tRNA forms a bond at C-4' of Adomet. This route ultimately leads to an anti diol and epoxide. Only Path B is consistent with the known absolute stereochemistry of Adomet and oQ-tRNA.

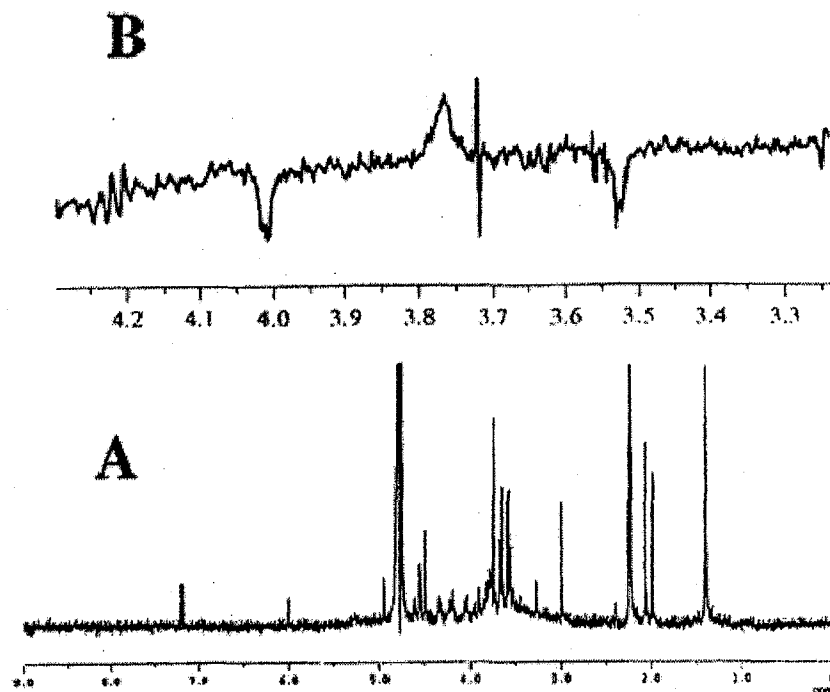


Figure 15. $[1\text{-}^{13}\text{C}]\text{AdoMet}$ labeling studies of the QueA reaction. 1-D ^1H spectra of $[^{13}\text{C}]\text{oQ}$ generated from $[1\text{-}^{13}\text{C}]\text{AdoMet}$. (A) The carbon-hydrogen coupled ^1H NMR spectrum. The carbon-hydrogen decoupled spectrum (not shown) was qualitatively identical to the coupled spectrum. (B) A portion of the ^1H NMR difference spectrum (decoupled minus coupled) showing the resonance of the hydrogen directly bonded to the ^{13}C -enriched spectrum (3.77 ppm, $J_{\text{C-H}} = 193$ Hz). The figure is reproduced from Kinze, SD *et al.*, *Org Lett.*, 2000, 2, 9, 1307-1310.

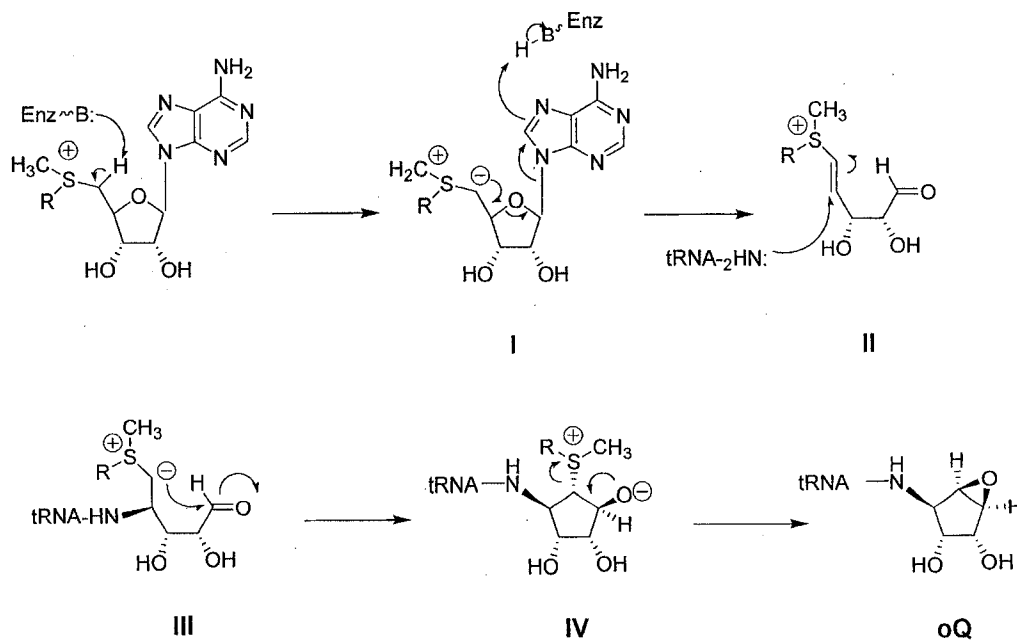


Figure 16. The proposed chemical mechanism of QueA. General base catalyzed deprotonation occurs as the initial step to form a sulfonium ylide (I). Collapse of the ylide leading to ring opening and the concomitant elimination of adenine forms a vinyl sulfonium (II). Nucleophilic attack on the re-face of the vinyl sulfonium by the primary amine of preQ₁-tRNA forms a second sulfonium ylide (III). Intramolecular attack on the si-face at C-1' forms the alkoxy-carbocycle (IV). Intramolecular S_N² of the nascent alkoxide releases methionine and forms the epoxide of oQ-tRNA.

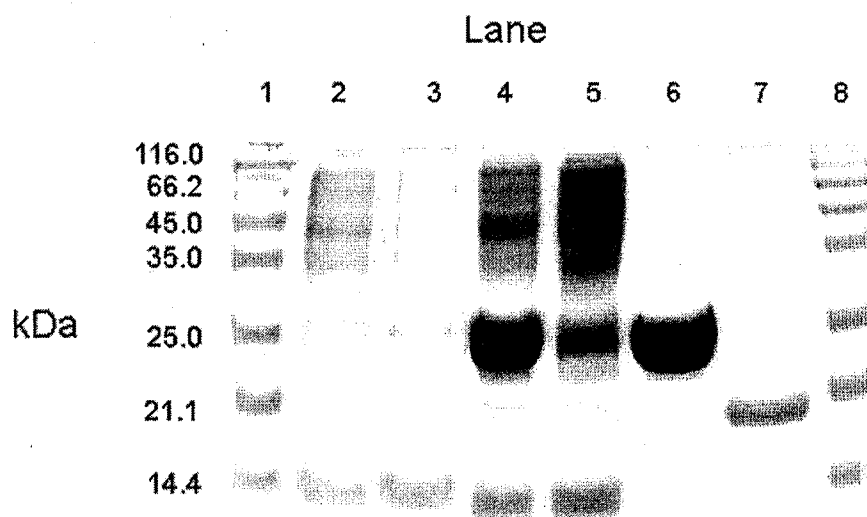


Figure 17. SDS-PAGE gel illustrating the purification of *B. subtilis* YkvM. Lane 1 and lane 8, molecular weight markers, lane 2, *E. coli* BL21 without the pET30-*ykvM* plasmid, lane 3, *E. coli* BL21 containing the pET30-*ykvM* plasmid prior to induction with IPTG, lane 4, *E. coli* BL21 containing the pET30-*ykvM* plasmid after 4 h induction with IPTG, lane 5, Ni²⁺-NTA column flow through wash, lane 6, recombinant his₆-YkvM, lane 7, native YkvM.

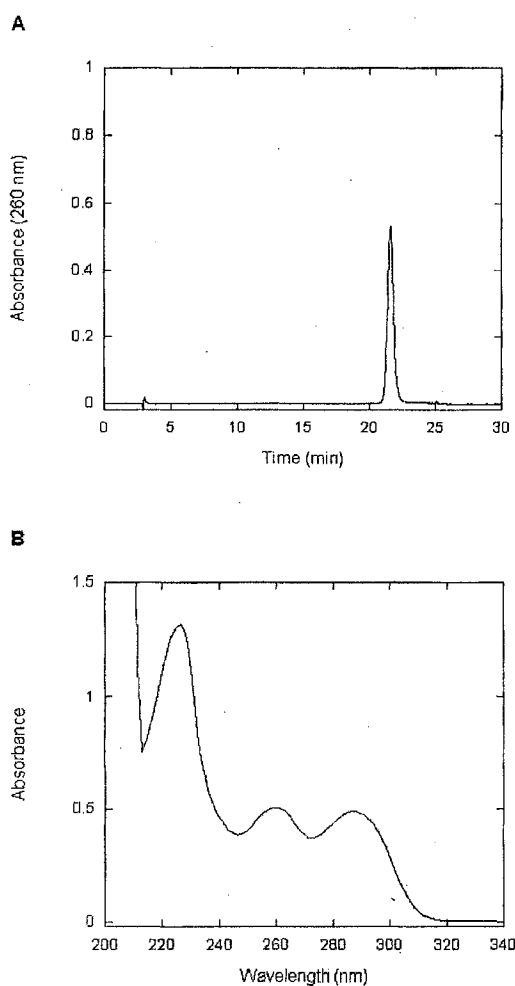


Figure 18. The purification and characterization of preQ₀. PreQ₀ was synthesized and described by Migawa, M. T., *et al.*, *Synth. Comm.*, 1996, 26(17), 3317-3322. For enzymatic work, preQ₀ was purified by semi-preparative HPLC (A) eluting at 22 min under an isocratic mobile phase of 4% acetonitrile in 20 mM ammonium acetate (pH 6.0). The product was identified by its characteristic UV-vis chromophore (B, [preQ₀] = 50 μM) with maxima at 226, 262, and 288 nm.

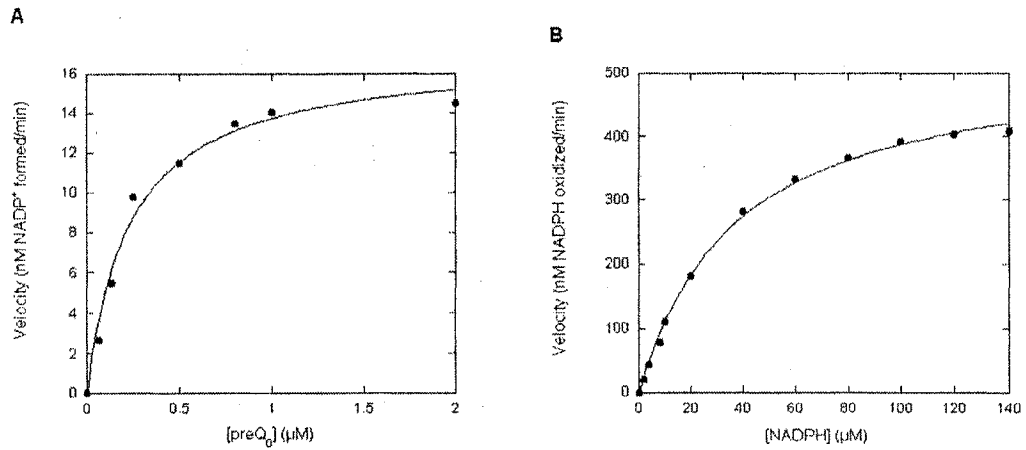


Figure 19. Steady state kinetic analysis of YkvM. Assays were performed in 100 mM Tris/HCl pH 7.5, 100 mM KCl, and 1 mM DTT. **(A)** For the determination of preQ₀ kinetic parameters, NADPH was held constant at 400 µM, and preQ₀ was varied between 0.066-2 µM. **(B)** For the determination of the NADPH kinetic parameters, preQ₀ was held at 20 µM while NADPH was varied between 5-140 µM.

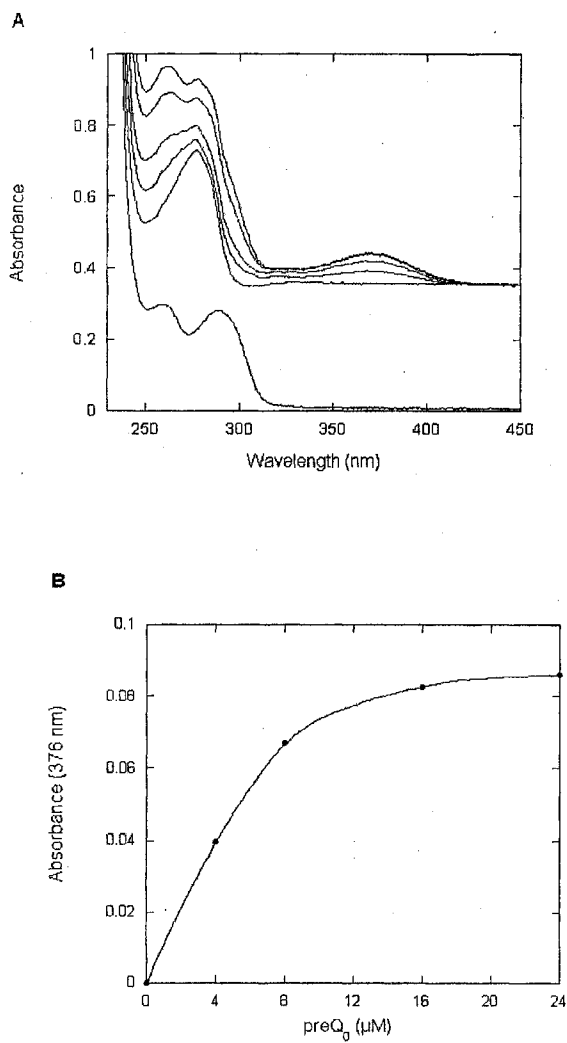


Figure 20. Titration of YkvM with preQ₀. **(A)** The UV-Vis spectrum of 20 μM preQ₀ (bottom curve), and above, a scan of protein alone, followed by successive additions of substrate 4 μM, 8 μM, 16 μM, and 24 μM. **(B)** A replot of the absorbance values of the new peak at 376 nm.

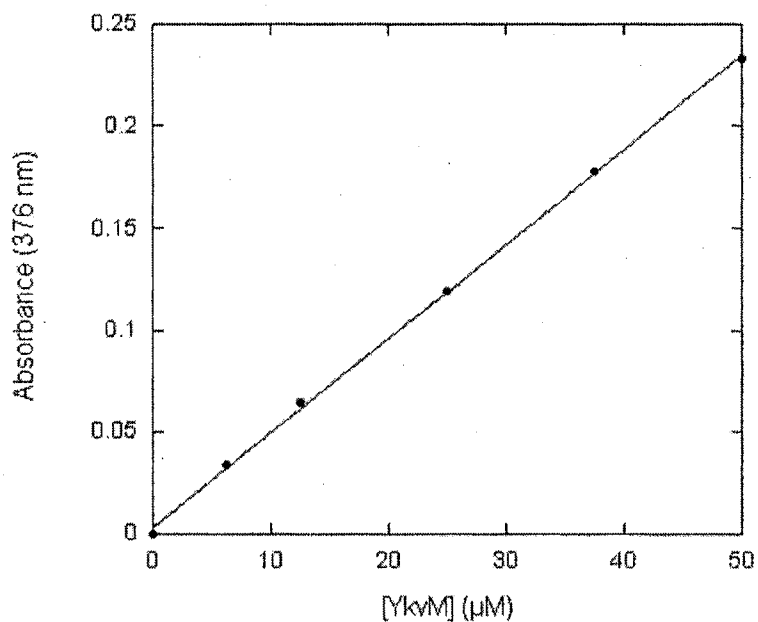


Figure 21. Measurement of the extinction coefficient of the absorbance band at 376 nm. Dilutions of a reaction mixture containing 10 mM phosphate (pH 7.5), 10 mM KCl, 1 mM DTT, 100 μM preQ₀, and 50 μM YkvM were made using a stock dilution buffer of 10 mM phosphate (pH 7.5), 10 mM KCl, and 1 mM DTT. A two-fold excess of preQ₀ was used to ensure for the complete saturation of the protein active sites. Linear regression analysis of the data from triplicate determinations indicate the extinction coefficient of the band at 376 nm is $4,353 \pm 89 \text{ M}^{-1}$.

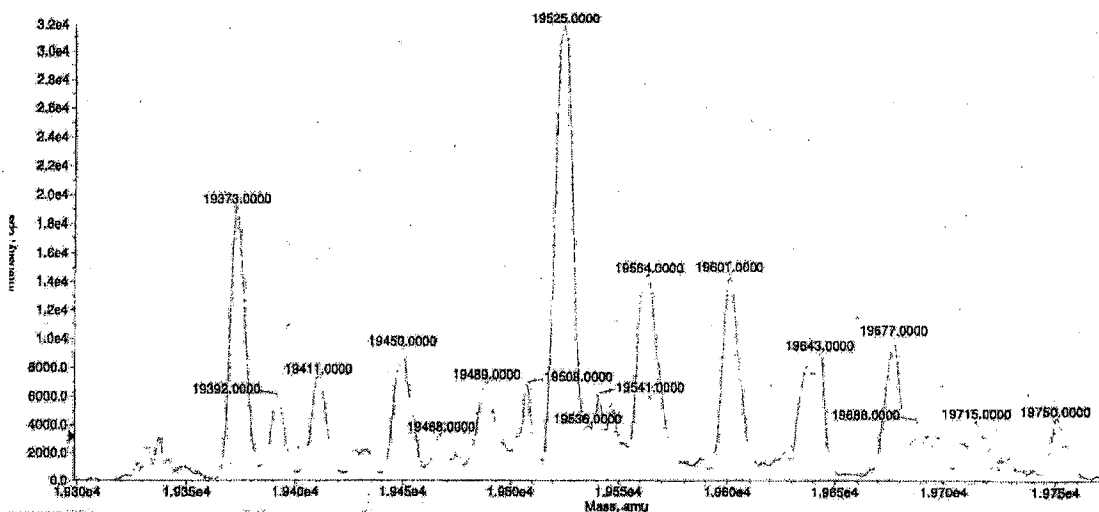


Figure 22. Molecular weight analysis of wild-type YkvM by mass spectrometry. The mass spectrum obtained for the native protein of YkvM showed the expected parental mass peak at 19 373 Da, and the associated potassium ion adducts (in ascending order), 19 411 Da, 19 450 Da, 19 489 Da, 19 525 Da, 19 564 Da, 19 601 Da.

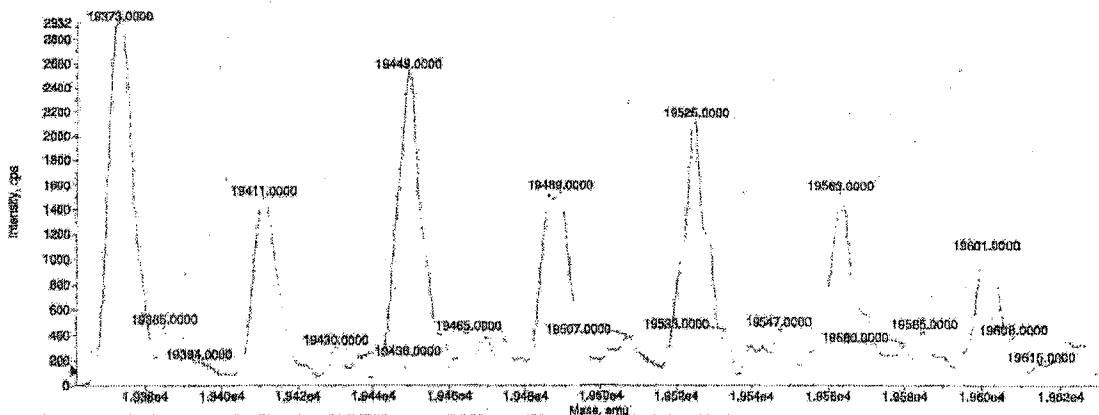


Figure 23. Detection of the YkvM-preQ₀ covalent adduct by mass spectrometry. A 5-fold excess of preQ₀ was incubated with YkvM for 5 min at room temperature before acidification and injection onto the mass spectrometer. The resulting spectrum showed, in addition to the parent peaks of YkvM (see Figure 22), a minor peak at 19 547 Da. This molecular mass is consistent with the covalent attachment of one molecule of preQ₀ (M.W. 175 Da). The additional series of peaks in this spectrum, 19 585 Da, and 19 625 Da are attributed to the potassium adducts of the protein-substrate complex.

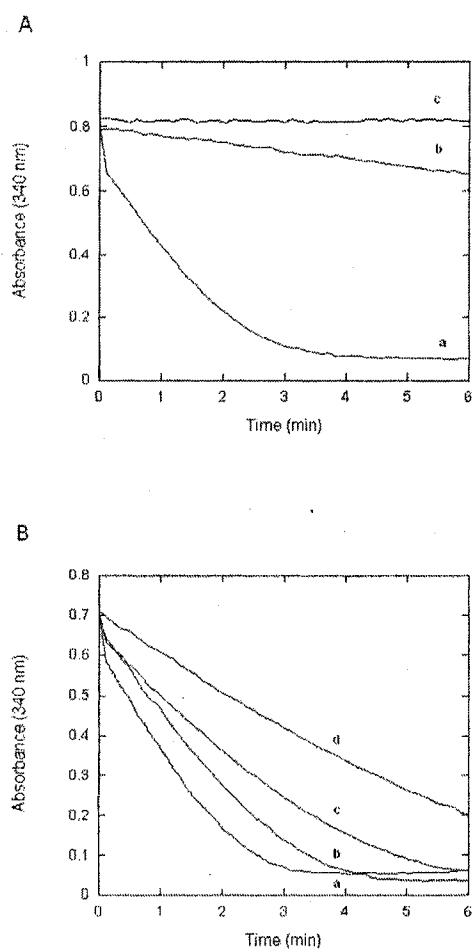


Figure 24. Thiol inactivation studies of YkvM. The inactivation of YkvM with iodoacetamide (**A**) and protection of enzyme (**B**) in the presence the substrate. Aliquots of a solution containing enzyme (5 μ M) and iodoacetamide (50 μ M) were removed at specified time points (**a**) 0 min, (**b**) 2 min, (**c**) 8 min, and diluted 20-fold into to a standard assay solution containing 100 μ M preQ₀ and 100 μ M NADPH prior to analysis. The protection assays, (**a**) 0 min, (**b**) 8 min, (**c**) 14 min, and (**d**) 20 min, were carried out in the same manner except the pre-incubation mixture included 100 μ M preQ₀.

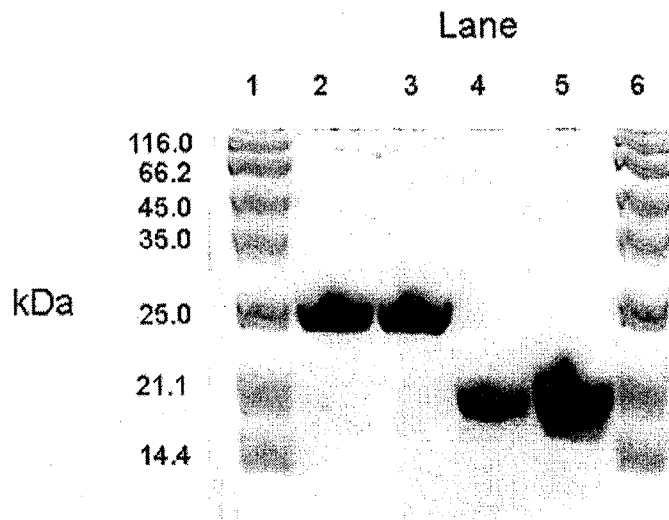


Figure 25. The purification of YkvM Cys⁵⁵ mutants Cys55Ser and Cys55Ala. Lane 1 and lane 6, molecular weight markers, lane 2, his₆-YkvM-C55S purified by Ni²⁺-NTA affinity chromatography, lane 3, his₆-YkvM-C55A purified by Ni²⁺-NTA affinity chromatography, lane 4, YkvM-C55S after treatment with Factor Xa and purification by Ni²⁺-NTA affinity chromatography, lane 5, YkvM-C55A after treatment with Factor Xa and purification by Ni²⁺-NTA affinity chromatography.

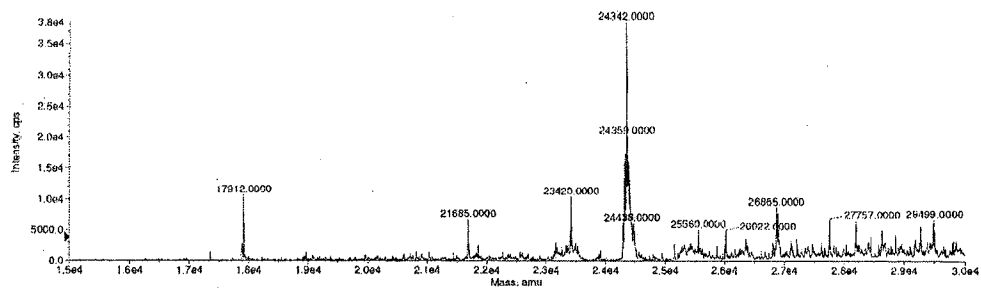
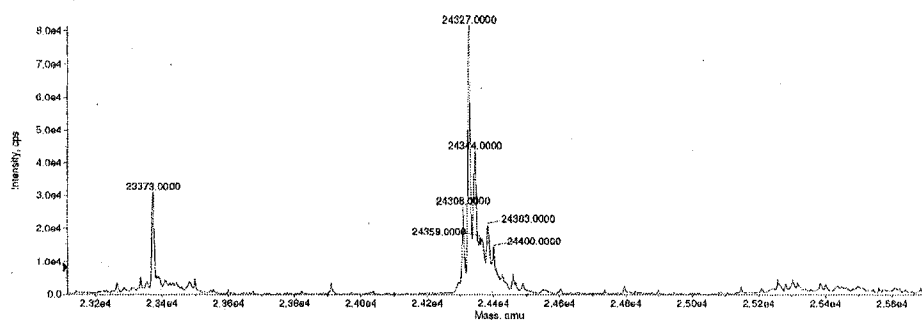
A**B**

Figure 26. Mass analysis of (A) YkvM C55S and (B) YkvM C55A. Prior to analysis, the proteins were dialyzed into 5 mM phosphate buffer (pH 7.5), 5 mM KCl, and 1 mM DTT. The parent molecular masses of the recombinant mutant proteins are consistent with the values of his₆-YkvM containing only the desired mutation.

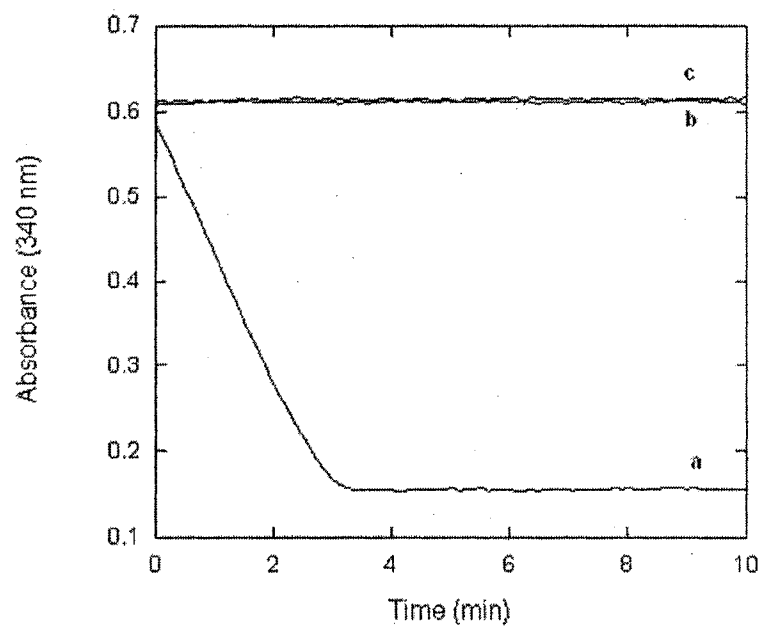


Figure 27. UV-Vis spectroscopy based assay of the YkvM Cys⁵⁵ mutants following the oxidation of NADPH at 340 nm. The assay solution contained 10 mM Tris (pH 7.5), 10 mM KCl, 1 mM DTT, 35 μM preQ₀, 100 μM NADPH and enzyme at 30°C. (a) 3 μM YkvM, (b) 650 μM C55A, (c) 270 μM C55S.

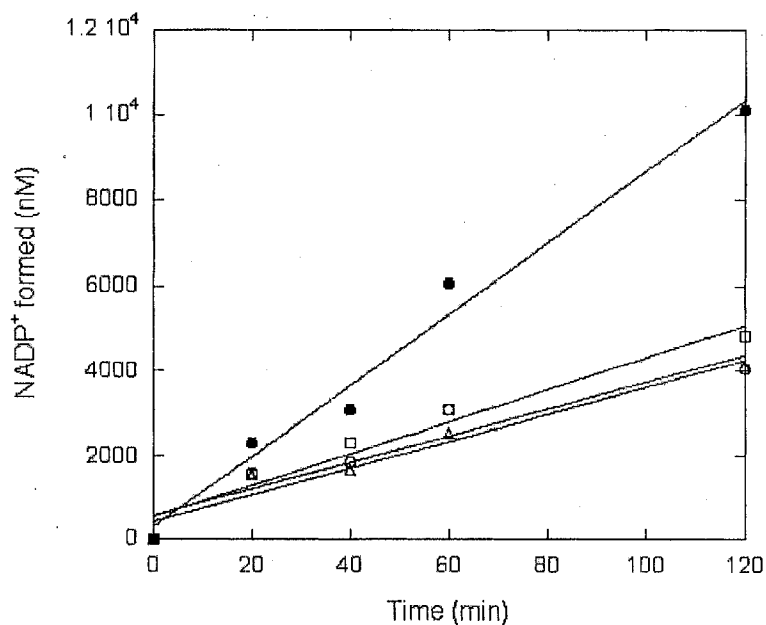


Figure 28. Fluorescence based activity assay of the YkvM Cys⁵⁵ mutants following the formation of the NADP⁺ alkaline degradation product. The assay solution contained 10 mM phosphate buffer (pH 7.5), 10 mM KCl, 1 mM DTT, 60 μM preQ₀, 400 μM NADPH and variable [protein] at 30°C. At the time points indicated, an aliquot of the reaction mixture was removed and subjected to workup as described in Materials and Methods. The plot shows the NADP⁺ formed from an assay containing 66 nM YkvM (●), 250 μM C55S (□), 300 μM C55A (Δ), and 66 nM YkvM with no substrate (○). This plot correlates to less than 1% of substrate turnover during the time period analyzed, and enzyme activity was calculated from the comparisons of the initial velocities obtained from a linear fit of these data.

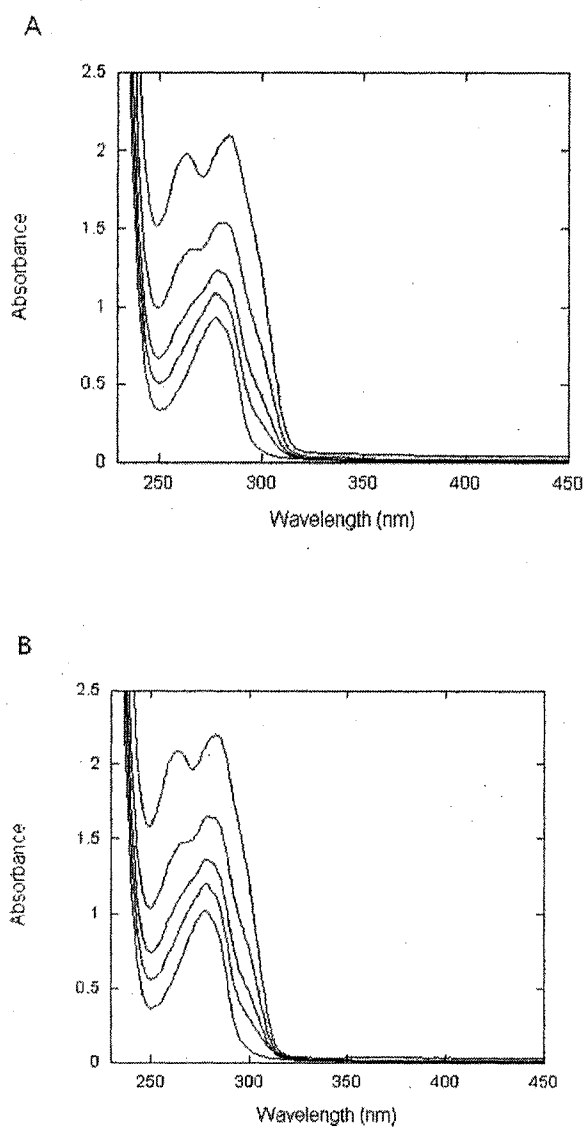


Figure 29. Substrate titrations studies of the YkvM mutants C55A (A) and C55S (B).

The reaction contained 50 μM protein (lowest curve), followed by successive additions of preQ₀ to 25 μM , 50 μM , 100 μM , and 200 μM . The absorbance band at 376 nm is not observed.

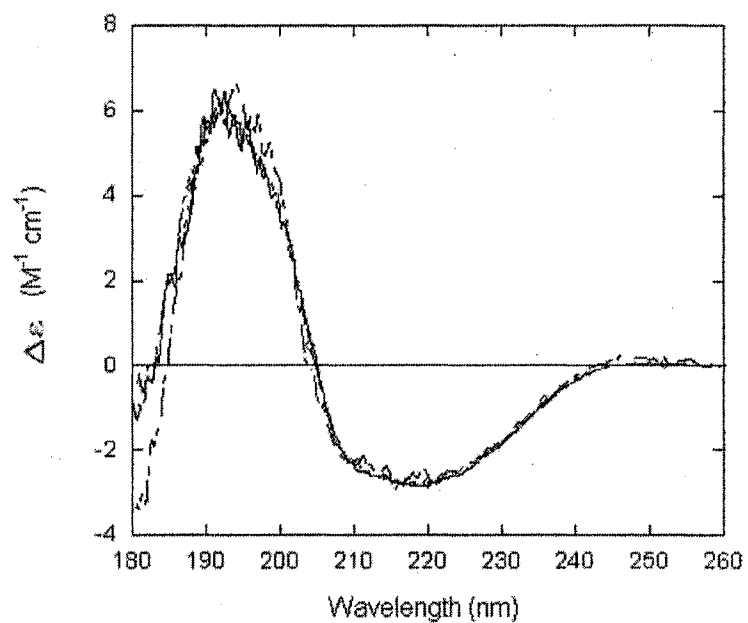


Figure 30. Comparison of circular dichroism spectra of YkvM (—), C55A (— —), and C55S (— —). The enzyme concentrations were at 2 mg mL^{-1} in 20 mM phosphate buffer (pH 7.5) and 20 mM NaF. The spectra were obtained as described in Materials and Methods.

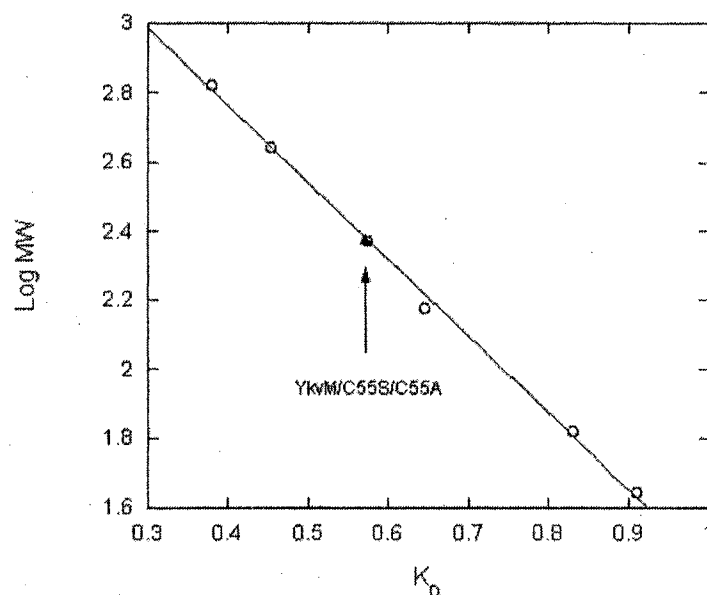


Figure 31. Size exclusion chromatography of YkvM and the Cys⁵⁵ mutants. Size exclusion chromatography was performed on a BioSep-SEC-S4000 column (Phenomenex). The mobile phase was 50 mM phosphate (pH 7.2) at a flow rate of 1 mL min⁻¹. The void volume (V_0) and the total volume (V_T) were measured with blue dextran (2,000 kDa) and DNP-aspartate (300 Da), respectively. Calibration of the column was conducted with the following protein standards: thyroglobulin (670 kDa), apo-ferritin (443 kDa), pyruvate kinase (237 kDa), alcohol dehydrogenase (150 kDa), bovine serum albumin (66 kDa), and ovalbumin (44 kDa). K_D values were calculated according to the equation $K_D = (V_e - V_0)/(V_T - V_0)$, where V_e is the elution volume of YkvM or the mutant proteins. The proteins YkvM, C55S and C55A (▲) elute with a volume corresponding to a native molecular weight of 235 kDa.

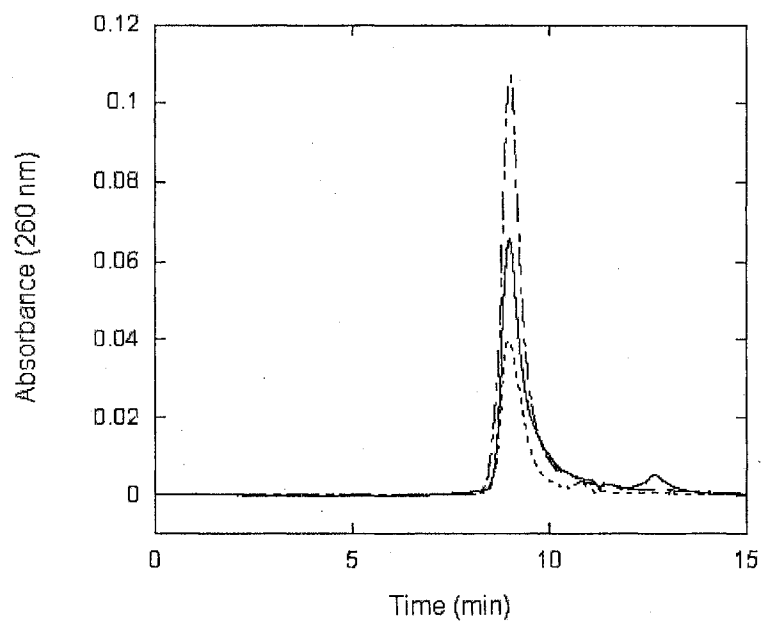


Figure 32. Comparative trace of YkvM (—), C55S (— —), and C55A (— —) by size exclusion chromatography. The traces were obtained as described for the protein standards.

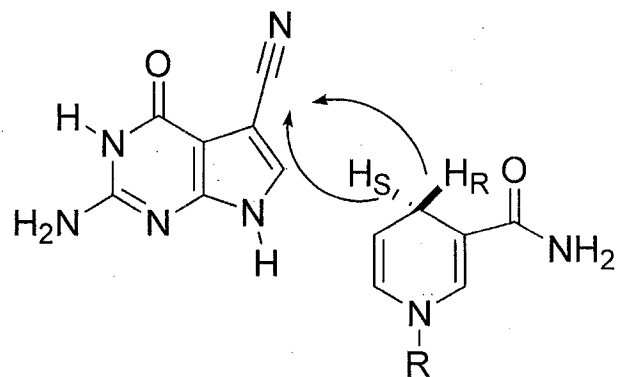


Figure 33. Stereospecificity of hydride transfer catalyzed by YkvM. According to Bentley's Rule, the active site of YkvM is oriented to promote exclusively either the *pro-R* or *pro-S* hydride of NADPH.

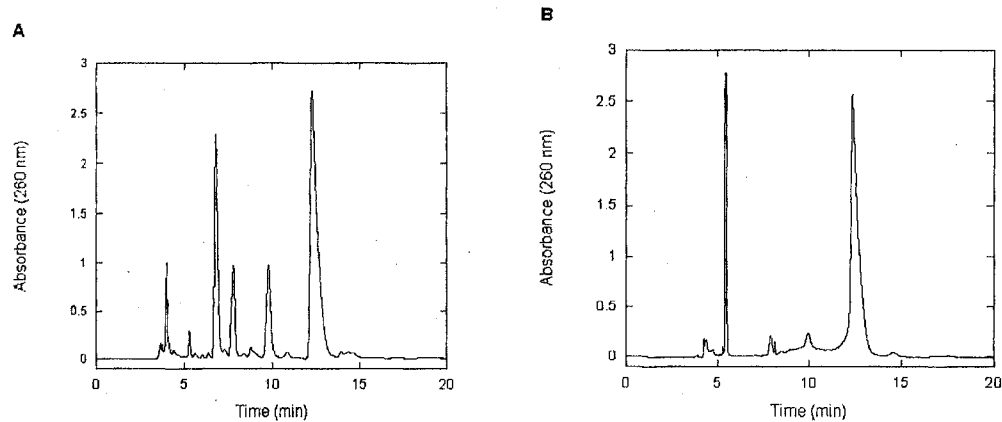


Figure 34. Purification of *pro-S* (A) and *pro-R* (B) deuterium labeled NADPH.

Reduced cofactors were purified on a semipreparative Luna C18 column (250 × 10 mm, 5 μm) from Phenomenex. The products were separated during a 20-min run of isocratic 75 mM NaCl buffered with MTEN (5 mM 4-morpholineethanesulfonic acid, 2.5 mM Tris base, 2.5 mM ethanolamine, and an additional 10 mM NaCl) adjusted to pH 8.2 (96). The flow rate was 3 mL min⁻¹. NADPH was eluted between 12.5-14 mins and was identified by the characteristic absorbance at 340 nm.

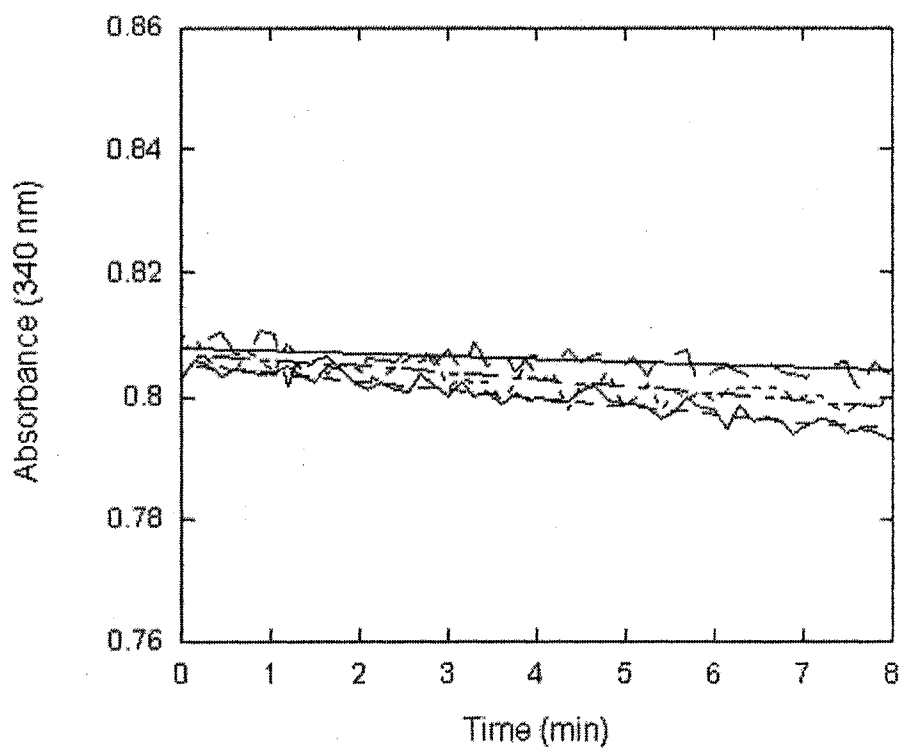


Figure 35. YkvM reaction using stereoisotopically labeled cofactor. The activity assays contained 10 mM phosphate buffer (pH 7.5), 10 mM KCl, 1 mM DTT, 20 μ M preQ₀, 1 μ M YkvM, and 130 μ M unlabeled (— —), stereospecifically *pro-S* (- -), or *pro-R* (—△—) deuterium labeled NADPH.

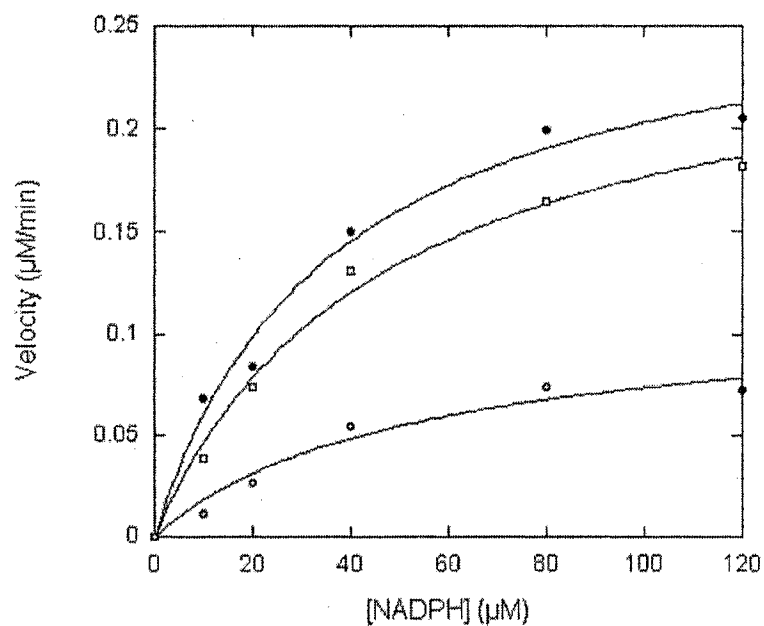


Figure 36. Steady-state kinetic analysis of YkvM using *pro-R* labeled, *pro-S* labeled, and unlabeled NADPH. YkvM assays were performed in 10 mM Tris (pH 7.5), 10 mM KCl, 1 mM DTT, 20 µM preQ₀, 1 µM YkvM and variable (10-120 µM) of (4*S*)-[4-²H]NADPH (□), (4*R*)-[4-²H]NADPH (○), or unlabelled NADPH (●). The reaction was monitored by following the oxidation of NADPH at 340 nm at 30°C. Assays were performed in triplicate, and the data points represent the mean values from these determinations. The data was fit to the rate equation describing NADPH (equation 3) using Kaleidagraph to extract the kinetic parameters.

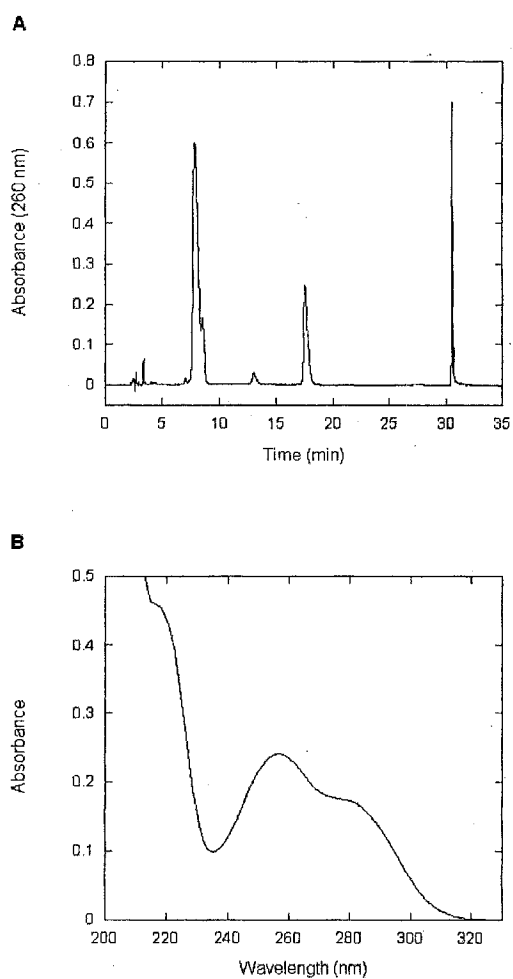


Figure 37. Purification and analysis of preQ₁ generated from deuterium labeled cofactors. (A) PreQ₁ was purified by semi-preparative column HPLC and the product was identified by (B) its characteristic chromophore consisting of a peak at 258 nm with a shoulder at 282 nm. The column was developed with an isocratic run of 20 mM ammonium acetate (pH 6.0) at a flow rate of 5 mL min⁻¹ to elute preQ₁ at 18 min.

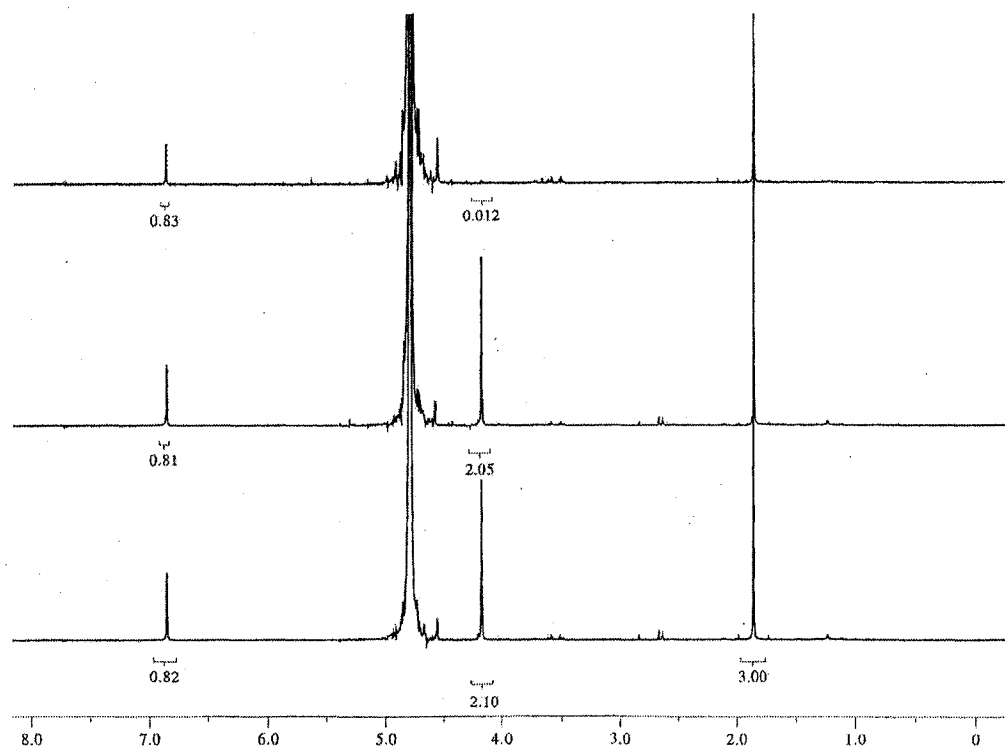


Figure 38. ^1H -NMR analysis of preQ_1 generated from deuterium labeled cofactors. The enzymatic products generated and purified as described in Experimental Procedures were dissolved in 0.6 mL D_2O and analyzed by ^1H -NMR. The overlay shown compares the spectra obtained from unlabelled NADPH (*bottom*), *pro-S* deuterium labeled NADPH (*middle*), and *pro-R* deuterium labeled NADPH (*top*).

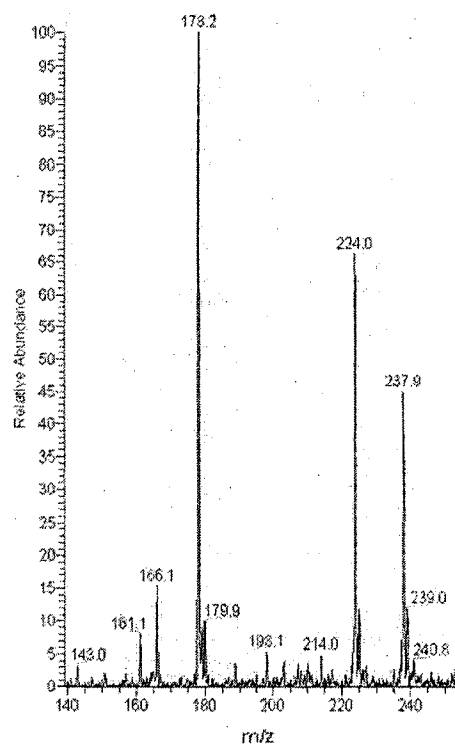


Figure 39. Mass spectrum of preQ₁ generated from unlabeled NADPH. Data was obtained by direct infusion into an electrospray ionization mass spectrometer and the data was collected in the negative mode. The spectrum shows free base form of preQ₁ (m/z 178.2) in addition to preQ₁ as the acetate salt (m/z 237.9).

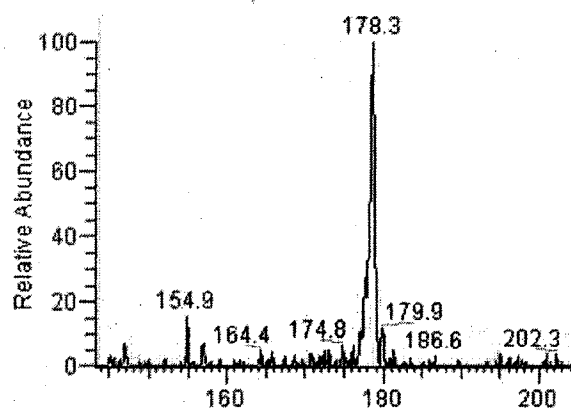
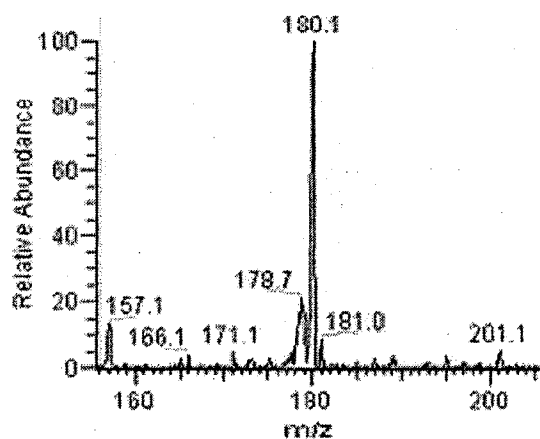
A**B**

Figure 40. Mass spectrum of preQ₁ generated from *pro-S* (A) and *pro-R* (B) stereospecifically deuterium labeled NADPH. The parent mass of PreQ₁ generated from *pro-S* labeled cofactor is consistent with preQ₁ generated from unlabelled NADPH and the calculated molecular weight of preQ₁, while preQ₁ recovered from incubations with *pro-R* deuterium labeled NADPH is marked by a *m/z* shift of 2 in the mass spectrum.

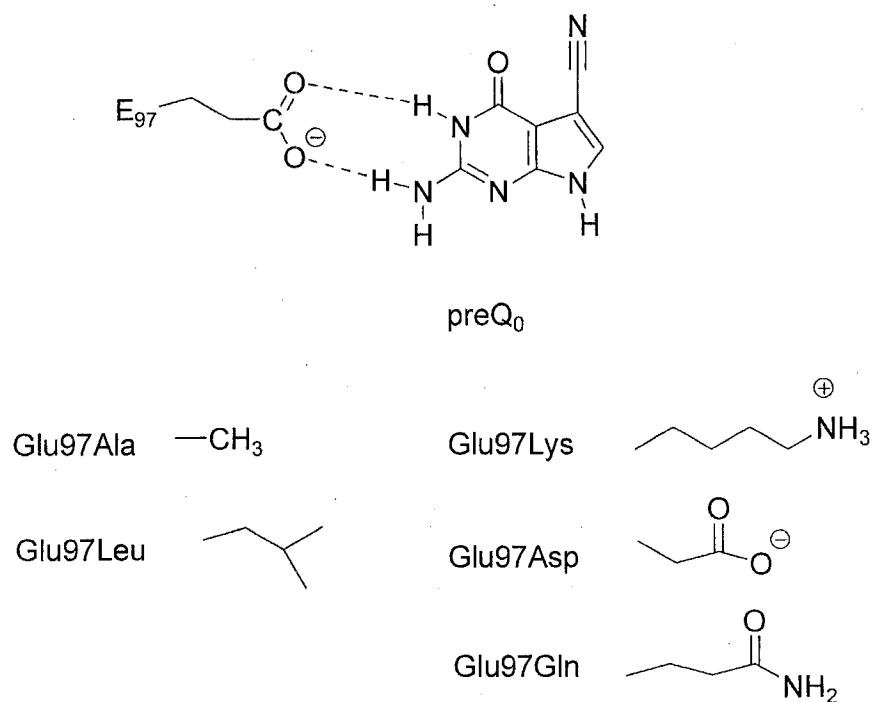


Figure 41. Proposed mode of substrate binding by the conserved residue Glu⁹⁷ of YkvM. Five single point mutations in the *ykvM* gene were obtained in order to examine the role of Glu⁹⁷ in the active site.

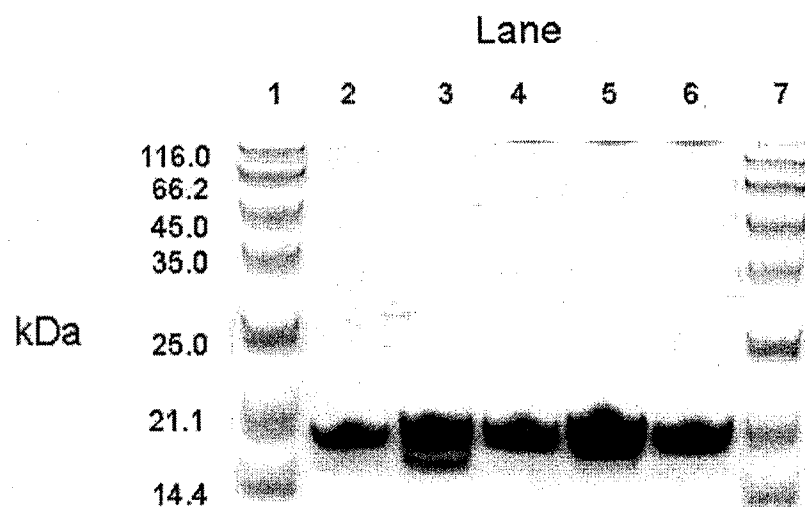


Figure 42. The purification of YkvM Glu⁹⁷ mutants. The SDS-PAGE gel shown here illustrates the purity of the mutant proteins after treatment of the purified polyhistidine tagged recombinant protein with Factor Xa and purification by Ni²⁺-NTA affinity chromatography. Lane 1 and lane 7, molecular weight markers, lane 2, Glu97Ala, lane 3, Glu97Leu, lane 4, Glu97Lys, lane 5, Glu97Gln, lane 6, Glu97Asp.

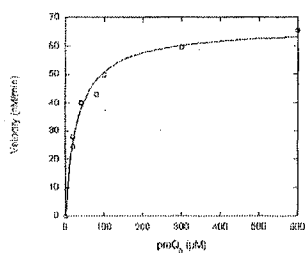
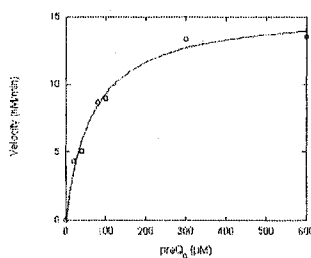
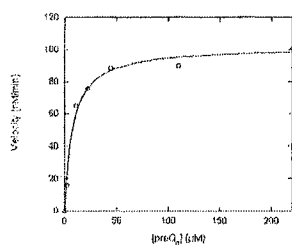
A**B****C**

Figure 43. Steady-state kinetic analysis of the Glu⁹⁷ mutants for preQ₀. **A.** Glu97Ala **B.** Glu97Gln **C.** Glu97Asp. Steady-kinetic analysis of the Glu97Ala, Glu97Gln, and Glu97Asp mutants were conducted following the formation of the fluorescence NADP⁺ alkaline degradation product. The assay solution contained 10 mM phosphate buffer (pH 7.5), 10 mM KCl, 1 mM DTT, 200 μM NADPH, and variable preQ₀ (0-600 μM) at 30°C. The reactions were initiated with enzyme (8.9 μM of Glu97Ala, 13 μM of Glu97Gln, 2 μM of Glu97Asp). Timed aliquots (up to 2 h incubation periods) were removed and subjected to the 0.3 M HCl and 9 M NaOH workup steps as described in Experimental Procedures. The data plots were fit to equation 1 to obtain the kinetic parameters for preQ₀.

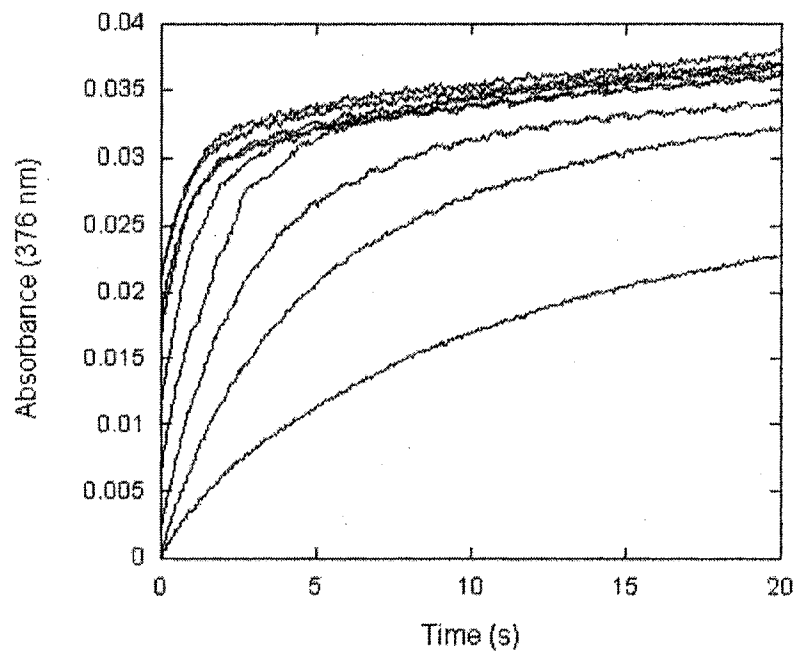


Figure 44. Stopped-flow spectrometric analysis of formation of the absorbance band at 376 nm. Equal volumes of enzyme solution (to a final concentration of 20 μM) were mixed with substrate solution containing variable concentrations of preQ₀ (to a final concentration of 0-200 μM) and monitored at 376 nm for 20 s. The final buffer concentrations were 10 mM phosphate buffer (pH 7.5) and 1 mM DTT.

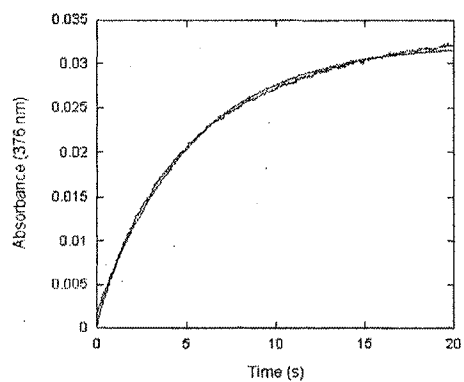
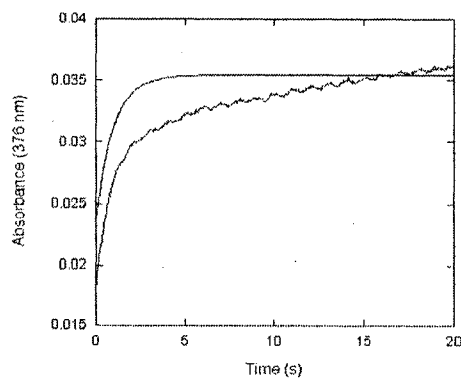
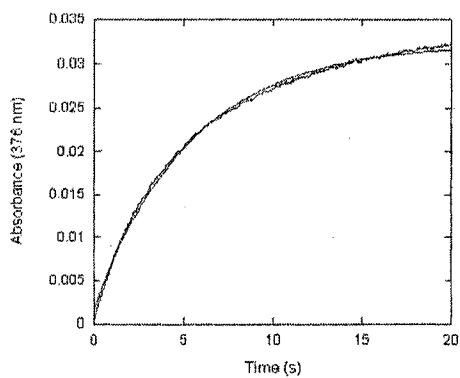
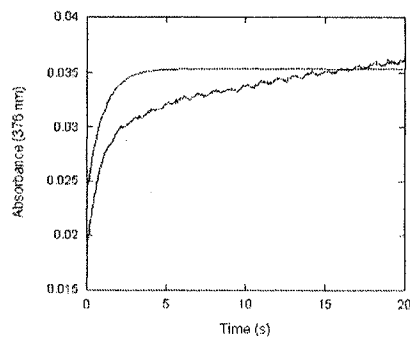
A**B****C****D**

Figure 45. Analysis of the kinetics of the formation of the absorbance band at 376 nm. Shown here is a comparison of the data obtained for 10 μM (**A**) and 120 μM (**B**) preQ₀ and fit to the single exponential, and the same data 10 μM (**C**) and 120 μM (**D**) preQ₀ and fit to the double exponential (Experimental Procedures).

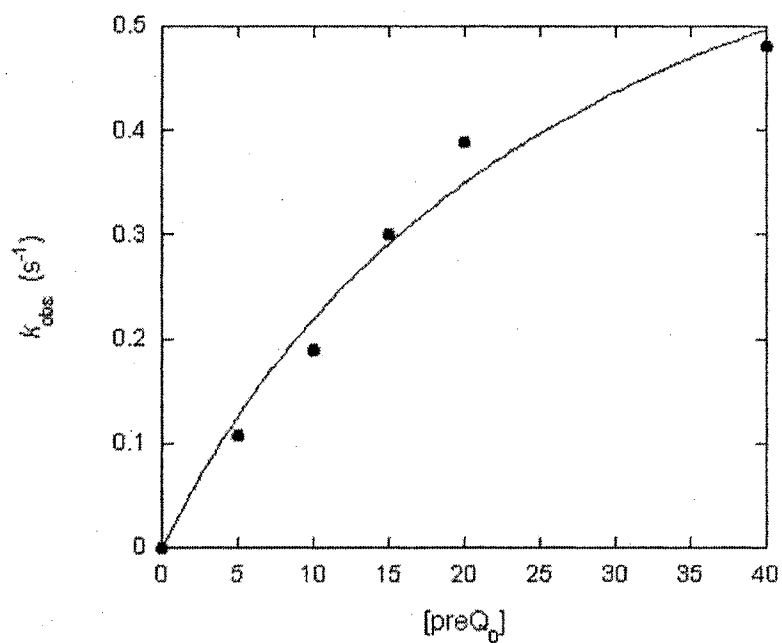


Figure 46. Replot of the k_{obs} of thioimide formation versus preQ_0 concentration data. The data obtained from the single exponential fit (up to 40 μM) were plotted, and the curve exhibits characteristics consistent with saturation kinetics.

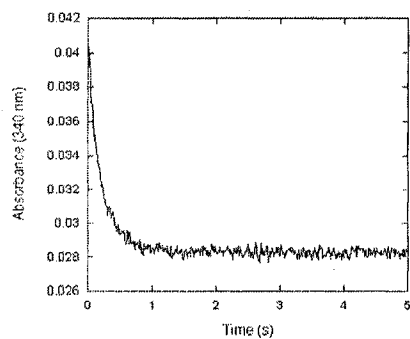
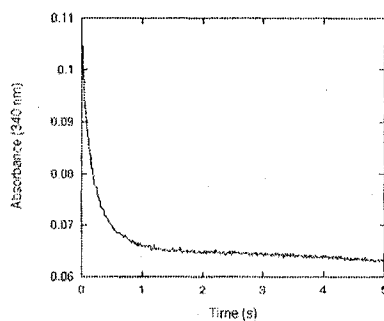
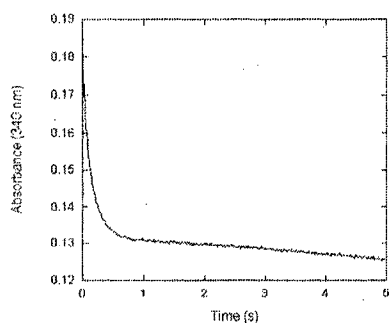
A**B****C**

Figure 47. Single turnover kinetics of YkvM monitoring the loss in absorbance at 340 nm. For single turnover experiments, the enzyme-preQ₀ solution contained a fixed concentration of YkvM (50 μM) and a substoichiometric concentration of preQ₀ (45 μM), and the cofactor solution contained NADPH at varying concentrations (0-50 μM). For each concentration of the cofactor used, the averaged reaction traces from at least three replicates were fit to either single-exponential or double-exponential functions. The plots illustrate the data collected from experiments containing (A) 6 μM (B) 18 μM and (C) 30 μM NADPH.

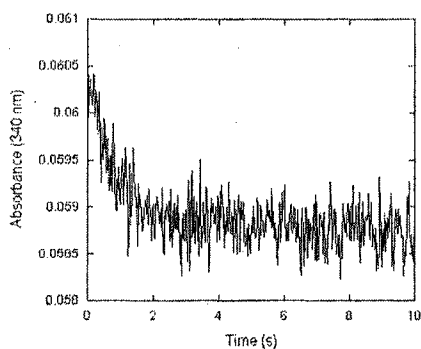
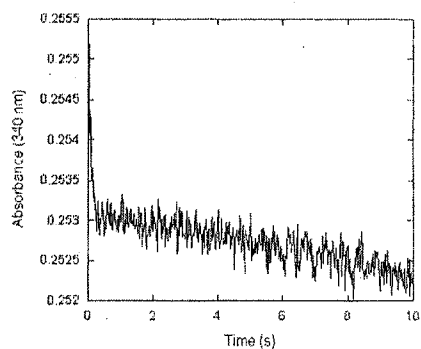
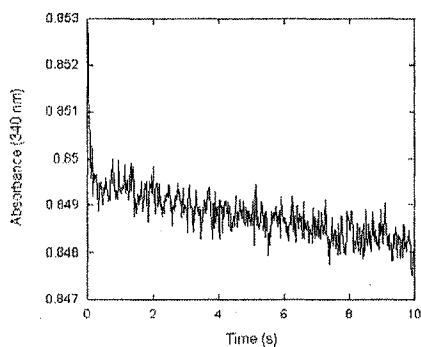
A**B****C**

Figure 48. Multiple turnover kinetics of YkvM monitoring the loss in absorbance at 340 nm. For stopped-flow multiple-turnover experiments, the enzyme solution contained a fixed concentration of YkvM (5 μM) and excess preQ₀ (20 μM), and the cofactor solution contained NADPH at concentrations in the range of 0-160 μM . For each concentration of the cofactor that was used, the averaged reaction traces from at least three replicates were fit to either the linear or “burst” equation. The plots illustrates the data collected from experiments containing (A) 10 μM (B) 40 μM and (C) 140 μM NADPH.

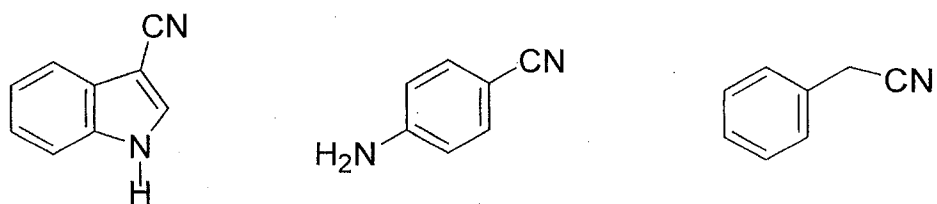


Figure 49. Substrate analogs with potential structural requirements for YkvM oxidoreductase activity (indole-3-nitrile, 4-aminobenzonitrile, phenylacetonitrile).

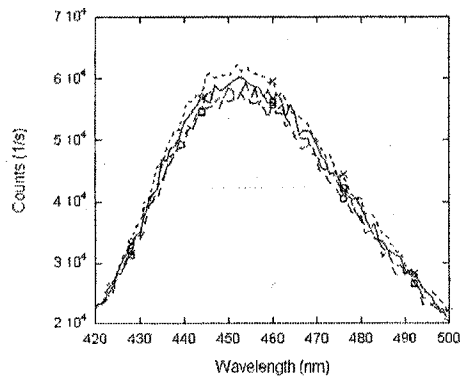
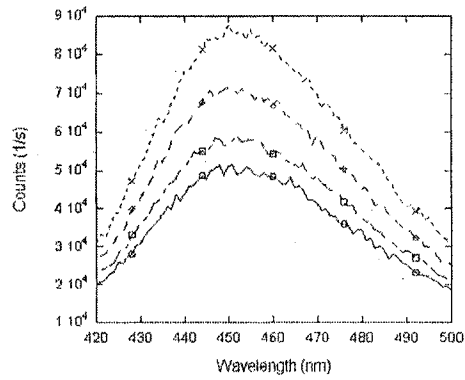
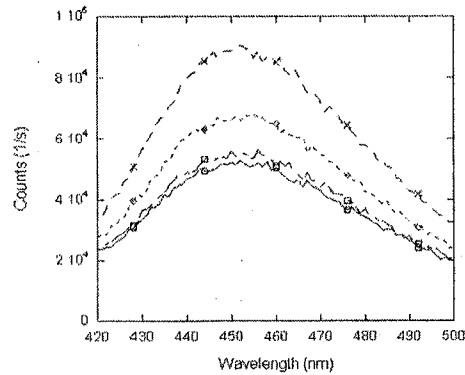
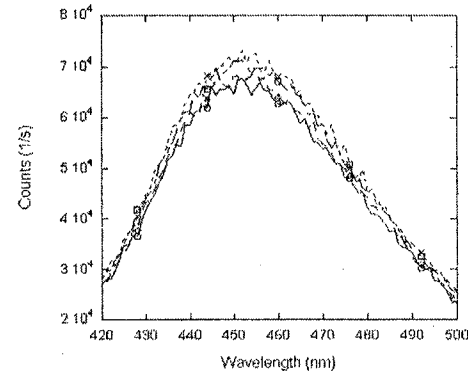
A**B****C****D**

Figure 50. Activity assays of indole-3-nitrile as a substrate for YkvM and the Glu⁹⁷ mutants. The reactions contained 10 mM phosphate buffer (pH 7.5), 10 mM KCl, 1 mM DTT, 100 μ M NADPH, 50 μ M enzyme, and 100 μ M indole-3-nitrile. At specified time intervals (0 min (\circ), 20 min, (\square), 40 min, (\diamond) and 60 min (x)), an aliquot of the reaction was removed and worked up as described in Experimental Procedures. **A.** No substrate added **B.** YkvM **C.** Glu97Ala **D.** Glu97Leu.

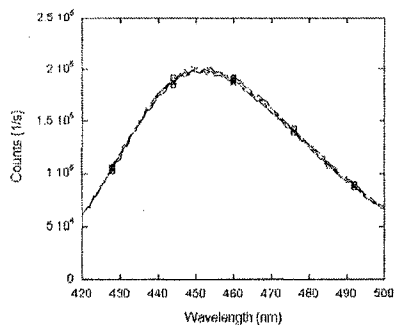
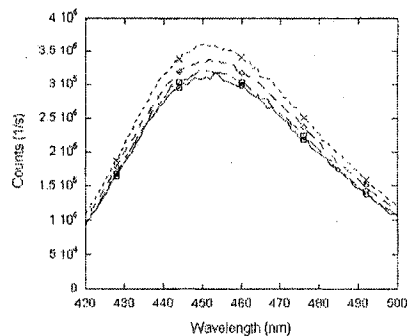
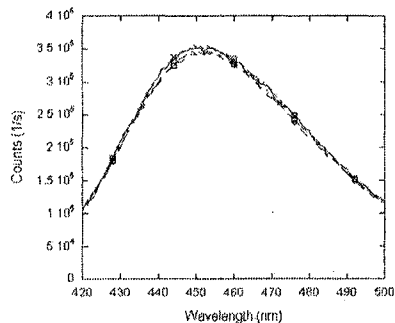
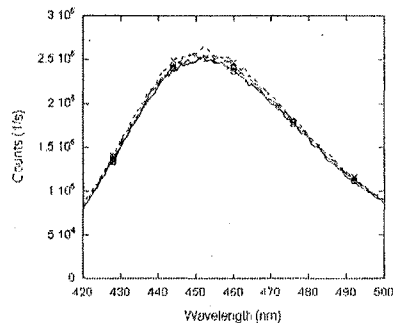
A**B****C****D**

Figure 51. Activity assays of 4-aminobenzonitrile as a substrate for YkvM and the Glu⁹⁷ mutants. The reactions contained 10 mM phosphate buffer (pH 7.5), 10 mM KCl, 1 mM DTT, 100 μ M NADPH, 50 μ M enzyme, and 100 μ M 4-aminobenzonitrile. At specified time intervals (0 min (\circ), 20 min, (\square), 40 min, (\diamond) and 60 min (x)), an aliquot of the reaction was removed and worked up as described in Experimental Procedures. **A.** No substrate added **B.** YkvM **C.** Glu97Ala **D.** Glu97Leu.

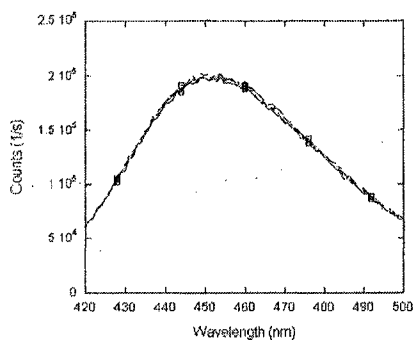
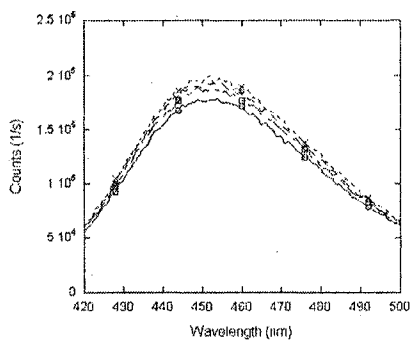
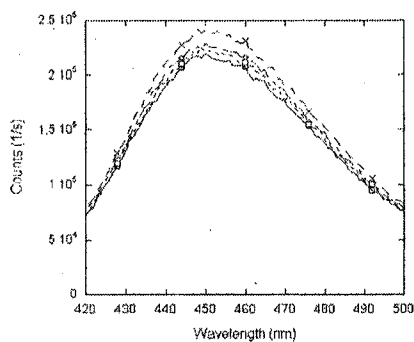
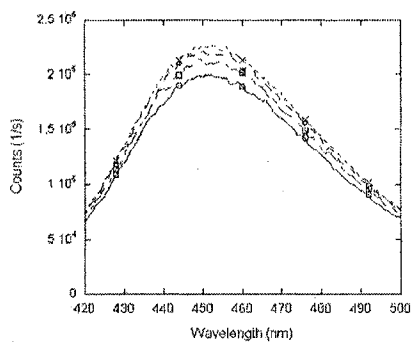
A**B****C****D**

Figure 52. Activity assays of phenylacetone nitrile as a substrate for YkvM and the Glu⁹⁷ mutants. The reactions contained 10 mM phosphate buffer (pH 7.5), 10 mM KCl, 1 mM DTT, 100 μ M NADPH, 50 μ M enzyme, and 100 μ M phenylacetone nitrile. At specified time intervals (0 min (\circ), 20 min, (\square), 40 min, (\diamond) and 60 min (x)), an aliquot of the reaction was removed and worked up as described in Experimental Procedures. **A.** No substrate added **B.** YkvM **C.** Glu97Ala **D.** Glu97Leu.

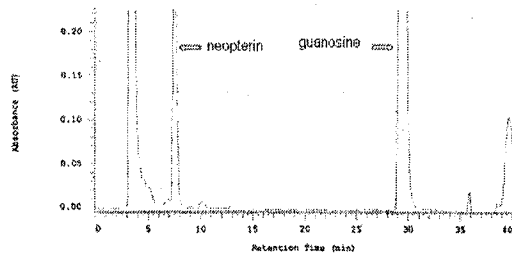
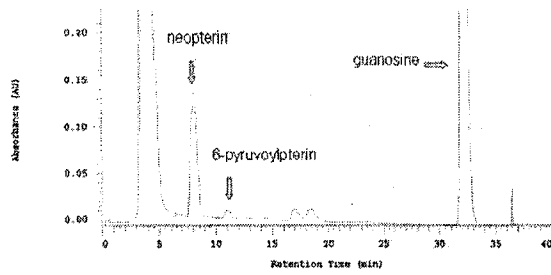
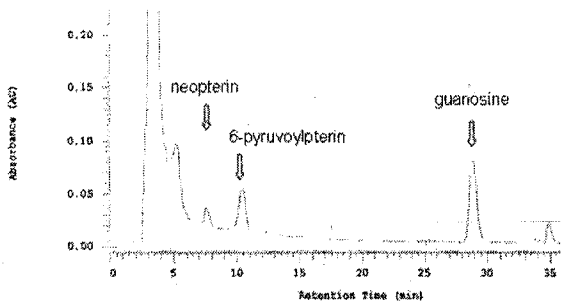
A**B****C**

Figure 53. Activity assays of YgcM coupled to FolE. The activity of YgcM was monitored by coupling the reaction with FolE, the GTP cyclohydrolase and in the presence and absence of magnesium. Peak identities were determined by comparison of the absorbance spectra with authentic samples **A**. FolE and GTP **B**. FolE, GTP, YgcM, no magnesium **C**. FolE, GTP, YgcM, 10 mM magnesium.

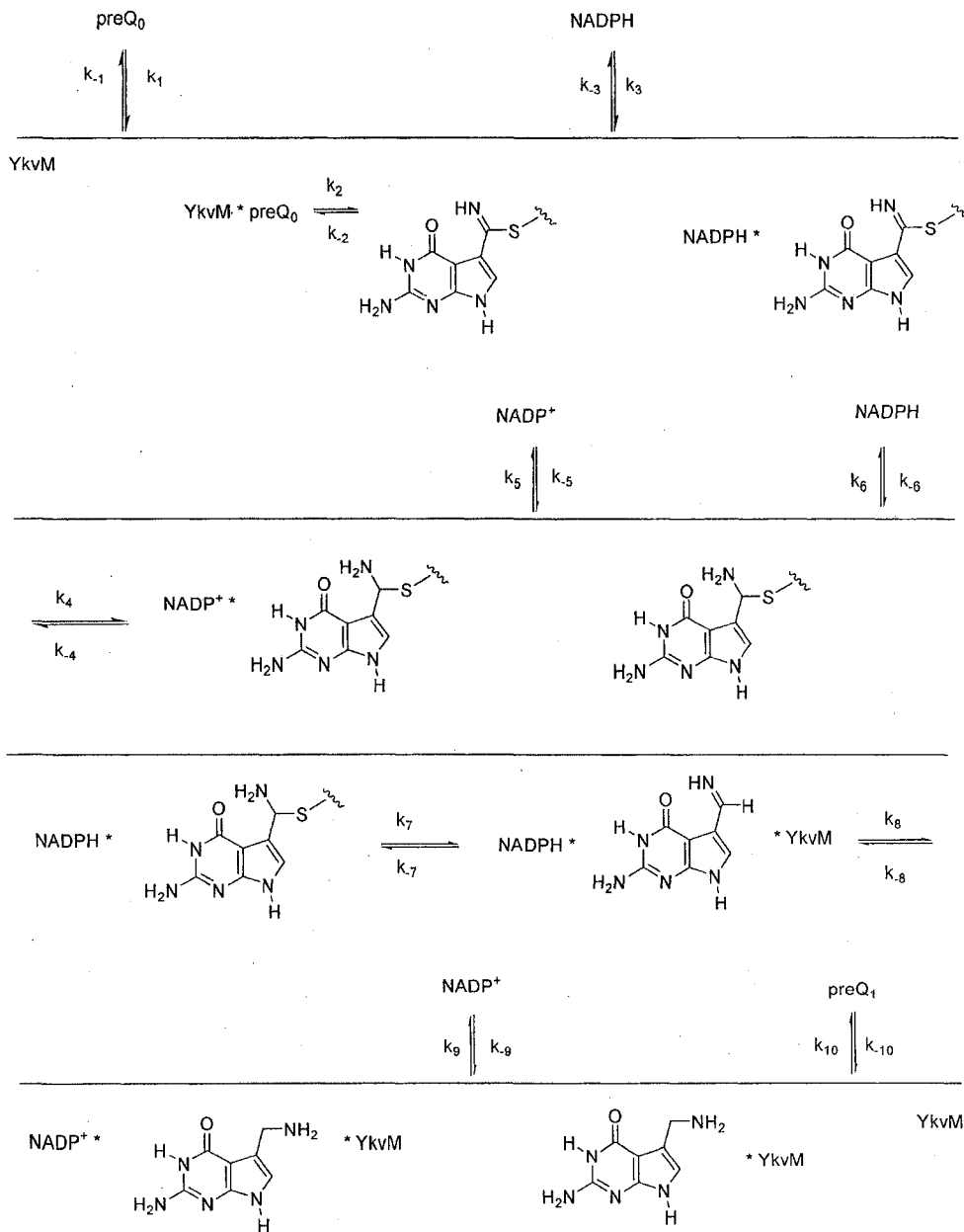


Figure 54. Proposed kinetic scheme of YkvM. This kinetic mechanism is based on the Bi-Uni-Uni-Bi Ter-Ter Ping Pong kinetic mechanism

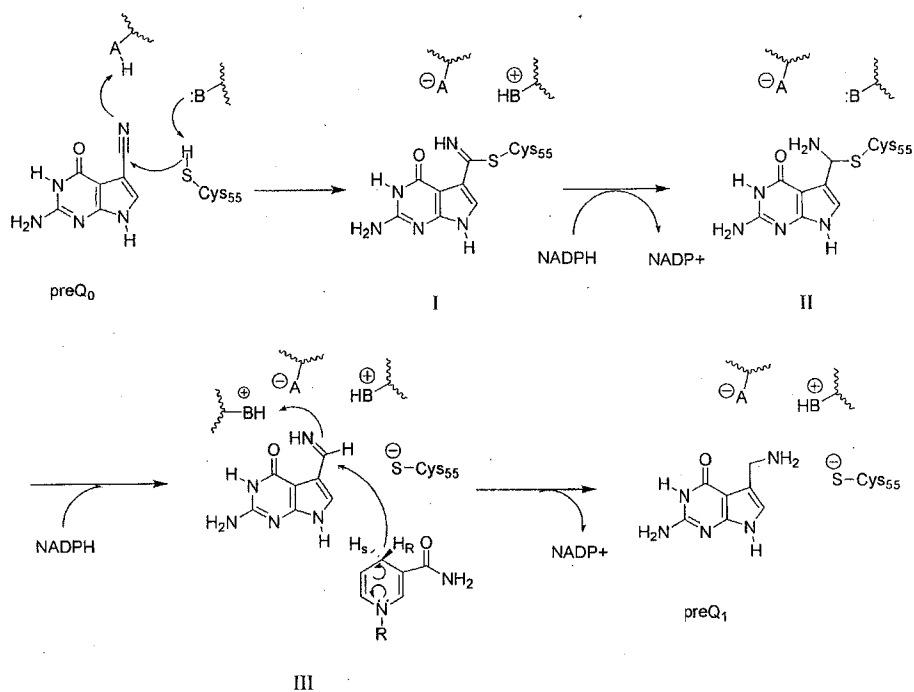
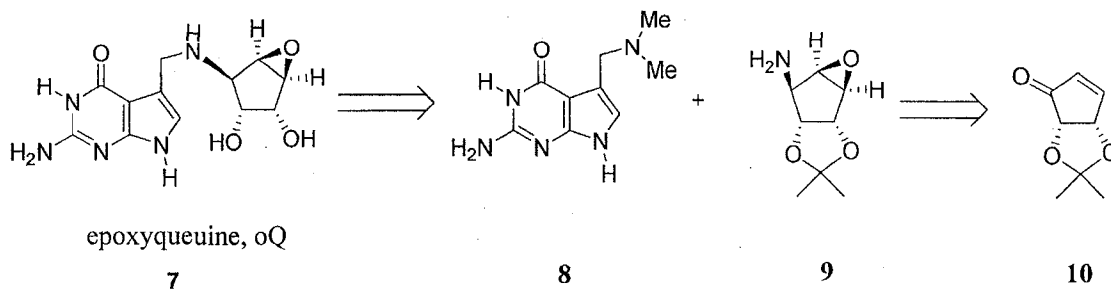
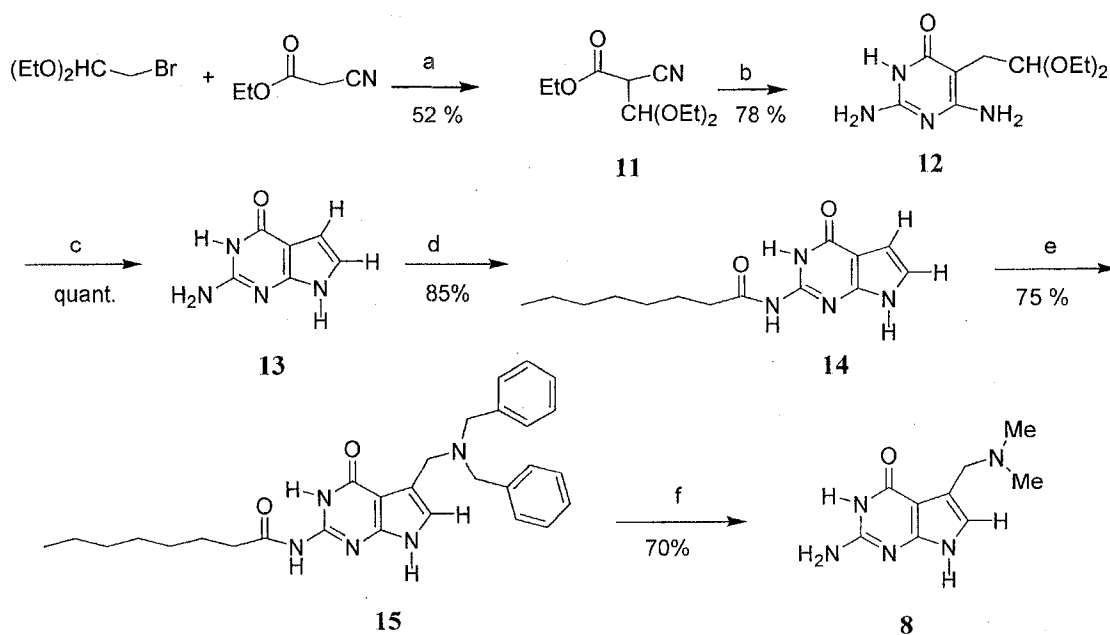


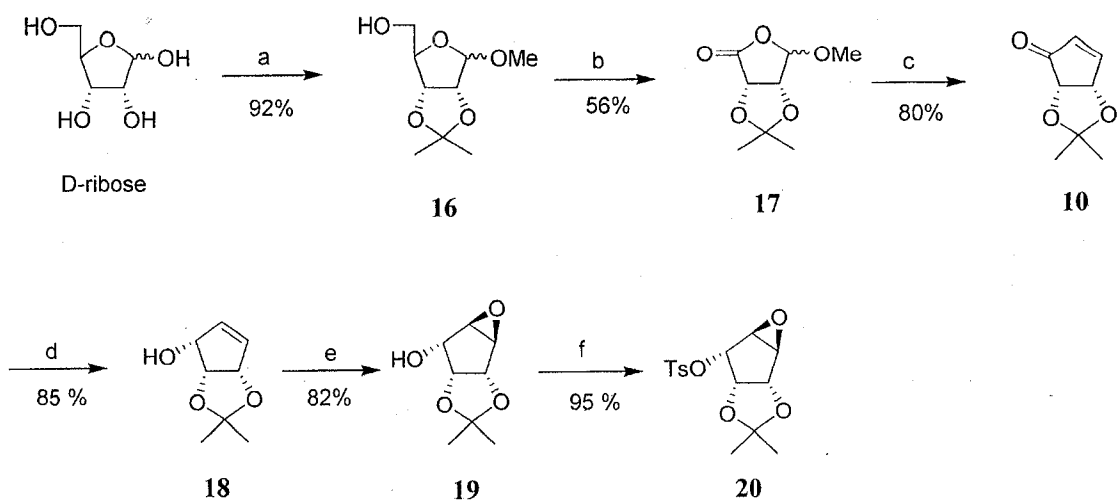
Figure 55. Proposed catalytic mechanism of YkvM. An active site thiolate attacks the nitrile of PreQ₀ to form the thioimidate covalent adduct **I**. NADPH delivers a hydride to give a thiohemiaminal intermediate **II** and release of NADP⁺ allows a second equivalent of NADPH to move into the active site. The thiohemiaminal collapses to imine **III** and is reduced by NADPH to give preQ₁.



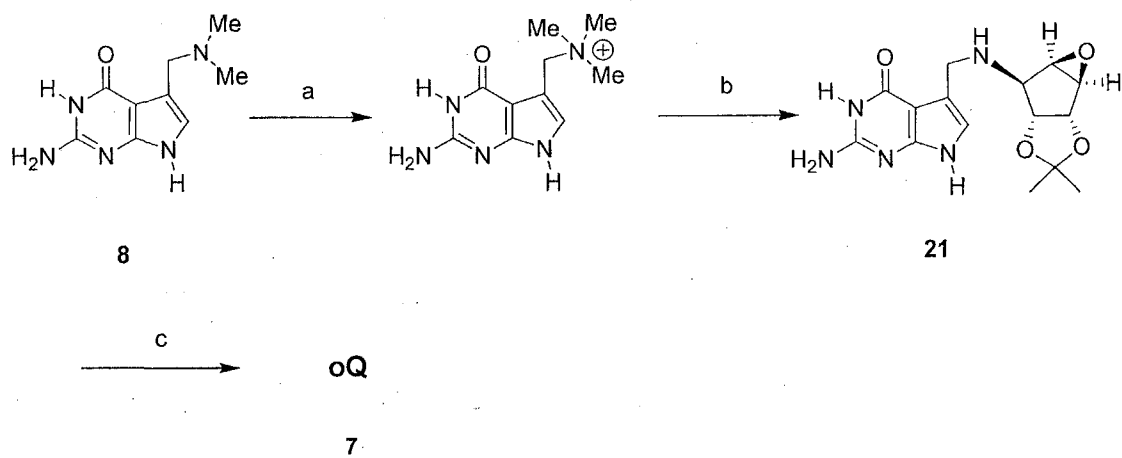
Scheme 1. Retrosynthetic analysis for the total synthesis of epoxyqueuine.



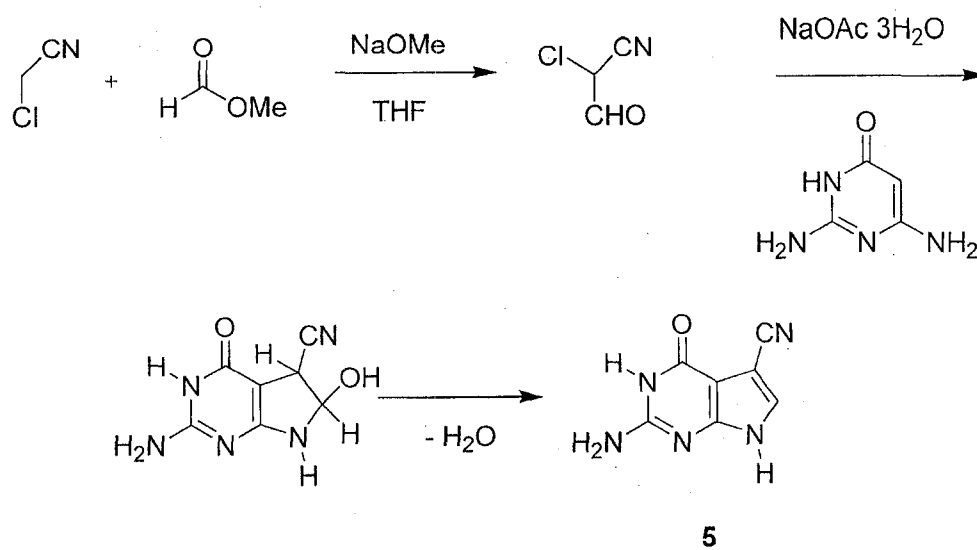
Scheme 2. Epoxyqueine pyrrolo[2,3-*d*]pyrimidine core structure synthesis. a) K_2CO_3 , NaI b) guanidine thiocyanate, NaOEt c) aq. HCl d) octanoyl-Cl, pyridine, cat. DMAP e) dibenzylamine, formalin, 80% acetic acid f) i. dimethylamine, MeOH-THF ii. KOH.



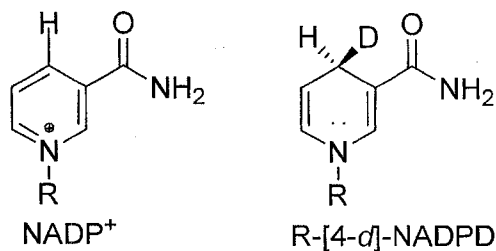
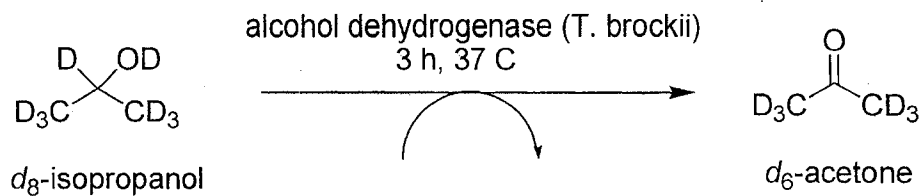
Scheme 3. Synthesis of an intermediate of the epoxycyclopentanediol moiety of oQ.
 a) Acetone, MeOH, HClO₄ b) PCC (4 equiv.), benzene c) dimethyl methylphosphonate, BuLi, THF d) NaBH₄, CeCl₃, MeOH e) trifluoroacetone, NaHCO₃, Oxone, CH₃CN f) TsCl, pyridine, cat. DMAP



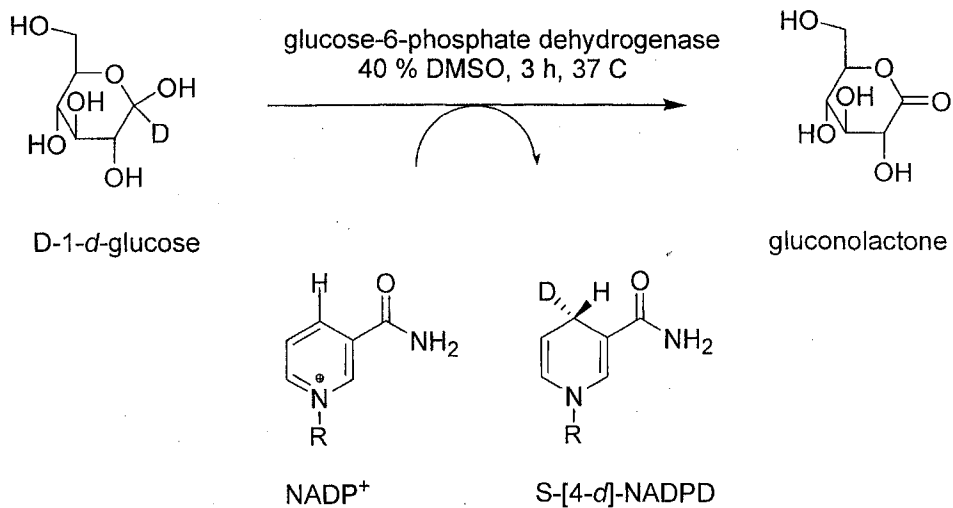
Scheme 4. Synthetic strategy for the coupling of the pyrrolo[2,3-*d*]pyrimidine core to ribosyl moiety. a) MeI, DMSO b) **11**, DMF c) I₂, MeOH.



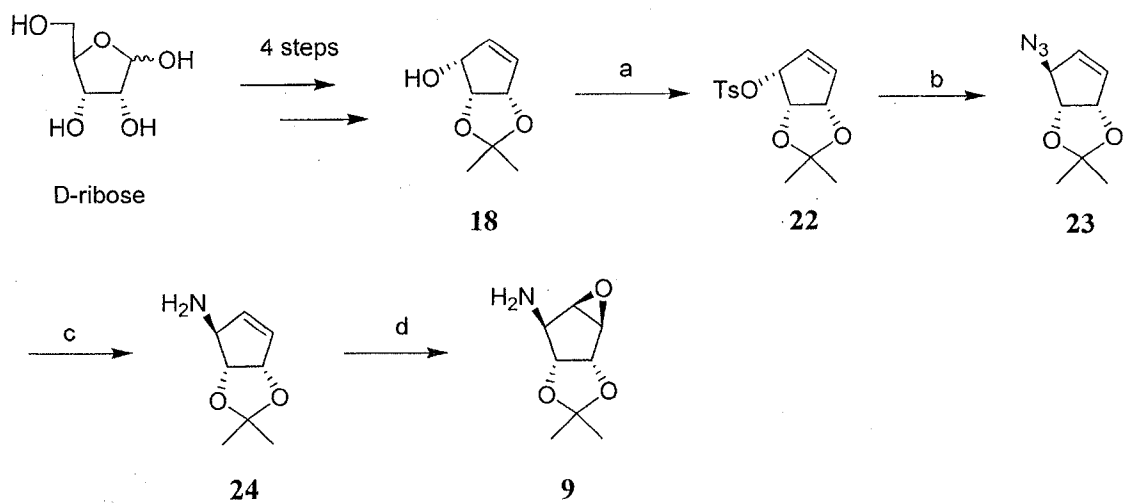
Scheme 5. Chemical synthesis of preQ₀. PreQ₀ was synthesized as described by Migawa *et al. Synth Comm.* 26, 3317-3322.



Scheme 6. Enzymatic synthesis of *pro-R* deuterium labeled NADPH. A total of 8 mg of $NADP^+$ (8.7 mM final concentration), 0.1 mL of d_8 -isopropanol (0.131 M final concentration), and 100 units of alcohol dehydrogenase (*Thermoanaerobium brockii*) were dissolved in 1 mL of 100 mM phosphate buffer (pH 8.0), 100 mM KCl, and 100 mM EDTA. The reaction was allowed to proceed at 37°C, and the formation of (4*R*)-[4- 2H]NADPH was monitored by following the increase in absorbance at 340 nm. The reduced cofactor was purified as described in Experimental Procedures.



Scheme 7. Enzymatic synthesis of *pro-S* deuterium labeled NADPH. The reaction contained 10 mg NADP^+ (9.8 mM final concentration), 4 mg 1-*d*-glucose (18.2 mM final concentration), 0.73 mL of 83 mM phosphate buffer (pH 8.0), 0.486 mL DMSO (40 % final concentration), and 30 units of glucose-6-phosphate dehydrogenase. The reaction was allowed to proceed at 37°C until a maximum absorbance at 340 nm was achieved (1 h).



Scheme 8. Alternate synthetic scheme for the elaboration of the ribosyl moiety of oQ. a) TsCl, pyridine, cat. DMAP b) $(\text{Bu})_4\text{NN}_3$, benzene c) LiAlH_4 , THF d) trifluoroacetone, NaHCO_3 , Oxone, CH_3CN .

REFERENCES

1. Voet, D., and Voet, J. (1995) *Biochemistry*, 2 ed., John Wiley & Sons, Inc.
2. Dunin-Horkawicz, S., Czerwoniec, A., Gajda, M. J., Feder, M., Grosjean, H., and Bujnicki, J. M. (2006) MODOMICS: A database of RNA modification pathways *Nuc. Acids Res.* 34, D145-D149.
3. Limbach, P. A., Crain, P. F. and McCloskey, J. A. (1994) Summary: the modified nucleosides of RNA. *Nuc. Acids Res.* 22, 2183-2196.
4. Rozenski, J., P. F. Crain, and J. A. McCloskey. (1999) The RNA Modification Database: 1999 update *Structure, Biosynthesis, and Function* 27, 196-197.
5. Bjork, G. R. (1995) *tRNA: Structure, Biosynthesis, and Function*, ASM Press, Washington, D. C.
6. Bjork, G. R., and Kohli, J. (1990) in *Chromatography and Modification of Nucleoside. Part B Biological Roles and Function of Modification* (Gehrke, C., and Kuo, K., Ed.) pp B13-B67, Elsevier, Amsterdam.
7. Anantharaman, V., Koonin, E. V., and Aravind, L. (2002) Comparative genomics and evolution of proteins involved in RNA metabolism *Nuc. Acids Res.* 30, 1427-1464.
8. <http://medlib.med.utah.edu/RNAmods/>.
9. Bjork, G. R. (1992) *Transfer RNA in Protein Synthesis*, CRC Press, Boca Raton.

10. Xie, W., Zhou, C., and Huang, R. H. (2007) Structure of tRNA Dimethylallyltransferase: RNA Modification through a Channel *J. Mol. Biol.* 367, 872-881.
11. Agris, P. F., Vendeix, F. A. P. and Graham, W. D. (2007) tRNA's Wobble Decoding of the Genome: 40 Years of Modification *J. Mol. Biol.* 366, 1-13.
12. Dao, V., R. H. Guenther, and P. F. Agris. (1992) The role of 5-methylcytidine in the anticodon arm of yeast tRNA(Phe): site-specific Mg²⁺ binding and coupled conformation transition in DNA analogs. *Biochemistry* 31, 11012-11019.
13. Zhao, X., and Horne, D.A. (1997) The role of cysteine residues in the rearrangement of uridine to pseudouridine catalyzed by pseudouridine synthase I. *J. Biol. Chem* 272, 1950-1955.
14. Cerutti, P., Holt, J. W., and Miller, N. (1968) Detection and determination of 5,6-dihydrouridine and 4-thiouridine in transfer ribonucleic acid from different sources. *J. Mol. Biol.* 34, 505-518.
15. Iwata-Reuyl, D. (2003) Biosynthesis of the 7-deazaguanosine hypermodified nucleosides of transfer RNA *Bioorganic Chem* 31, 24-43.
16. Ohgi, T., T. Kondo, T., and Goto, T. (1979) Total synthesis of optically pure nucleoside Q. Determination of absolute configuration of natural nucleoside Q *J. Am. Chem. Soc.* 101, 1931-1939.

17. Kasai, H., Kuchino, Y., Nihei, K., and Nishimura, S. (1975) Distribution of the modified nucleoside Q and its derivatives in animal and plant transfer RNAs *Nuc. Acids Res.* 2, 1931-1939.
18. Kasai, H., Nakaanishi, K., Macfarlane, R. D., Torgerson, D. F., Ohasi, Z., McCloskey, J. A., Gross, H. J., and Nishimura, S. (1976) The structure of Q nucleoside isolated from rabbit liver transfer ribonucleic acid. *J. Am. Chem. Soc.* 98, 5044-5046.
19. Salazar, J. C., Ambrogelly, A., Crain, P. F., McCloskey, J. A., and Soll, D. (2004) A truncated aminoacyl-tRNA synthetase modifies RNA. *Proc. Natl. Acad. Sci. USA* 101, 7536-41.
20. Blaise, M., Becker, H. D., Keith, G., Cambillau, C., Lapointe, J., Giege, R., and Kern, D. (2004) A minimalist glutamyl-tRNA synthetase dedicated to aminoacylation of the tRNA^{Asp} QUC anticodon *Nucleic. Acids Res.* 32, 2768-75.
21. Harada, F., and Nishimura, S. (1972) Possible anticodon sequences of tRNA^{His}, tRNA^{Asn}, and tRNA^{Asp} from *Escherichia Coli* B. Universal presence of nucleoside Q in the first position of the anticodons of the transfer ribonucleic acids. *Biochemistry* 11, 301-8.
22. Gregson, J. M., Crain, P. F., Edmonds, C. G., Gupta, R., Hashizume, T., Phillipson, D. W., McCloskey, J. A. (1993) Structure of the archaeal transfer RNA nucleoside G*-15 (2-amino-4, 7-dihydro-4-oxo-7-beta-D-

ribofuranosyl-1H-pyrrolo[2,3-d]pyrimidine-5-carboximidamide
(archaeosine)). *J. Biol. Chem.* 268, 10076-86.

23. Bai, Y., Fox, D. T., Lacy, J. A., Van Lanen, S. G., and Iwata-Reuyl, D. (2000) Hypermodification of tRNA in thermophilic archaea. Cloning, overexpression, and characterization of tRNA-guanine transglycosylase from *Methanococcus jannaschii*. *J. Biol. Chem.* 275, 28731-8.
24. Kersten, H., Kersten, W. (1990) Biosynthesis and Function of Queuine and Queuosine tRNA., in *Chromatography and Modification of Nucleosides Part B*.
25. Okada, N., Shindo-Okada, N., Sato, S., Itoh, Y. H., Oda, K., and Nishimura, S. (1978) Detection of unique tRNA species in tumor tissues by *Escherichia coli* guanine insertion enzyme. *Proc. Natl. Acad. Sci. USA* 75, 4247-51.
26. Marks, T., and Farkas, W. R. (1997) Effects of a Diet Deficient in Tyrosine and Queuine on Germfree Mice *Biochem. Biophys. Res. Comm.* 230, 233-7.
27. Carlson, B. A., Kwon, S. Y., Chamorro, M., Oroszlan, S., Hatfield, D. L., and Lee, B. J. (1999) Transfer RNA modification status influences retroviral ribosomal frameshifting *Virology* 255, 2-8.
28. Hatfield, D., Feng, Y.-X., Lee, B. J., Rein, A., Levin, J. G., and Oroszlan, S. (1989) Chromatographic analysis of the aminoacyl-tRNAs which are required for translation of codons at and around the ribosomal frameshift sites of HIV, HTLV-1, and BLV *Virology* 173, 736-742.

29. Durand, J. M., Okada, N., Tobe, T., Watarai, M., Fukuda, I., Suzuki, T., Nakata, N., Komatsu, K., Yoshikawa, M., and Sasakawa, C. (1994) *vacC*, a virulence-associated chromosomal locus of *Shigella flexneri*, is homologous to *tgt*, a gene encoding tRNA transglycosylase (Tgt) of *Escherichia coli* K-12. *J. Bacteriol.* 176, 4627-34.
30. Durand, J. M., Dagberg, B., Uhlin, B. E. and Bjork, G. R. (2000) Transfer RNA modification, temperature and DNA superhelicity have a common target in the regulatory network of the virulence of *Shigella flexneri*: the expression of the *virF* gene. *Mol. Microbiol.* 35, 924-35.
31. Huang, B. S., Wu, R. T., and K. Y. Chien. (1992) Relationship of the queuine content of transfer ribonucleic acids to histopathological grading and survival in human lung cancer *Cancer Res.* 52, 4696-4700.
32. Langgut, W., and T. Reisser. (1995) Involvement of protein kinase C in the control of tRNA modification with queuine in HeLa cells *Nucleic Acids Res.* 23, 2488-2491.
33. Muralidhar, G., Ochieng, J., and Trewyn, R. W. (1989) Altered queuine modification of transfer RNA involved in the in vitro transformation of chinese hamster embryo cells. *Cancer Res.* 49, 7110.
34. Katze, J. R., and Beck, W. T. (1980) Administration of queuine to mice relieves modified nucleoside queuosine deficiency in Erlich Ascites tumor tRNA. *Biochem. Biophys. Res. Comm.* 96, 313.

35. Singhal, R. P. (1983) Queuine: An addendum. *Prog. Nuc. Acids Res. Molec. Biol.* 28, 75-80.
36. Noguchi, S., Nishimura, Y., Hirota, Y., and Nishimura, S. (1982) Isolation and characterization of an *Escherichia coli* mutant lacking tRNA-guanine transglycosylase. *J. Biol. Chem.* 257, 6544-6550.
37. Kirtland, G. M., Morris, T. D., Moore, P. H., O'Brian, J. J., Edmonds, C. G., McCloskey, J. A. and Katze, J. R. (1988) Novel Salvage of queuine from queuosine and absence of queuine synthesis in *Chlorella pyrenoidosa* and *Chlamydomonas reinhardtii*. *J. Bacteriol.* 170, 5633.
38. Kersten, H. (1988) The nutrient factor queuine: biosynthesis, occurrence in transfer RNA and function. *Biofactors* 1, 27-9.
39. Shindo-Okada, N., Okada, N., Ohgi, T., Goto, T., and Nishimura, S. (1980) Transfer ribonucleic acid guanine transglycosylase isolated from rat liver. *Biochemistry* 19, 395-400.
40. Kuchino, Y., Kasai, H., Nihel, K., and Nishimura, S. (1976) Biosynthesis of the modified nucleoside Q in transfer RNA. *Nuc. Acids Res.* 3, 393-398.
41. Elstner, E. F., and Suhadolnik, R. J. (1971) The biosynthesis of the nucleoside antibiotics. IX Purification and properties of guanosine triphosphate 8-formylhydrolase that catalyzes production of formic acid from the ureido carbon of guanosine triphosphate. *J. Biol. Chem.* 246, 6973-6981.

42. Suhadolnik, R. J., and Uematsu, T. (1970) Biosynthesis of the pyrrolopyrimidine nucleoside antibiotic, toyocamycin. VIII Origin of the pyrrole carbons and the cyano carbon. *J. Biol. Chem.* 246, 6973-6981.
43. Yim, J. J., and Brown, G. M. (1976) Characteristics of guanosine triphosphate cyclohydrolase I purified from escherichia coli. *J. Biol. Chem.* 1976, 5087-5094.
44. Burg, A. W., and Brown, G. M. (1968) The biosynthesis of folic acid. VIII Purification and properties of the enzyme that catalyzes the production of formate from carbon atom 8 of guanosine triphosphate. *J. Biol. Chem.* 243, 2349-2358.
45. Okada, N., Noguchi, S., Nishimura, S., Ohgi, T., Goto, T., Crain, P. F. and McCloskey, J. A. (1978) Structure determination of a nucleoside Q precursor isolated from E. coli tRNA: 7-(aminomethyl)-7-deazaguanosine. *Nuc. Acids Res.* 5, 2289-96.
46. Okada, N., Noguchi, S., Kasai, H., Shindo-Okada, N., Goto, T., and Nishimura, S. (1979) Novel mechanism of post-transcriptional modification of tRNA. *J. Biol. Chem.* 254, 3067-3073.
47. Okada, N., and Nishimura, S. (1979) Isolation and characterization of a guanine insertion enzyme, a specific tRNA transglycosylase, from Escherichia coli. *J. Biol. Chem.* 254, 3061-6.
48. Slany, R. K., Bosl, M. and Kersten, H. (1994) Transfer and isomerization of the ribose moiety of Adomet during the biosynthesis of queuosine tRNAs, a

new unique reaction catalyzed by the QueA protein from *Escherichia coli*.
Biochimie 76, 389-93.

49. Phillipson, D. W., Edmonds, C. G., Crain, P. F., Smith, D. L., Davis, D. R., and McCloskey, J. A. (1987) Isolation and structure elucidation of an exoxide derivative of the hypermodified nucleoside queuosine from *Escherichia coli* transfer RNA. *J. Biol. Chem.* 262, 3462-3471.
50. Slany, R. K., Bosl, M., Crain, P. F., and Kersten, H. (1993) The ribosyl moiety of Adomet is the precursor of the cyclopentenediol moiety of the tRNA base queuine. *Biochemistry* 32, 7811-7817.
51. Frey, B., McCloskey, J. A., Kersten, W., and Kersten, H. (1988) New function of vitamin B12: Cobamide-dependent reduction of epoxyqueuosine to queuosine in tRNAs of *Escherichia coli* and *Salmonella typhimurium*. *J. Bacteriol.* 170, 2078-2082.
52. Morris, R. C., Brown, K. G., and Elliot, M.S. (1999) The effect of queuosine on tRNA structure and function. *J. Biomol. Struct. Dyn.* 16, 757-74.
53. Morris, R. C., and Elliot, M. S. (2001) Queuosine Modification of tRNA: a case for convergent evolution. *Mol. Genet. Metab.* 74, 147-159.
54. Watanabe, M., Matsuo, M., Tanaks, S., Akimoto, H., Asahi, S., Nishimura, S., Katze, J. R., Hashizume, T., Crain, P. F., McCloskey, J. A., and Okada, N. (1997) Biosynthesis of archaeosine, a novel derivative of 7-deazaguanosine specific to archaeal tRNA, proceeds via a pathway

- involving base replacement on the tRNA polynucleotide chain. *J. Biol. Chem.* 272, 20146-51.
55. Watanabe, M., Nemeki, N., Matsuo-Takasaki, M., Nishimura, S., and Okada, N. (2001) tRNA recognition of tRNA-guanine transglycosylase from a hyperthermophilic Archaeon, pyrococcus Horikoshii. *J. Biol. Chem.* 276, 2387-2394.
56. Reader, J. S., Metzgar, D., Schimmel, P., and de Crecy-Lagard, V. (2004) Identification of Four Genes Necessary for Biosynthesis of the Modified Nucleoside Queuosine *J. Biol. Chem.* 279, 6280-6285.
57. Auerbach, G., and Nar, H. (1997) *Biol. Chem.* 378, 15-192.
58. Woo, H. J., Hwang, Y. K., Kim, Y. J., Kang, J. Y., Choi, Y. K., Kim, C. G., Park, Y. S. (2002) *Escherichia coli* 6-pyruvoyltetrahydropterin synthase ortholog encoded by *ygeM* has a new catalytic activity for conversion of sepiapterin to 7,8-dihydropterin. *FEBS Lett.* 523, 234-238.
59. Jo, J., Jang, Y.S., Kim, K. Y., Kim, M. H., Kim, I. J., Chung, W. I. (1997) Isolation of ALU1-P gene encoding a protein with aluminum tolerance activity from *Arthrobacter viscosus* *Biochem. Biophys. Res. Comm.* 239, 835-839.
60. Gaur, R., and Varshney, U. (2005) Genetic Analysis Identifies a Function for the *queC* (*ybaX*) Gene Product at an Initial Step in the Queuosine Biosynthetic Pathway in *Escherichia coli* *J. Bacteriol.* 187, 6893-6901.

61. Sofia, H. J., Chen, G., Hetzler, B. G., Reyes-Spindola, J. F., Miller, N. E. (2001) Radical SAM, a novel protein superfamily linking unresolved steps in familiar biosynthetic pathways with radical mechanisms: functional characterization using new analysis and information visualization methods. *Nuc. Acids Res.* 29, 1097-1106.
62. Van Lanen, S. G., Reader, J. S., Swairjo, M. A., de Crecy-Lagard, V., Lee, B., and Iwata-Reuyl, D. (2005) From cyclohydrolase to oxidoreductase: Discovery of nitrile reductase activity in a common fold. *PNAS* 102, 4264-4269.
63. Roth, A., Winkler, W. C., Regulski, E. E., Lee, B. W. K., Lim, J., Jona, I., Barrick, J. E., Ritwik, A., Kim, J. N., Welz, R., Iwata-Reuyl, D., and Breaker, R. R. (2007) A riboswitch selective for the queuosine precursor preQ₁ contains an unusually small aptamer domain *Nat. Struct. Mol. Biol* 14, 308-317.
64. Winkler, W. C., Nahvi, A., Sudarsan, N., Barrick, J. E., and Breaker, R. R. (2003) An mRNA structure that controls gene expression by binding S-adenosylmethionine *Nat. Struct. Mol. Biol* 10, 701-707.
65. Winkler, W. C., Cohen-Chalamish, S., and Breaker, R. R. (2002) An mRNA structure that controls gene expression by binding FMN *PNAS* 99, 15908-15913.

66. Mandal, M., and Breaker, R. R. (2004) Adenine riboswitches and gene activation by disruption of a transcription terminator *Nat. Struct. Mol. Biol* 11, 29-35.
67. Mandal, M., Boese, B., Barrick, J. E., Winkler, W. C., and Breaker, R. R. (2003) Riboswitches Control Fundamental Biochemical Pathways in *Bacillus subtilis* and Other Bacteria *Cell* 113, 577-586.
68. Colloch, N., Poupon, A., and Morion, J.P. (2000) Sequence and Structural Features of the T-Fold, an Original Tunneling Building Unit *Proteins: Structure, Function, and Genetics* 39, 142-154.
69. Swairjo, M. A., Reddy, R.R., Lee, B., Van Lanen, S. G., Brown, S., de Crecy-Lagard, V., Iwata-Reuyl, D., and Schimmel, P. (2005) Crystallization and preliminary X-ray characterization of the nitrile reductase QueF: a queuosine-biosynthesis enzyme. *Acta Crystallography Sect F Struct Biol Cryst Commun.* F61, 945-948.
70. Auerbach, G., Herrmann, A., Bracher, A., Bader, G., Gutlich, M., Fischer, M., Neukamm, M., Garrido-Franco, M., Richardson, J., Nar, H., Huber, R., and Bacher, A. (2000) Zinc plays a key role in human and bacterial GTP cyclohydrolase I *PNAS* 97, 13567-13572.
71. Feingold, D. S., and Franzen, J. S. (1981) Pyridine nucleotide-linked four electron transfer dehydrogenases *Trends Biochem. Sci* 6, 103-105.
72. Campbell, R. E., Sala, R. F., van de Rijn, I., and Tanner, M. E. (1997) Properties and Kinetic Analysis of UDP-glucose Dehydrogenase from

- Group A Streptococci. IRREVERSIBLE INHIBITION BY UDP-CHLOROACETOL *J. Biol. Chem.* 272, 3416-3422.
73. Ge, X., Campbell, R. E., van de Rijn, I., and Tanner, M. E. (1998) Covalent Adduct Formation with a Mutated Enzyme: Evidence for a Thioester Intermediate in the Reaction Catalyzed by UDP-Glucose Dehydrogenase *J. Am. Chem. Soc* 120, 6613-6614.
74. Teng, H., Segura, and Grubmeyer, C. (1993) Conserved Cysteine Residues of Histidinol Dehydrogenase Are Not Involved in Catalysis *J. Biol. Chem* 268, 14182-14188.
75. Barbosa, J. A. R. G., Sivaraman, J., Li, Y., Larocque, R., Matte, A., Schrag, J. D., and Cygler, M. (2002) Mechanism of action and NAD⁺-binding mode revealed by the crystal structure of L-histidinol dehydrogenase *PNAS* 99, 1859-1864.
76. Teng, H., Grubmeyer, C. (1999) Mutagenesis of Histidinol Dehydrogenase Reveals roles for Conserved Histidine Residues *Biochemistry* 38, 7363-7371.
77. Banerjee, A., Sharma, R., and Banerjee, U. C. (2002) The nitrile degrading enzymes: current status and future prospects *Appl. Microbiol. Biotechnol.* 60, 33-44.
78. Stevenson, D. E., Feng, R., and Storer, A. C. (1990) Detection of covalent enzyme-substrate complexes of nitrilase by ion-spray mass spectroscopy *FEBS* 277, 112-114.

79. Kobayashi, M., Yanada, N., Nagasawa, T., and Yamada, H. (1992) Primary Structure of an Aliphatic Nitrile-Degrading Enzyme, Aliphatic Nitrilase, from *Rhodococcus rhodochrous* K22 and Expression of Its Gene and Identification of Its Active Site Residue *Biochemistry* 31, 9000-9007.
80. Katze, J. R., Simonian, M. H., Mosteller, R. D. (1977) Role of methionine in the synthesis of nucleoside Q in *Escherichia coli* transfer ribonucleic acid. *J. Bacteriol.* 132, 174-79.
81. Okada, N., Yasuda, T., and Nishimura, S. (1977) Detection of nucleoside Q precursors in methyl-deficient *E. coli* tRNA. *Nuc. Acids Res.* 4, 4063-4075.
82. Reuter, K., Slany, K., Ullrich, F., and Kersten, H. (1991) Structure and organization of *Escherichia coli* genes involved in biosynthesis of the deazaguanine derivative queuine, a nutrient factor for eukaryotes. *J. Bacteriol.* 173, 2256-64.
83. Kinzie, S. D., Thern, B., and Iwata-Reuyl, D. (2000) Mechanistic studies of the tRNA-modifying enzyme QueA: a chemical imperative for the use of Adomet as a "ribosyl" donor. *Org. Lett.* 2, 1307-10.
84. Hoops, G. C., Townsend, L. B., and Garcia, G. A. (1995) Mechanism-based inactivation of tRNA-guanine transglycosylase (TGT) from *Escherichia coli* by 5-fluoromethyl-2-aminopyrrolo[2,3-d]pyrimidin-4-one. *Biochemistry* 34, 15539-15544.
85. Davoll, J. (1960) Pyrrolo[2,3-d]pyrimidines. *J. Chem. Soc.*, 131-138.

86. Akimoto, H., E. Imamiya, T. Hitaka, H. Nomura and S. Nishimura. (1988) Synthesis of Queuine, the Base of Naturally Occurring Hypermodified Nucleoside (Queuosine), and Its Analogues. *J. Soc. Perkin Trans. I* 1988, 1937-1644.
87. Johnson, C. R., and Penning, T. D. (1988) Triply convergent synthesis of (-) - prostaglandin E₂ methyl ester. *J. Am. Chem. Soc.* 110, 4726-4735.
88. Medich, J. R., Kunnen, K. B., and Johnson, C. R. (1987) Synthesis of the carbocyclic nucleoside (-) - Neplanocin A. *Tet. Lett.* 28, 4131-4134.
89. Shuto, S., Obara, T., Saito, Y., Andrei, G., Snoeck, R., De Clerq, E., and Matuda, A. (1996) New Neplanocin analogues. 6. Synthesis and Potent Antiviral Activity of 6'-Homoneplanocin A. *J. Med. Chem.* 39, 2392-2399.
90. Ohrui, H., Konno, M., and Meguro, H. (1987) Synthesis of (4S, 5S)-4,5-Dihydroxy-4,5-O-isopropylidene-2-cyclopenten-1-one from D-ribose. *Agric. Biol. Chem.* 51, 625-626.
91. Flann, C. J., and Mash, E. A. (1988) Homochiral ketals in organic synthesis. Enantioselective synthesis of (4S,5S)-4,5-dihydroxycyclopent-2-en-1-one isopropylidene ketal. *Synth. Comm.* 18, 391-402.
92. Deardorff, D. R., Shambayati, S., Myles, D. C., and Heerding, D. (1988) Studies on the synthesis of (-) - Neplanocin A. *J. Org. Chem.* 53, 3614-3615.

93. Takano, S. I. K., and Ogasawara, K. (1989) A new route to (+)-2,3-(isopropylidenedioxy)-4-cyclopentenone via the optically active dicyclopentadiene intermediate. *Chem. Lett.*, 359-362.
94. Johnson, C. R., Esker, J. L., and Van Zandt, M. C. (1994) Chemoenzymatic synthesis of 4-substituted riboses. *J. Org. Chem.* 59, 5854-5855.
95. Biadatti, T., Esker, J. L., and Johnson, C. R. (1996) Chemoenzymatic synthesis of a versatile cyclopentenone: (+)-(3aS,6aS)-2,2-dimethyl-3ab,6ab-dihydro-4H-cyclopenta-1,3-dioxol-4-one. *Tetrahedron:Asy.* 7, 2313-2320.
96. Ali, S. M., Ramesh, K., and Borchart, R. T. (1990) Efficient enantioselective syntheses of carbocyclic nucleoside and prostaglandin synthons. *Tet. Lett.* 31, 1509-1512.
97. Borcharding, D. R., Scholtz, S. A., and Borchardt, R. T. (1987) Synthesis of analogues of Neplanocin A: Utilization of optically active dihydroxycyclopentenones derived from carbohydrates. *J. Org. Chem.* 52, 5457-5461.
98. Wang, P., Luigi, A., Agrofoglio, M., Newton, G., and Chu, C. K. (1999) Chiral synthesis of carbocyclic analogues of L-ribofuranosides. *J. Org. Chem.* 64, 4173-4178.
99. Carey, F. A., and Sundberg, R. J. (1991) *Advanced Organic Chemistry Part A: Structure and Mechanisms*, 4 ed., Plenum Publishing, New York, NY.

100. Hudlicky, T., Fleming, A., and Radesca, L. (1989) [2+3] and [3+4] Annulation of enones, enantiocontrolled total synthesis of (-)-Retigeranic Acid. *J. Am. Chem. Soc.* *111*, 6691-6707.
101. Moon, H. R., Kim, H. O., Lee, K. M., Chun, M. W., Kim, J. H., and Jeong, L. S. Stereoselective synthesis of a novel apio analogue of Neplanocin A as potential S-adenosylhomocysteine hydrolase inhibitor. *Org. Lett.*
102. Acena, J. L., Arjona, O., Leon, M. L., and Plumet, J. (2000) Total synthesis of (+)-7-deoxypancratistatin from furan. *Org. Lett.* *2*, 3683-3686.
103. de Almeida, M. V., Hyaric, M. L., Siqueira, L. J. A., Pinto, L. D., Valle, M. S., and Alves, W. A. (2001) Synthesis of furan derivatives condensed with carbohydrates. *Molecules* *6*, 728-735.
104. Danishefsky, S. J., DeNino, M. P., and Chen, S. J. (1988) Stereoselective total syntheses of the naturally occurring enantiomers of N-acetylneuraminic acid and 3-deoxy-D-manno-2-octulosonic acid. A new and stereospecific approach to sialo and 3-deoxy-D-manno-2-octulosonic acid conjugates *J. Am. Chem. Soc.* *110*, 3929.
105. Kim, J. H., Yang, M. S., Lee, W. S., and Park, K. H. (1998) Chiroselective synthesis of 1,4-dideoxy-1,4-imino-D-arabinitol and 1,4-dideoxy-1,4-imino-L-xylitol via one-pot cyclisation. *J. Chem. Soc., Perkin Trans. 1.*, 2877.

106. Gill, S. C., and von Hippel, P. H. (1989) Calculation of Protein Extinction Coefficients from Amino Acid Sequence Data *Analytical Biochemistry* 182, 319-326.
107. Sambrook, J., Fritsch, E. F., and Maniatis, T. (1989) (Nolan, C., Ed.) pp A.3, Cold Spring Harbor Laboratory Press.
108. Campos, A., Zhang, R., Alkire, R. W., Matsumura, P., and Westbrook, E. W. (2001) Crystal structure of the global regulator FlhD from *Escherichia coli* at 1.8 Å resolution *Molecular Microbiology* 39, 567-580.
109. Tsotsou, G. E., Edward, A., Cass, G. and Gilardi, G. (2002) High Throughput Assay for Cytochrome P450 BM3 for Screening Libraries of Substrates and Combinatorial Mutants. *Biosensors and Bioelectronics* 17, 119-131.
110. Lowry, O. H., and Passonneau, J. V. (1972) *A Flexible System of Enzymatic Analysis*, Academic Press, New York.
111. Kaplan, N. O., Colowick, S. P., and Barnes, C. C. (1951) Effect of Alkali on Diphosphopyridine Nucleotide *J. Biol. Chem* 191, 461.
112. Segal, I. H. (1975) *Enzyme Kinetics*, John Wiley & Sons, New York.
113. Jeong, S. S., and Gready, J. E. (1994) A Method of Preparation and Purification of (4R)-Deuterated-Reduced Nicotinamide Adenine Dinucleotide Phosphate *Analytical Biochemistry* 221, 273-277.

114. McCracken, J. A., Wang, L., and Amnon, K. (2004) Synthesis of R and S tritiated reduced B-nicotinamide adenine dinucleotide 2' phosphate. *Analytical Biochemistry* 324, 131-136.
115. Mostad, S. B., Helming, H. L., Groom, C. and Glasfeld, A. (1997) The Stereospecificity of Hydrogen Transfer to NAD(P)⁺ Catalyzed by Lactol Dehydrogenase *Biochem. Biophys. Res. Comm.* 233, 681-686.
116. Pollack, V. V., and Barber, M. J. (2001) Kinetic and Mechanistic Properties of Biotin Sulfoxide Reductase *Biochemistry* 40, 1430-1440.
117. Balacco, G. (1994) SwaN-MR: a Complete and Expansible NMR Software for the Macintosh *J. Chem. Inf. Comput. Sci* 34, 1235-1241.
118. Migawa, M. T., J. M. Hinkley, G. C. Hoops, and L. B. Townsend. (1996) A Two Step Synthesis of the Nucleoside Q Precursor 2-Amino-5-Cyanopyrrolo[2,3-d]pyrimidine-4-one (PreQ₀). *Synth. Commun.* 26, 3317-3322.
119. Van Lanen, S. G., Reader, J. S., Swairjo, M. A., de Crecy-Lagard, V., Lee, B., and Iwata-Reuyl, D. (2005) From cyclohydrolase to oxidoreductase: Discovery of nitrile reductase activity in a common fold. *Proc. Natl. Acad. Sci. USA* 102, 4264-4269.
120. Viola, R. E., Cook, P. F. and Cleland, W. W. (1979) Stereoselective Preparation of Deuterated Reduced Nicotinamide Adenine Nucleotides and Substrates by Enzymatic Synthesis *Analytical Biochemistry* 96, 334-340.

121. Gemal, A. L., and J. L., Luche. (1981) Lanthanoids in Organic Synthesis. 6. The Reduction of α -Enones by Sodium Borohydride in the Presence of Lanthanoid Chlorides: Synthetic and Mechanistic Aspects. *J. Am. Chem. Soc.* 103, 5454-5459.
122. Kurihara, M., Ito, S., Tsutsumi, N., and Miyata, N. (1994) Stereoselective epoxidation with dioxiranes generated from ketones. *Tet. Lett.* 35, 1577-1580.
123. Yang, D., Wong, M. K., and Yip, Y. C. (1995) Epoxidation of olefins using methyl(trifluoromethyl)dioxirane generated in situ. *J. Org. Chem.* 60, 3887-3889.
124. Smith, E. L., Austen, B. M, Blumenthal, K. M. and Nye, J. F. (1975) in *The Enzymes, 3rd ed.* pp 2293-367, Academic Press, New York.
125. Dick, R. A. a. K., T. W. (2004) The catalytic and kinetic mechanisms of NADPH-dependent alkenal/one oxidoreductase *J. Biol. Chem* 279, 17269-17277.
126. Van Lanen, S. G., Kinzie, S. D., Matthieu, S., Link, T., Culp, J. and Iwata-Reuyl, D. (2003) tRNA Modification by S-Adenosylmethionine:tRNA Ribosyltransferase-Isomerase *J. Biol. Chem* 278, 10491-10499.
127. Hoops, G. C., Townsend, L. B., and Garcia, G. A. (1995) tRNA-Guanine Transglycosylase from *Escherichia coli*: Structure-Activity Studies Investigating the Role of the Aminomethyl Substituent of the Herocyclic substrate PreQ₁ *Biochemistry* 34, 15381-15387.

128. Kasai, H., Shino-Okada, N., Noguchi, S. and Nishimura, S. (1979) Specific fluorescent labeling of 7-(aminomethyl)-7-deazaguanosine located in the anticodon of tRNA^{Tyr} isolated from *E. coli* mutant *Nuc. Acids Res.* 7, 231-238.
129. Weigele, M., DeBernardo, S. L., Teng, J. P. and Leimgruber, W. (1972) A Novel Reagent for the Fluorometric Assay of Primary Amines *J. Am. Chem. Soc.* 94, 5927-5928.
130. Udenfriend, S., Stein, S., Bohlen, P., and Dairman, W. (1972) Fluorescamine: A Reagent for Assay of Amino Acids, Peptides, Proteins, and Primary Amines in the Picomole Range *Science* 178, 871-872.
131. Takahashi, M., Pischetsrieder, M., and Monnier, V. M. (1997) Isolation, Purification, and Characterization of Amadoriase Isoenzymes (Fructosyl Amine-oxygen Oxidoreductase EC 1.5.3) from *Aspergillus* sp. *J. Biol. Chem.* 272, 3437-3443.
132. Wang, W., Manier, M., Jain, R., Jacobs, J., Trias, J., and Yuan, Z. (2001) A Fluorescence-Based Homogeneous Assay for Measuring Activity of UDP-3-O-(R-3-Hydroxymyristoyl)-N-acetylglucosamine Deacetylase *Analytical Biochemistry* 290, 338-346.
133. Matsuura, K., Tamada, Y., Deyashiki, Y., Miyabe, Y., Nakanishi, M., Ohya, I., Hara, A. (1996) Activation of human liver 3-alpha-hydroxysteroid dehydrogenase by sulphobromophthalein *Biochem. J.* 313, 179-184.

134. Hara, A., Matsuura, K., Tamada, Y., Sato, K., Miyabe, Y., Deyashiki, Y., and Ishida, N. (1996) Relationship of human liver dihydrodiol dehydrogenases to hepatic bile-acid-binding protein and an oxidoreductase of human colon cells *Biochem. J.* 313, 373-376.
135. Held, P. (2003), Bio-Tek Instruments.
136. Dufour, E., Storer, A. C., and Menard, R. (1995) Engineering nitrile hydratase activity into a cysteine protease by a single mutation *Biochemistry* 34, 16382-16388.
137. Hirayama, K. (1967) *Handbook of Ultraviolet and Visible Absorption Spectra of Organic Compounds*, Plenum Press Data Division, New York, USA.
138. Ge, X., Penney, L. C., van de Rijn, I., and Tanner, M. E. (2004) Active Site Residues and Mechanism of UDP-Glucose Dehydrogenase *Eur J Biochem* 271, 14-22.
139. Bentley, R. (1970) *Molecular Asymmetry in Biology*, Vol. 2, Academic Press, New York.
140. Ridley, W. P., and Kirkwood, S. (1973) The stereospecificity of hydrogen abstraction by uridine diphosphoglucose dehydrogenase *Biochem. Biophys. Res. Commun.* 54, 955-960.
141. Grubmeyer, C. T., Insinga, S., Bhatia, M. and Moazami, N. (1989) *Salmonella typhimurium* Histidinol Dehydrogenase: Complete Reaction Stereochemistry and Active Site Mapping *Biochemistry* 28, 8174-8180.

142. Glasfield, A., Lenz, G.F. and Benner, S. A. (1990) The stereospecificities of seven dehydrogenases from *Acholeplasma laidlawii*. The simplest historical model that explains dehydrogenase stereospecificity *J. Biol. Chem.* 265, 11692-11699.
143. Reynolds, K. A., and Holland, K. A. (1997) The mechanistic and evolutionary basis of stereospecificity for hydrogen transfers in enzyme-catalysed processes *Chemical Society Reviews* 26, 337-343.
144. Nambiar, K. P., Stauffer, D. M., Koldziej, P. A., and Benner, S. A. (1983) A Mechanistic Basis for the Stereoselectivity of Enzymatic Transfer of Hydrogen from Nicotinamide Cofactors *J. Am. Chem. Soc* 105, 5886-5890.
145. Kurz, L. C., and Frieden, C. (1980) Anomalous Equilibrium and Kinetic alpha-Deuterium Secondary Isotope Effects Accompanying Hydride Transfer from Reduced Nicotinamide Adenine Dinucleotide *J. Am. Chem. Soc* 102, 4198-4203.
146. Cook, P. F., Oppenheimer, N. J., and Cleland, W. W. (1981) Secondary Deuterium and Nitrogen-15 Isotope Effects in Enzyme-Catalyzed Reactions. Chemical Mechanism of Liver Alcohol Dehydrogenase *Biochemistry* 20, 1817-1825.
147. Nar, H., Huber, R., Auerbach, G., Fischer, M., Hosl, C., Ritz, H., Bracher, A., Meining, W., Eberhardt, S., and Bacher, A. (1995) Active site topology and reaction mechanism of GTP cyclohydrolase I *Proc. Natl. Acad. Sci. USA* 92, 12120-12125.

148. Lee, S., Ahn, C., Park, E., Hwang, D. S., and Yim, J. (2002) Biochemical Characterization of Oligomerization of *Escherichia coli* GTP Cyclohydrolase I *Journal of Biochemistry and Molecular Biology* 35, 255-261.
149. Kuzmic, P. (1996) Program DYNAFIT for the Analysis of Enzyme Kinetic Data: Application to HIV Protease *Analytical Biochemistry* 237, 260-273.

Appendix A. Buffers

LB media: 10 g tryptone, 5 g NaCl, 10 g yeast extract per 1 L, pH 7.0

Buffer A: 100 mM Tris (pH 8.0), 100 mM KCl, 1 mM β -mercaptoethanol, 1 mM PMSF, and 1% Triton X-100

Buffer B: 100 mM Tris (pH 8.0), 100 mM KCl, 1 mM β -mercaptoethanol, 1 mM PMSF, 1% Triton X-100, and 20 mM imidazole

Buffer C: 100 mM Tris (pH 8.0), 100 mM KCl, 1 mM β -mercaptoethanol, and 20 mM imidazole

Buffer D: 100 mM Tris (pH 8.0), 100 mM KCl, 1 mM β -mercaptoethanol, and 50 mM imidazole

Buffer E: 100 mM Tris (pH 8.0), 100 mM KCl, 1 mM β -mercaptoethanol, and 100 mM imidazole

Buffer F: 100 mM Tris (pH 8.0), 100 mM KCl, 1 mM β -mercaptoethanol, and 200 mM imidazole

Buffer G: 100 mM Tris (pH 8.0), 100 mM KCl, and 1 mM β -mercaptoethanol

M9 media: 6 g $\text{Na}_2\text{HPO}_4 \cdot 7\text{H}_2\text{O}$, 3 g KH_2PO_4 , 0.5 g NaCl, 1 g NH_4Cl , in 1000 mL $\text{MQ-H}_2\text{O}$

Appendix B. Primer Sequences

Sequence Name	Sequence 5' → 3'	Description
C55A-s	CCGGAATTCACATCTTTAGCTCCTAAAACAGGC	C55A sense strand primer
C55A-as	CTGGCCTGTTTTAGGAGCTAAAGATGTGAATTCCGG	C55A antisense strand primer
C55S-s	CCGGAATTCACATCTTTA <u>TC</u> TCTCCTAAAACAGGC	C55S sense strand primer
C55S-as	CTGGCCTGTTTTAGGAGATAAAAGATGTGAATTCCGG	C55S antisense strand primer
E97A-s	GTGACTTCCACGCGGACTGCATGAATATCATCATGAAC	E97A sense strand primer
E97A-as	GTTTCATGATGATATTCATGCAGTCCGCGTGGAAGTCAC	E97A antisense strand primer
E97L-s	GTGACTTCCAC <u>CT</u> GGACTGCATGAATATCATCATGAAC	E97L sense strand primer
E97L-as	GTTTCATGATGATATTCATGCAGTCCAGGTGGAAGTCAC	E97L antisense strand primer
E97K-s	GTGACTTCCACAAGGACTGCATGAATATCATCATGAAC	E97K sense strand primer
E97K-as	GTTTCATGATGATATTCATGCAGTCC <u>TT</u> GTGGAAGTCAC	E97K antisense strand primer
E97Q-s	GTGACTTCCACCAGGACTGCATGAATATCATCATGAAC	E97Q sense strand primer
E97Q-as	GTTTCATGATGATATTCATGCAGTCC <u>TG</u> TGGAAGTCAC	E97Q antisense strand primer
E97D-s	GTGACTTCCACGACGACTGCATGAATATCATCATGAAC	E97D sense strand primer
E97D-as	GTTTCATGATGATATTCATGCAGTCC <u>TC</u> GTGGAAGTCAC	E97D antisense strand primer
YgcM-s	GGTATTGAGGGTTCGCATGATGTCCACCACG	<i>E. coli ygcM</i> pET30Xa vector, sense strand primer
YgcM-as	AGAGGAGAGTTAGAGCCTCATTGCCC	<i>E. coli ygcM</i> pET30Xa vector, antisense strand primer
Ybax-s	GGTATTGAGGGTTCGCATGAAACGTGC	<i>E. coli ybax</i> pET30Xa vector, sense strand primer
Ybax-as	AGAGGAGAGTTAGAGCCTTACTTCAACCC	<i>E. coli ybax</i> pET30Xa vector, antisense strand primer

* underlined bases indicate desired point mutation

Appendix C. Derivation of the Initial Velocity Equations for the Ter-Ter Ping Pong Mechanism

$$\frac{v}{V_{\max}} = \frac{[A][B][C]}{K_{ia}K_{mB}[C] + K_{mC}[A][B] + K_{mB}[A][C] + K_{mA}[B][C] + [A][B][C]}$$

where: $[B] = [C]$ (NADPH binds and reacts twice) and assuming $K_{mB} = K_{mC}$,

$$\frac{v}{V_{\max}} = \frac{[A][B]^2}{K_{ia}K_{mB}[B] + K_{mB}[A][B] + K_{mB}[A][B] + K_{mA}[B]^2 + [A][B]^2}$$

Collecting the terms $K_{mB}[A][B]$,

$$\frac{v}{V_{\max}} = \frac{[A][B]^2}{K_{ia}K_{mB}[B] + 2K_{mB}[A][B] + K_{mA}[B]^2 + [A][B]^2}$$

Solving for A, divide by $[B]^2$,

$$\frac{v}{V_{\max}} = \frac{[A]}{\frac{K_{ia}K_{mB}}{[B]} + \frac{2K_{mB}[A]}{[B]} + K_{mA} + [A]}$$

Rearrangement of the terms and expression in the form of the Michelis-Menton,

$$\frac{v}{V_{\max}} = \frac{[A]}{K_{mA} \left(1 + \frac{K_{ia}K_{mB}}{K_{mA}[B]} \right) + [A] \left(1 + \frac{2K_{mB}}{[B]} \right)}$$

As derived before,

$$\frac{v}{V_{\max}} = \frac{[A][B]^2}{K_{ia}K_{mB}[B] + 2K_{mB}[A][B] + K_{mA}[B]^2 + [A][B]^2}$$

Solving for B, divide by [A][B],

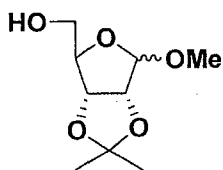
$$\frac{v}{V_{\max}} = \frac{[B]}{\frac{K_{ia}K_{mB}}{[A]} + 2K_{mB} + \frac{K_{mA}[B]}{[A]} + [B]}$$

Rearrangement of the terms and expression in the form of the Michelis-Menton gives,

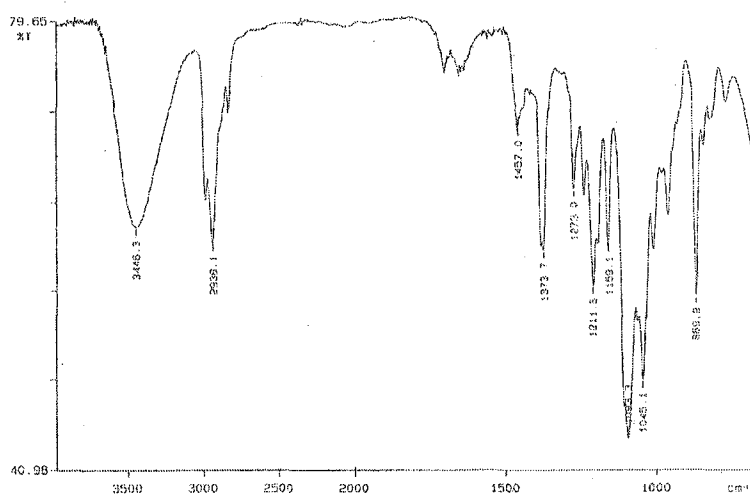
$$\frac{v}{V_{\max}} = \frac{[B]}{K_{mB} \left(2 + \frac{K_{ia}}{[A]} \right) + [B] \left(1 + \frac{K_{mA}}{[A]} \right)}$$

Appendix D. Characterization of Synthetic Compounds

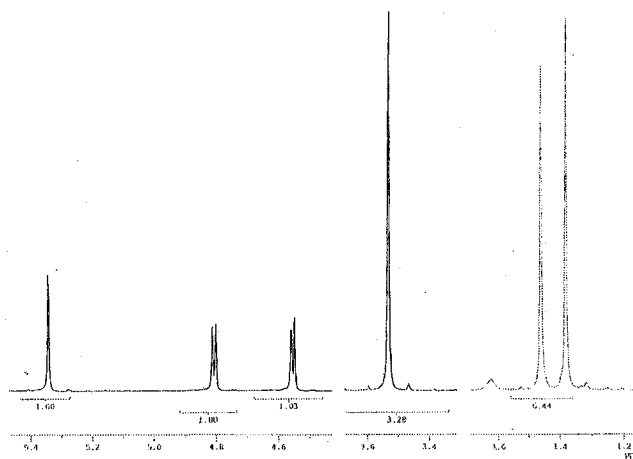
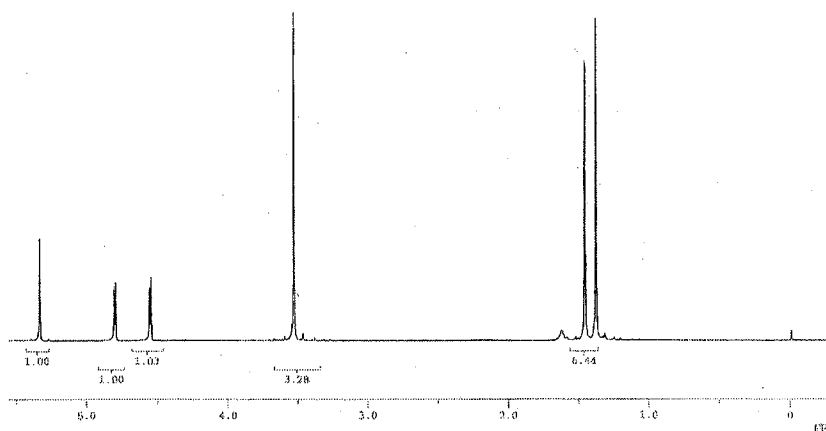
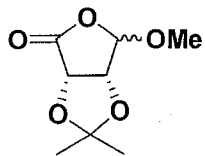
Methyl 2,3-O-Isopropylidene-D-ribofuranoside



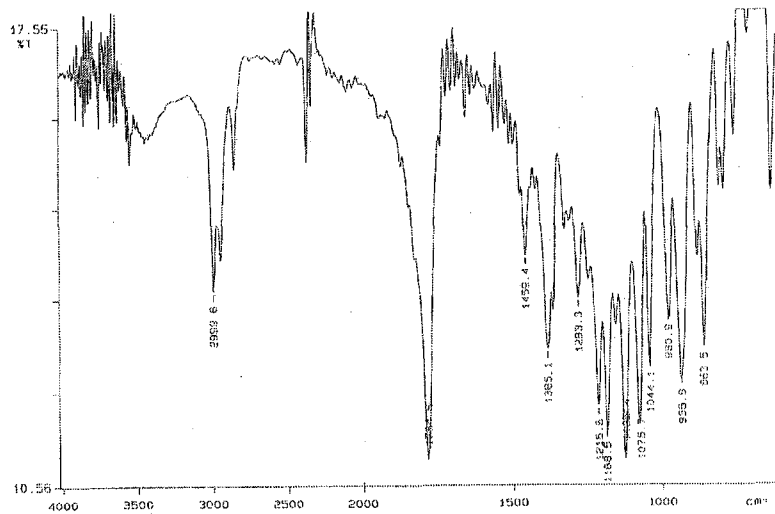
$^1\text{H-NMR}$ (CDCl_3): 1.32 (3H, s, CCH_3), 1.48 (3H, s, CCH_3), 3.2 (1H, s, OH), 3.44 (3H, s, OCH_3), 3.67 (2H, d, $J=3.7$ Hz, H-5), 4.41 (1H, t, $J=3.7$, H-4), 4.71/4.85, (2H, ab pair, $J=6.3$ Hz, H-2/H-3), 5.00 (1H, s, H-1).



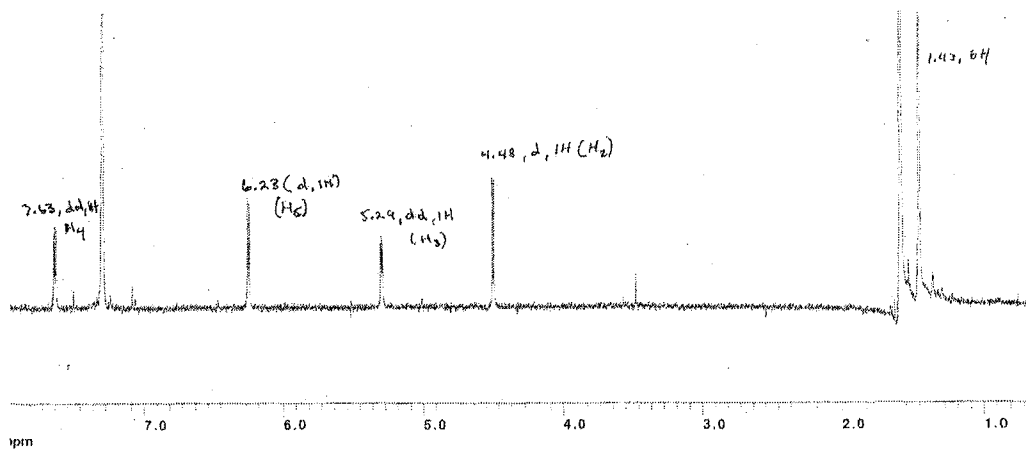
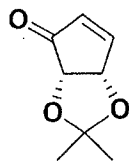
2,3-O-Isopropylidene-4-methoxy-erythruronofuranoside



$^1\text{H-NMR}$ (CDCl_3): 1.38 (3H, s, CH_3), 1.46 (3H, s, CH_3), 3.53 (3H, s, OCH_3), 4.55 (1H, d, $J=5.37$ Hz, H-3), 4.80 (1H, d, $J=5.37$ Hz, H-2), 5.34 (1H, s, H-1).

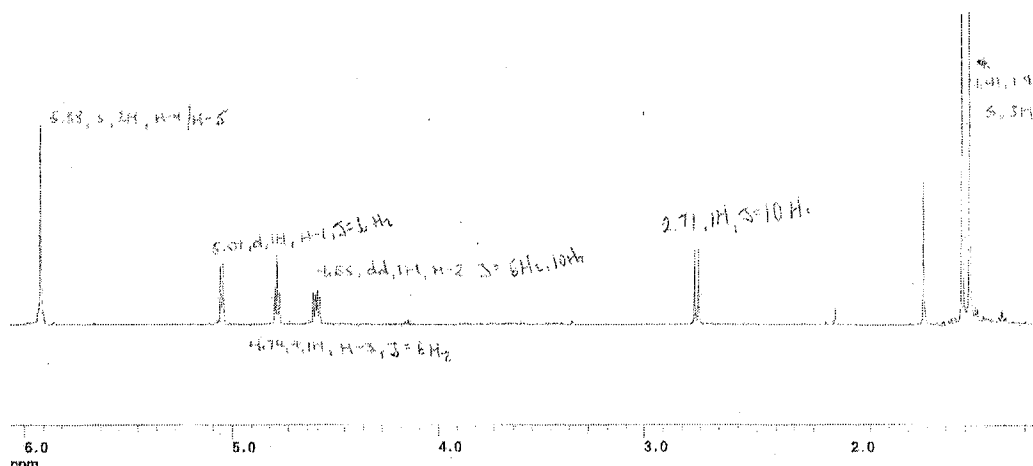
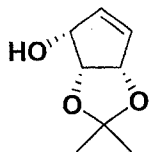


2,3-O-Isopropylidene-4-cyclopentenone



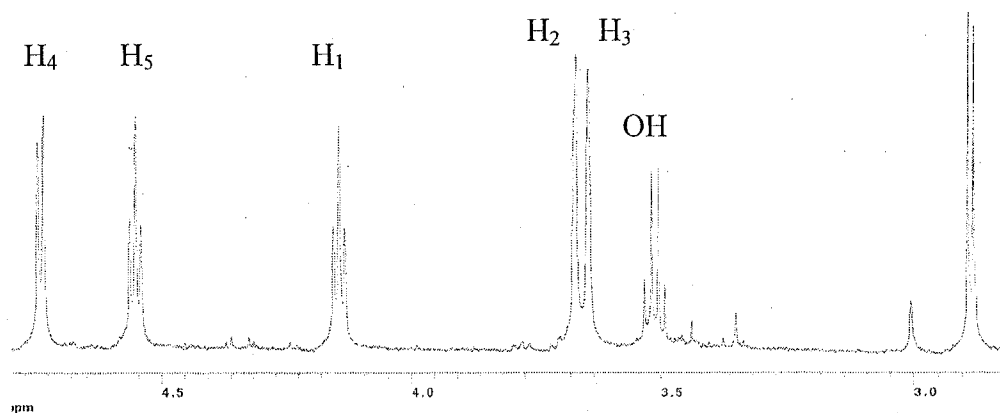
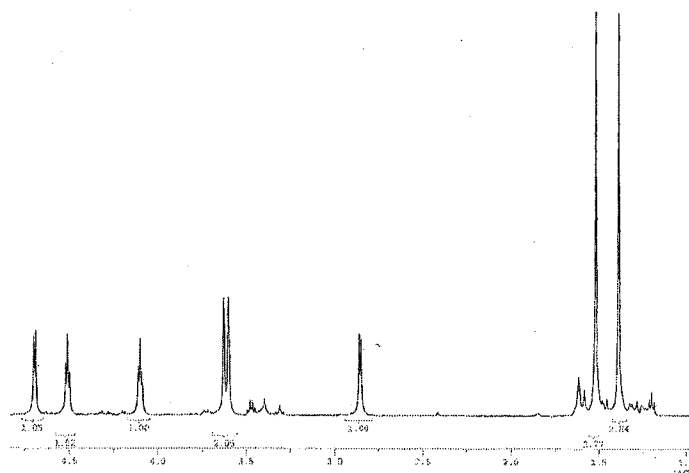
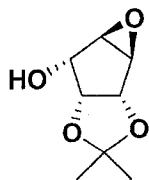
$^1\text{H-NMR}$ (CDCl_3): 1.43 (6H, s, $2\times\text{CH}_3$), 4.48 (1H, d, $J=5$ Hz, H-2), 5.29 (1H, dd, $J_1=5\text{Hz}$, $J_2=2$ Hz, H-3), 6.22 (1H, d, $J=6\text{Hz}$, H-5), 7.60 (1H, dd, $J_1=6\text{Hz}$, $J_2=2\text{Hz}$, H-4).

2,3-O-isopropylidene-4-cyclopenten-1-ol

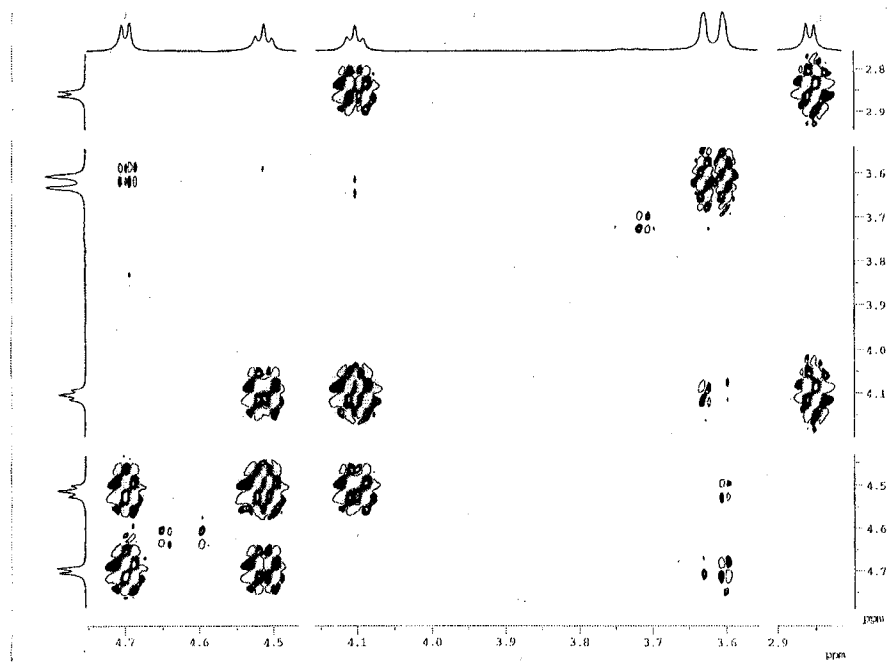


$^1\text{H-NMR}$ (CDCl_3): 5.88 (2H, s, H-4 and H-5), 5.01 (1H, d, $J=6$ Hz, H-1), 4.74 (1H, t, $J=6$ Hz, H-3), 4.55 (1H, dd, $J=6$ Hz, H-2), 2.71 (1H, d, $J=6$ Hz, OH), 1.43 (3H, s, CH_3), 1.41 (3H, s, CH_3).

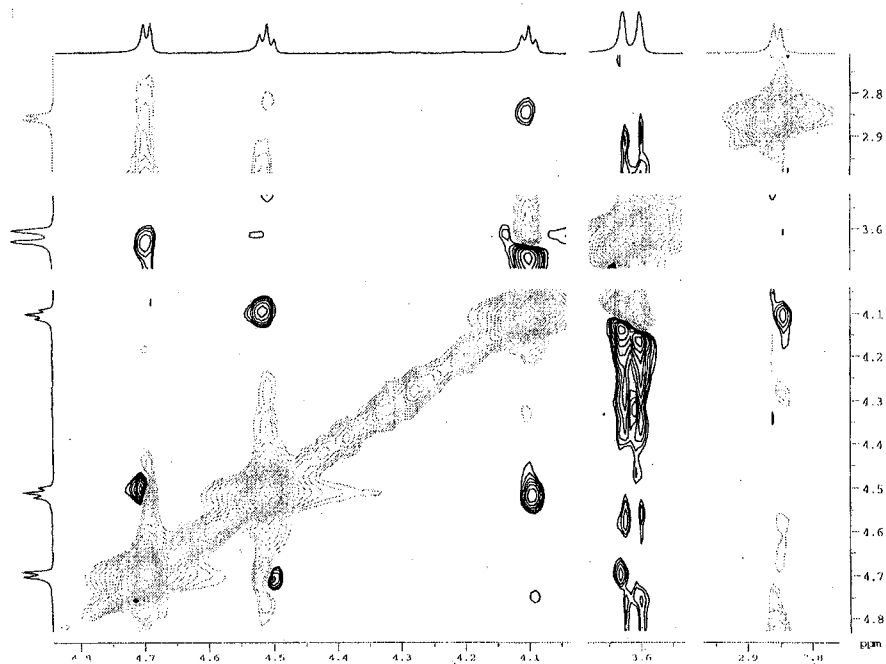
2,3-epoxy-4,5-isopropylidene cyclopentan-1-ol



$^1\text{H-NMR}$ (CDCl_3): 1.42 (3H, s, CH_3), 1.57 (3H, s, CH_3), 2.9 (1H, d, $J=5$ Hz, OH), 3.65 (1H, d, $J=2$ Hz, H-3), 3.67 (1H, d, $J=2$ Hz, H-2), 4.14 (1H, t, $J=6$ Hz, H-1), 4.55 (1H, t, $J=6$ Hz, H-5), 4.7 (1H, d, $J=5$ Hz, H-4).

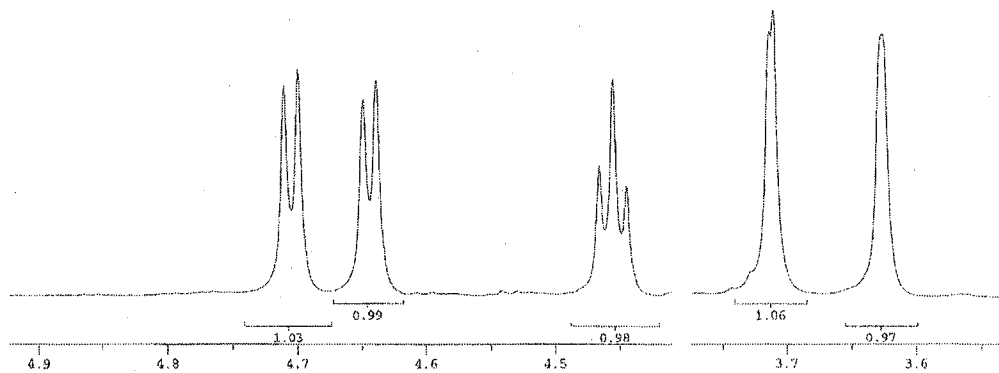
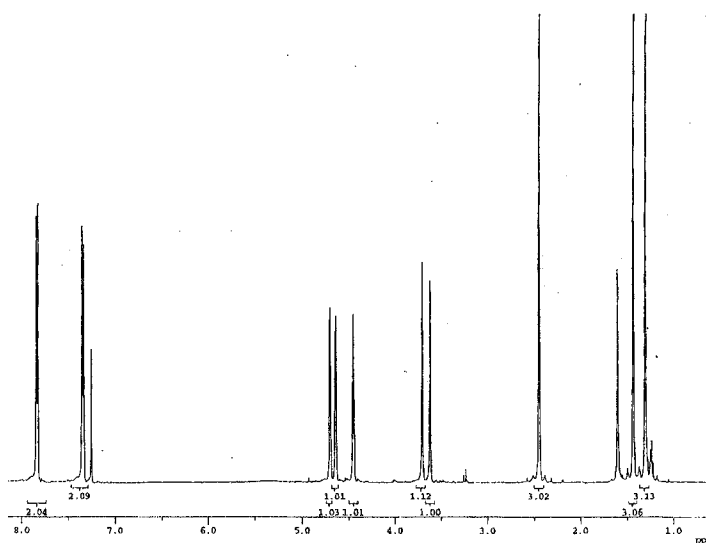
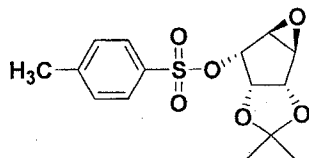


COSY spectrum of (1*R*,2*R*,3*S*,4*R*,5*S*)-2,3-epoxy-4,5-*O*-isopropylidene-cyclopentan-1-ol. (The ring protons are shown here)



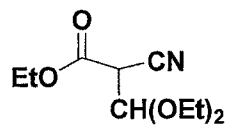
NOESY spectrum of (1*R*,2*R*,3*S*,4*R*,5*S*)-2,3-epoxy-4,5-*O*-isopropylidene-cyclopentan-1-ol. (The ring protons are shown here)

2,3-epoxy-4,5-isopropylidene-1-tosyl-cyclopentane

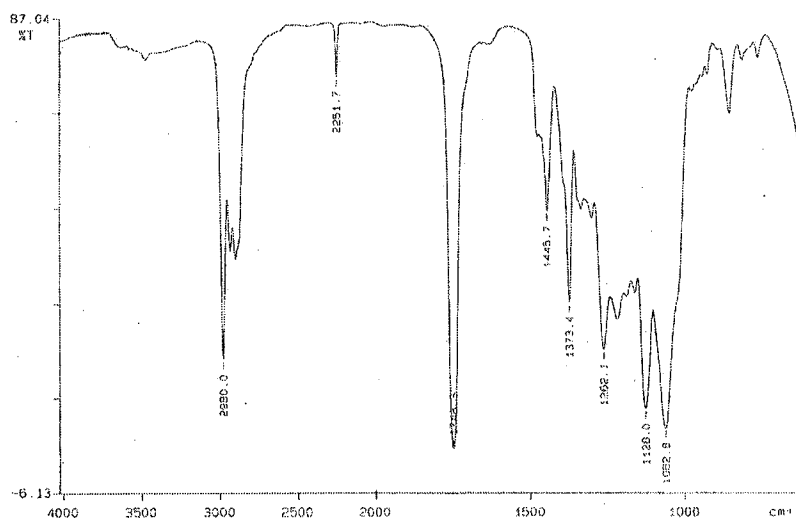


$^1\text{H-NMR}$ (CDCl_3): 1.42 (3H, s, CH_3), 1.57 (3H, s, CH_3), 2.45 (3H, s, CH_3), 3.63 (1H, s, H-3), 3.71 (1H, d, $J=2$ Hz, H-2), 4.45 (1H, t, $J=6$ Hz, H-1), 4.64 (1H, d, $J=5$ Hz, H-5), 4.70 (1H, d, $J=5$ Hz, H-4), 7.35 (2H, d), 7.84 (2H, d).

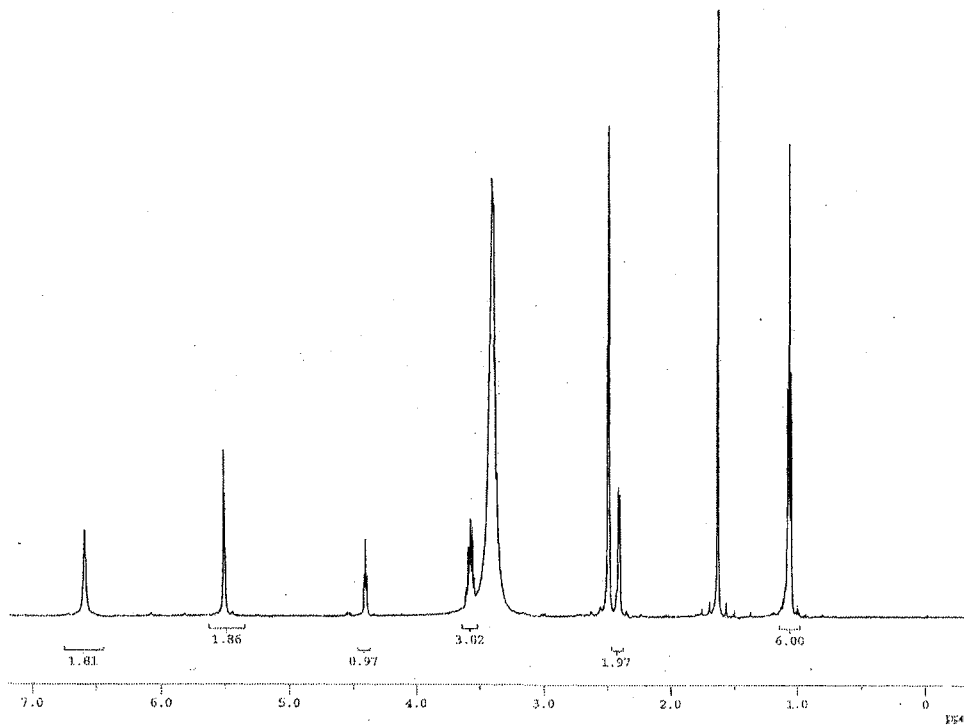
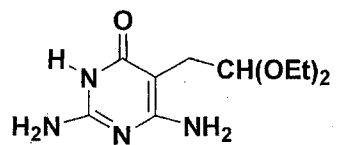
Ethyl 2,2-diethoxyethylcyanoacetate



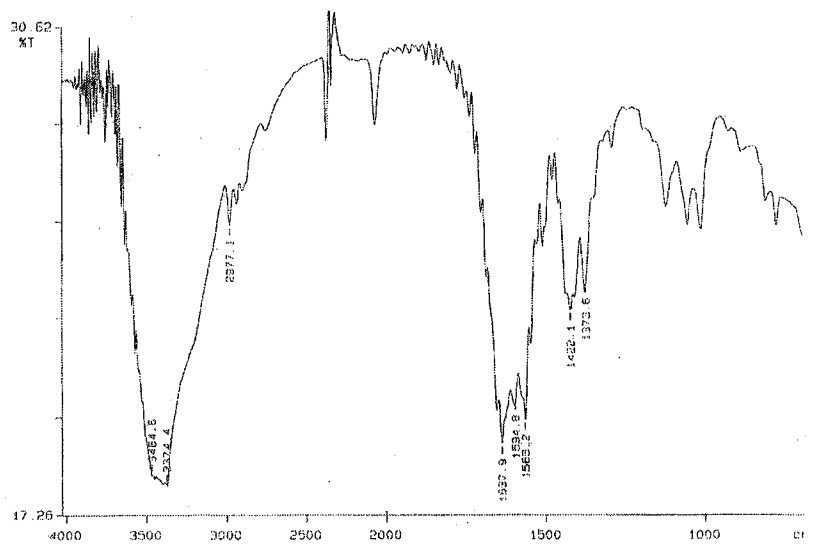
¹H-NMR (CDCl₃): 1.22 (6H, m), 1.33 (3H, t), 2.25 (2H, dm), 3.46 (1H, t), 3.52 (2H, m), 3.66 (2H, m), 4.27 (2H, q), 4.7 (1H, t).



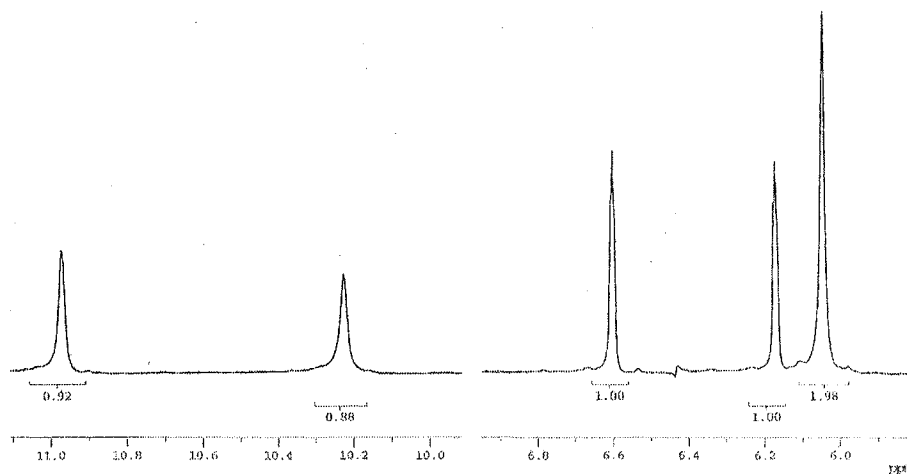
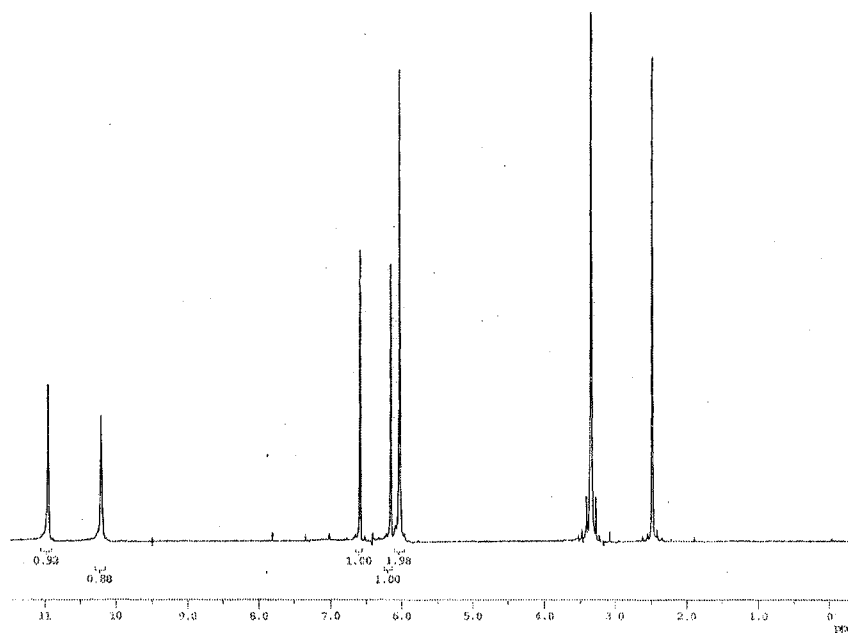
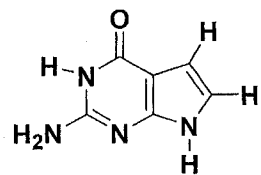
2,4-Diamino-5(2,2-diethoxyethyl)-6-hydroxypyrimidine



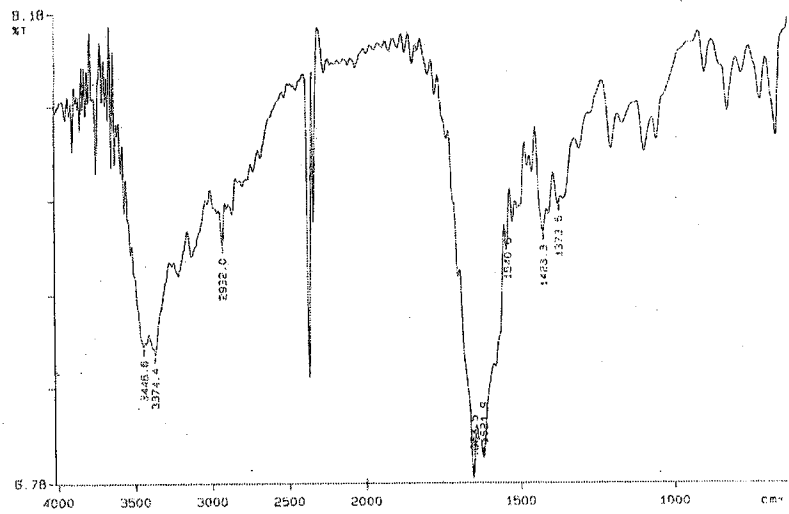
¹H-NMR (*d*₆-DMSO): 1.08 (6H, t), 2.42 (2H, d), 3.59 (4H, m), 4.43 (1H, t), 5.89 (2H, s), 6.00 (2H, s), 9.88 (1H, br s).



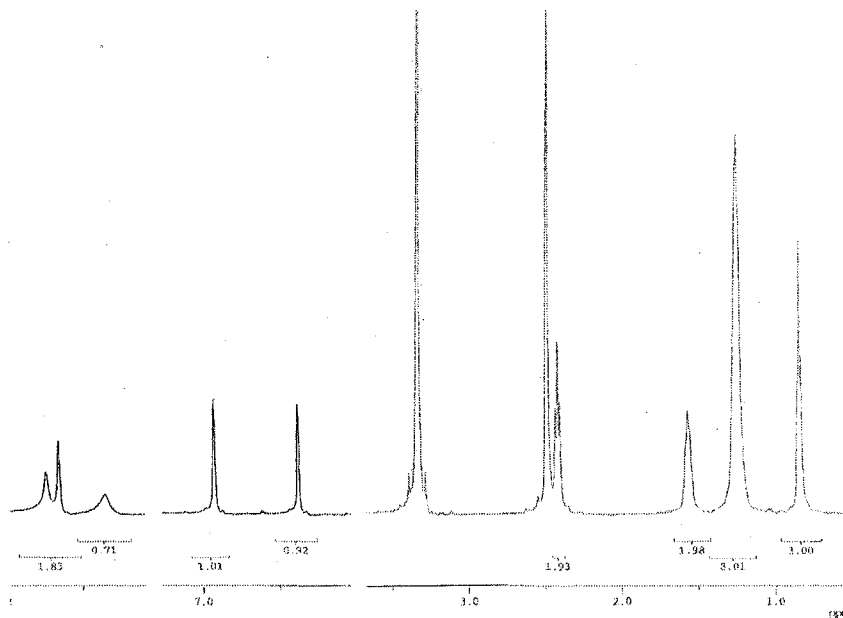
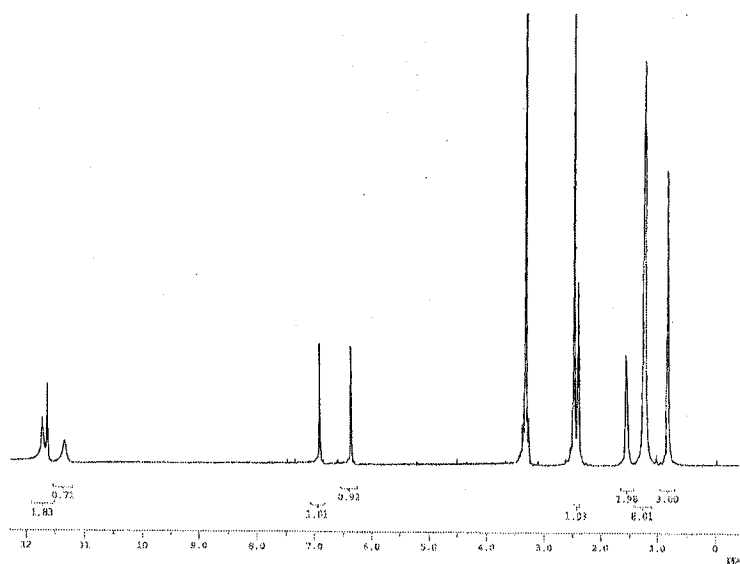
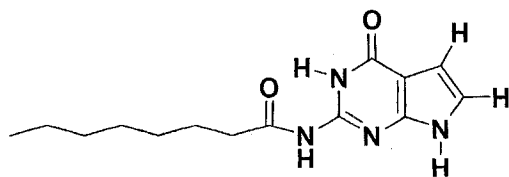
2-Amino-pyrrolo[2,3-*d*]pyrimidin-4-one



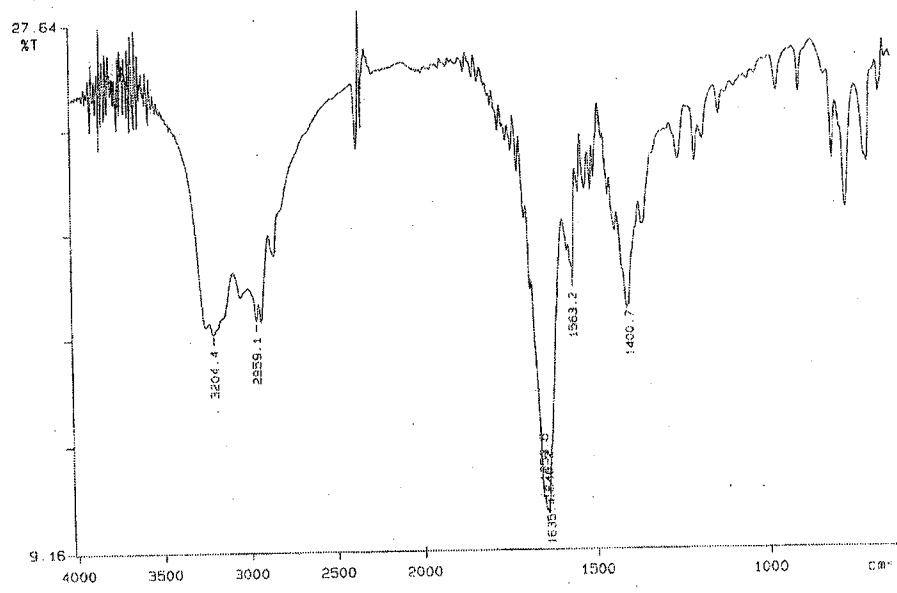
$^1\text{H-NMR}$ (d_6 -DMSO): 6.26, (1H, d), 6.69 (1H, d), 10.79 (1H br s), 11.25 (1H, br s).



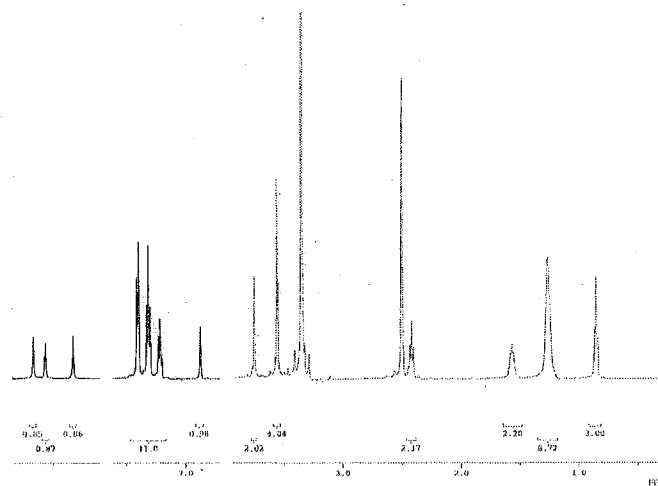
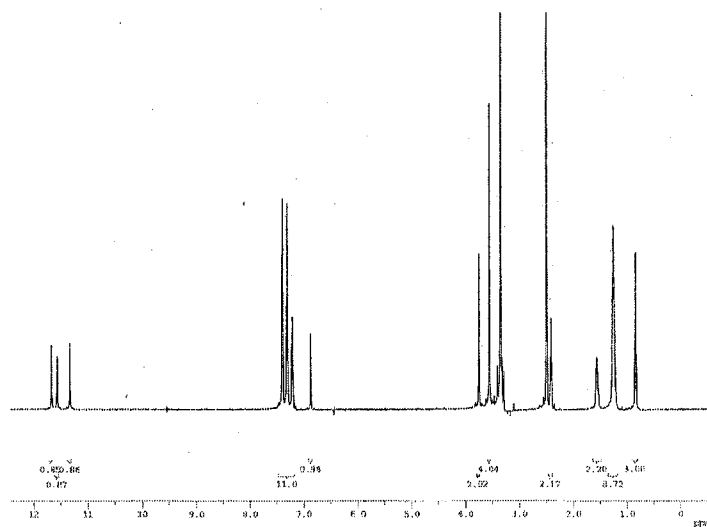
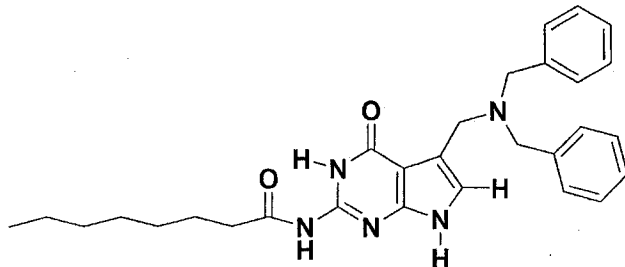
2-Octanoyl-pyrrolo[2,3-d]pyrimidin-4-one



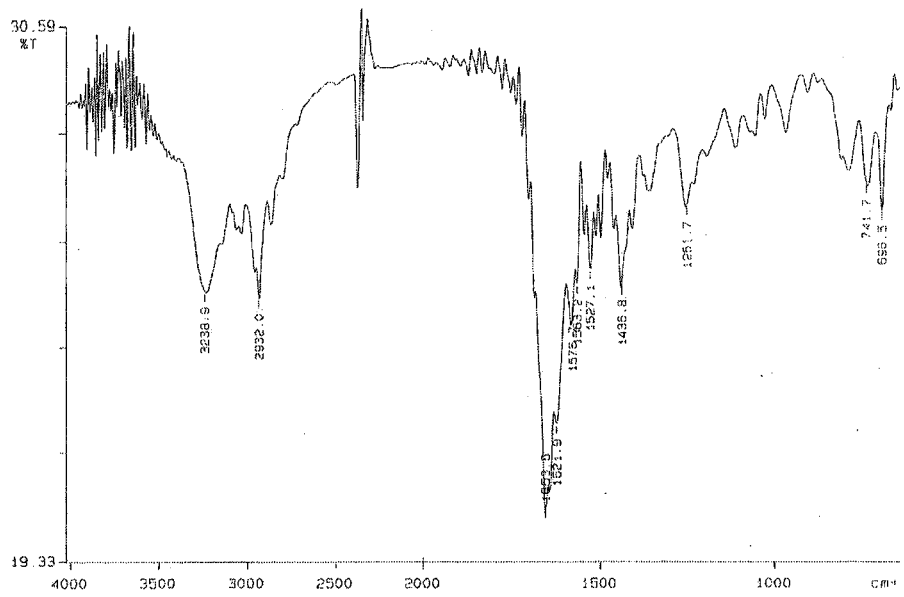
¹H-NMR (*d*₆-DMSO): 0.89 (3H, t), 1.29 (8H, s), 1.75 (2H, m), 2.47 (2H, t).



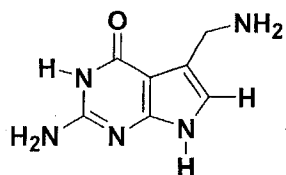
2-Octanoyl-5-(N,N-dibenzylaminomethyl)pyrrolo[2,3-d]pyrimidin-4-one



¹H-NMR (*d*₆-DMSO): 0.85 (3H, t), 1.26 (8H, br s), 1.57 (2H, m), 2.44 (2H, m), 3.56 (4H, s), 3.76 (2H, s), 6.88 (1H, d), 7.21-7.42 (10H, m).

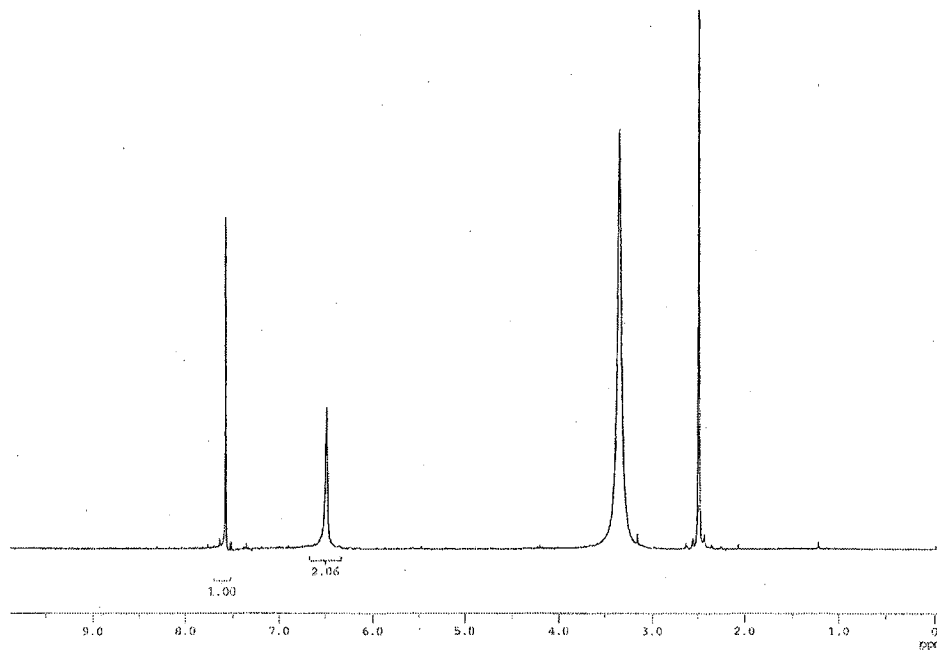
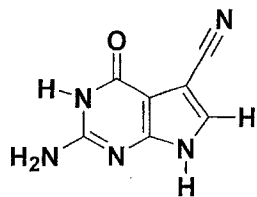


2-amino-5-(aminomethyl)pyrrolo[2,3-*d*]pyrimidin-4-one (PreQ₁)



¹H-NMR (*d*₄-MeOH): 4.13 (2H, s), 6.81 (1H, s) (see Figure 38).

2-amino-5-cyanopyrrolo[2,3-*d*]pyrimidin-4-one (PreQ₀)



¹H-NMR (*d*₆-DMSO): 6.38 (2H, s), 7.61 (1H, s), 10.70 (1H, s), 11.97 (1H, s).